CAPITAL UNIVERSITY OF SCIENCE AND TECHNOLOGY, ISLAMABAD

Investigation of a Williamson Hybrid Nanofluid Flow using the Cattaneo-Christov Heat Flux, Magnetic Field, Forchheimer Flow and Chemical Reaction

by

Hassan Shahzad

A thesis submitted in partial fulfillment for the degree of Master of Philosophy

in the

Faculty of Computing
Department of Mathematics

2023

This thesis is dedicated to my cherished parents, whose boundless love, unwavering support and belief in my abilities have been the driving force behind my academic journey. Their sacrifices, encouragement, and constant presence have inspired me to persevere and reach for excellence. I am forever grateful for the values and guidance they have instilled in me, which have shaped my character and ambitions. This work is a testament to their selfless dedication and the profound impact they have had on my life. I am privileged to have such remarkable parents who have always stood by me with unwavering love and care.

CERTIFICATE OF APPROVAL

Investigation of a Williamson Hybrid Nanofluid Flow using the Cattaneo-Christov Heat Flux, Magnetic Field, Forchheimer Flow and Chemical Reaction.

by

Hassan Shahzad

(MMT213027)

THESIS EXAMINING COMMITTEE

S No	Examiner	Name	Organization
(a)	External Examiner	Dr. Farman Ullah Khan	HITEC University
(b)	Internal Examiner	Dr. Rashid Ali	CUST University
(c)	Supervisor	Dr. Muhammad Sagheer	CUST University

Dr. Muhammad Sagheer
Thesis Supervisor
November, 2023

Dr. Muhammad Sagheer
Head
Dept. of Mathematics
November, 2023

Dr. M. Abdul Qadir
Dean
Faculty of Computing
November, 2023

Author's Declaration

I, **Hassan Shahzad** hereby state that my MPhil thesis titled "**Investigation of a Williamson Hybrid Nanofluid Flow using the Cattaneo-Christov Heat Flux, Magnetic Field, Forchheimer Flow and Chemical Reaction.**" is my own work and has not been submitted previously by me for taking any degree from Capital University of Science and Technology, Islamabad or anywhere else in the country/abroad.

At any time if my statement is found to be incorrect even after my graduation, the University has the right to withdraw my MPhil Degree.

(Hassan Shahzad)

Registration No: MMT213027

Plagiarism Undertaking

I solemnly declare that research work presented in this thesis titled "**Investigation of a Williamson Hybrid Nanofluid Flow using the Cattaneo-Christov Heat Flux, Magnetic Field, Forchheimer Flow and Chemical Reaction.**" is solely my research work with no significant contribution from any other person. Small contribution/help wherever taken has been duly acknowledged and that complete thesis has been written by me.

I understand the zero tolerance policy of the HEC and Capital University of Science and Technology towards plagiarism. Therefore, I as an author of the above titled thesis declare that no portion of my thesis has been plagiarized and any material used as reference is properly referred/cited.

I undertake that if I am found guilty of any formal plagiarism in the above titled thesis even after award of MPhil Degree, the University reserves the right to withdraw/revoke my MPhil degree and that HEC and the University have the right to publish my name on the HEC/University website on which names of students are placed who submitted plagiarized work.

(Hassan Shahzad)

Registration No: MMT213027

Acknowledgement

I would like to express my deepest gratitude and appreciation to all those who have contributed to the successful completion of this thesis.

First and foremost, I am immensely grateful to my supervisor, Dr. Muhammad Sagheer, for his unwavering guidance, encouragement, and support throughout this research journey. His expertise and valuable insights have been instrumental in shaping the direction and quality of this work.

I am also deeply grateful to my mother and sister for their unwavering love, encouragement, and belief in me. Their constant support and understanding have been a source of strength during the challenging moments of this academic pursuit. Their sacrifices and words of encouragement have kept me motivated and focused.

A special note of thanks goes to my father, whose boundless love, encouragement, and sacrifices have been the bedrock of my academic journey. His unwavering belief in me has been a driving force behind my achievements, and I am forever grateful for his guidance and wisdom.

In conclusion, this thesis would not have been possible without the collective efforts of all those mentioned above.

(Hassan Shahzad)
Registration No: MMT213027

Abstract

This research has provided a comprehensive understanding of water-based Williamson hybrid nanofluid flow, considering various physical parameters. The investigation is focused on a two-dimensional steady boundary layer flow over a stretching sheet. The governing equations are modelled and analyzed, incorporating Cattaneo-Christov heat flux, magnetic field effects, diffusion, Forchheimer flow, and chemical reaction parameter. Numerical techniques; the shooting method, effectively solved the converted coupled system of ordinary differential equations. Notably, the study identifies the significant role of Cattaneo-Christov heat flux and magnetic field effects in enhancing heat transfer efficiency, thereby improving thermal diffusion within the system. Furthermore, the inclusion of diffusion and Forchheimer flow led to noticeably effect the velocity, temperature and concentration profiles and their rates of change. The study also reveals initial uncertain behavior observed in nanoparticle concentration before reaching stable values for certain parameter combinations. This transient behavior is crucial to understand the dynamics of nanofluid flow and its practical implications in engineering applications.

Contents

List of Figures

List of Tables

Abbreviations

BCs	Boundary conditions
HNF	Hybrid Nano Fluid
IVPs	Initial value problem
MHD	Magnetohydrodynamics
NF	Nano Fluid
ODEs	Ordinary differential equation
PDEs	Partial differential equation
RK-4	Range kutta order 4

Symbols

$\widetilde{u}, \widetilde{v}$	Velocity components
$\tilde{\mu}$	Viscosity
$\widetilde{\nu}$	Kinematic viscosity
$\widetilde{\rho}$	Density
$\widetilde{B}_o$	Magnetic field strenght
$\widetilde{¥}$	Temperature of nanoparticles
$\widetilde{K}$	Thermal conductivity
$\widetilde{\rho}\widetilde{c}_p$	Heat capacity
$\widetilde{¥}_f$	Wall constant temperature
$\widetilde{¥}_\infty$	Ambient temperature of fluid
$\widetilde{C}$	Concentration
$\widetilde{C}_f$	Nanoparticles concentration at the stretching surface
$\widetilde{C}_\infty$	Ambient concentration
$\widetilde{q}_r$	Radiative heat flux
λ_T	Relaxiation time constant
$\widetilde{B}_o$	Magnatic field constant
$\widetilde{\sigma}^*$	Stefan Boltzmann constant
$\widetilde{k}^*$	Absorption coefficient
ζ	Similarity variable
$f(\zeta)$	Dimensionless velocity
$\theta(\zeta)$	Dimensionless temperature
$\phi(\zeta)$	Dimensionless concentration
Γ	Fluid relaxation time
$\widetilde{Q}_o$	Heat source

$\widetilde{h}_f$	Cofficient of heat transfer
w_e	Non-Newtonian Williamson parameter
M	Magnetic field parameter
K_p	Porosity medium parameter
Pr	Prandtl number
Ec	Eckert number
Q	Heat source
Fr	Forchheimer number
$\widetilde{D}_B$	Brownian motion
$\widetilde{D}_{¥}$	Thermophoresis motion
Nb	Brownian motion parameter
Nt	Thermophoresis motion parameter
Le	Lewis number
γ	Chemical reaction parameter
Re	Reynolds number
Re_x	Local Reynolds number
Sh_x	Local Sherwood number
Nu	Nusselt number
Nu_x	Local Nusselt number
Cf	Skin fraction coefficient

Subscripts

p	Nanoparticle
nf	Nanofluid
hnf	Hybrid nanofluid

Chapter 1

Introduction

1.1 Background

The Williamson fluid flow model is a non-Newtonian fluid model that was introduced by Williamson in 1929 [1]. This model describes the behavior of certain viscoelastic fluids. It defines the stress tensor as a combination of the rate of strain tensor and the relaxation time tensor, making it suitable for studying viscoelastic fluids that exhibit both elastic and viscous behavior. Since its introduction, the Williamson fluid flow model has been extensively studied and applied in various fields of engineering and science.

Bouslimi et al. [2] conducted a numerical investigation of the magnetohydrodynamic flow of a Williamson nanofluid over a stretching sheet within a porous medium. Their study comprehensively considered significant physical effects, encompassing Joule heating, nonlinear thermal radiation, and chemical reaction. Meanwhile, Jalili et al. [3] employed the semi-analytical Akbari-Ganji Method (AGM) to explore the thermal analysis of Williamson fluid flow, elucidating the impact of the Lorentz force and variable viscosity on a stretching plate. Guedri et al. [4] meticulously examined the behavior of a two-phase dusty thermally developed Marangoni forced convective flow of Williamson material, leveraging a novel finite difference scheme for their numerical simulation. In addition, Kumar et al.

[5] performed a numerical investigation of the flow and heat transfer characteristics of a Williamson fluid over a permeable stretching cylinder using the bvp4c solver in MATLAB. A number of researchers have also conducted comprehensive reviews on the Williamson fluid, including works by Shaheen et al. [6], Jangid et al. [7], and Taj and Salahuddin [8].

Nanofluids, which encompass nanoparticles uniformly suspended within a base fluid, have garnered considerable research attention due to their heightened thermophysical attributes in contrast to the conventional heat transfer fluids. The inception of nanofluid studies can be attributed to Choi and Eastmam [9]. Buongiorno [10] introduced a non-homogeneous equilibrium model, elucidating the role of Brownian motion and thermophoretic diffusion in augmenting heat transfer. Khan and Pop [11] conducted an inquiry into the boundary-layer flow of nanofluids over a stretching sheet, delving into the effects of Brownian motion and thermophoresis to unravel their behavior near the sheet, employing an implicit finite-difference method. Nadeem et al. [12] delved into the flow characteristics of non-Newtonian Williamson fluid over a stretching sheet, utilizing the Homotopy Analysis Method (HAM). Bhatti and Rashidi [13] explored the impact of thermo-diffusion and thermal radiation on nanofluid flow over a porous stretching sheet, employing the combined approaches of the Successive Linearization Method (SLM) and Chebyshev Spectral Collocation Method (CSC). Krishnamurthy et al. [14] harnessed numerical techniques, employing the Runge-Kutta-Fehlberg fifth-order method coupled with the shooting technique, to investigate the effects of a chemical reaction on the magnetohydrodynamics (MHD) boundary layer flow and melting heat transfer of the Williamson nanofluid within a porous medium. Hayat et al. [15] probed the mixed convective three-dimensional flow of the Williamson nanofluid, considering the influence of a chemical reaction and employing the Optimal Homotopy Analysis Method (OHAM). Furthermore, Zhu et al. [16] conducted a comprehensive numerical investigation to analyze the heat and mass transfer attributes of the Williamson nanofluid over a stretching/shrinking sheet. This study was conducted through the combined application of the Successive Over Relaxation (SOR) Method and Finite Difference Method (FDM).

Hybrid nanofluids, have emerged as modern and innovative solutions for heat and

mass transfer, finding applications in heat exchangers, cooling systems, automotive engine cooling, solar thermal systems, and refrigeration. Yahya et al. [17] conducted a study on the thermal characteristics of a Williamson hybrid nanofluid MoS_2+ZnO mixed with engine oil flowing over a stretched sheet. They employed the Runge-Kutta method with a shooting technique for their analysis. In a similar vein, Jamshed et al. [18] employed the Keller box numerical technique to investigate the flow of a Williamson hybrid nanofluid Ag−Cu/EO over a stretching surface. Amjad et al. [19] presented a numerical solution using the MATLAB function bvp4c for the analysis of magnetized Williamson nanofluid flow over an exponentially stretching permeable surface. Their study accounted for temperature-dependent viscosity and thermal conductivity. Furthermore, Alhowaity et al. [20] adopted a numerically computational approach, specifically the parametric continuation method, to perform a heat transfer analysis of hybrid nanofluid flow with thermal radiation. Ongoing research continues to explore the diverse applications and behavior of hybrid nanofluids [21–25].

Heat and mass transfer are crucial in various applications, including space cooling, renewable energy production, aerospace engineering, and medical therapies like magnetic drug targeting [26]. While Fourier's law of thermal conduction has been extensively used for studying heat transfer, it has limitations, such as predicting an infinite speed of heat propagation. To address this, Cattaneo [27] proposed a generalized form of Fourier's law by introducing the relaxation time. Later, Christov [28] modified the Cattaneo model using Oldroyd's upper convected derivative to maintain frame-indifferent formulations.

Recently, researchers have explored the applications of the Cattaneo-Christov model in different fluid flow scenarios. Ashraf et al. [29] investigated the magnetohydrodynamic flow of Jeffrey nanofluid with modified Cattaneo-Christov fluxes. Algehyne et al. [30] studied the behavior of magnetized hybrid nanomaterial flow near a stretching wall. Salmi et al. [31] investigated heat generation in chemically reactive flow of Prandtl liquid, considering Ohmic heating. Overall, the Cattaneo-Christov flux model provides a valuable framework for understanding and analyzing heat and mass transfer phenomena in various fluid flow scenarios.

Several other researchers have also contributed to the exploration of this model in different contexts, as referenced in the mentioned articles [32–35].

Magnetohydrodynamics (MHD) stands as an interdisciplinary realm, blending the core principles of classical electromagnetism with the intricacies of fluid dynamics. Its purview encompasses the behavior of electrically conductive fluids when subjected to magnetic fields. Hussaini et al. [36] embarked on an exploration of convective MHD nanofluid flow. Their study unfurled over an impermeable stretching surface, considering the interplay of Soret diffusivity. This investigation harnessed the potency of the Runge-Kutta-Fehlberg method, augmented by the precision of the shooting technique. Likewise, Jalili et al. [37] navigated the MHD nanofluid landscape employing the finite element method. Their investigation extended beyond fluid flow and encompassed the intricate interplay of heat transfer within a circular porous medium. Within this realm, the dominant influences of Lorentz and buoyancy forces took precedence, and they ingeniously incorporated a cassini oval cavity into the framework governed by Darcy's law. Venturing further, Hussaini and Abdulkadir [38] embarked on a discourse that dissected the tangible impacts of diverse factors on MHD nanofluid flow. Here, the trinity of heat generation/absorption, magnetic fields, and solar radiation converged upon a stretching surface. This intricate interplay was meticulously deciphered using the Runge-Kutta-Fehlberg method in tandem with the deft precision of the shooting approach. On a different trajectory, Sarala et al. [39] steered their efforts towards the investigation of MHD nanofluid flow dynamics. An oscillating plate entered the narrative, further emboldened by chemical reactions and radiation. The analytical arsenal of Laplace transformation was summoned to tackle this intricate choreography of the phenomenon. As the symphony of research continued, Sadighi et al. [40] crafted an analytical melody resonating with the nuances of MHD heat and mass transfer nanofluid flow. This composition involved a porous cylinder graced with the presence of an inclined magnetic field, curvature, concentration power-law exponent, chemical reactions, and the interplay of viscous dissipation effects. The harmonious notes of the Forbenius method orchestrated the unraveling of this intricate composition. Meanwhile, Dawar et al. [41] unfurled an innovative canvas portraying a non-homogeneous convective nanofluid flow within

the embrace of MHD. This model resonated with the dynamism of rotating inclined thin layers, basking in the embrace of incident solar energy. The homotopy analysis method emerged as the guiding maestro in this creative endeavor. Further afield, Sivasankaran et al. [42] embarked on a journey that resonated with the echoes of chemical reactions. Their exploration wove through the intricate labyrinth of double diffusive unsteady incompressible MHD squeezing copper-water nanofluid flow between parallel plates. A systematic approach, known as the Differential Transformation Method (DTM), was enlisted in conjunction with the rhythmic cadence of the Runge-Kutta-Fehlberg method. In a parallel pursuit, Raghunath [43] charted an investigation into the symphony of unsteady MHD nanofluid flow. This endeavor unfolded past a vertical porous plate, with chemical reactions, radiation, and Soret effects orchestrating the intricate dynamics. The cadence of the perturbation technique served as the guiding rhythm, unraveling the intricate tapestry of the phenomenon. Since those seminal endeavors, the field of MHD mass and heat transfer has unfurled its wings, extending its reach to encompass various fluid types and an array of diverse physical properties [44–47].

In the context of existing research, notable gaps beckon for a deeper exploration of non-Newtonian Williamson nanofluid behavior. While previous studies have probed specific aspects of fluid dynamics, a comprehensive framework integrating diverse factors remains lacking. Against this backdrop, this research emerges with the aim to bridge these gaps by harmonizing various elements, forming a unified understanding of fluid dynamics. At its core is the investigation of a complex hybrid nanofluid, namely MoS_2+GO/H_2O, introducing a novel layer of complexity. To unravel this intricate interplay, sophisticated numerical techniques take center stage, employing the shooting method in conjunction with fourth-order Runge-Kutta numerical integration. This combination provides a potent toolkit to dissect the behaviors of the hybrid nanofluid. In doing so, this research not only illuminates new facets of fluid dynamics but also elevates the stature of numerical methodologies within the discipline. In essence, by addressing these research gaps and embarking on a multifaceted exploration, this study not only reshapes our understanding of fluid behavior but also charts a path towards innovative applications in engineering and science.

1.2 Thesis Structure

Chapter 2 serves as an introduction to the thesis and provides essential definitions and terminologies that are crucial for understanding the concepts discussed in subsequent chapters. This chapter aims to establish a foundational understanding of the key terms and concepts that will be used throughout the thesis.

In **Chapter 3**, we present a comprehensive numerical study of the flow of Williamson HNF MoS_2+ZnO/EO over a stretched sheet in the Cartesian coordinate system. The proposed numerical model incorporates heat and mass transfer phenomena across the stretched sheet. To obtain the numerical outcomes of the governing flow equations, the shooting technique is utilized. This chapter explores the flow characteristics and heat transfer performance of the Williamson hybrid nanofluid under various operating conditions.

Building upon the model discussed in Chapter 3, **Chapter 4** extends the investigation to a water-based hybrid nanofluid (MoS_2+GO). In this chapter, we introduce the impact of Forchheimer flow in the momentum equation along with other additional effects, such as Cattaneo-Christov heat flux, thermal radiation, magnetic field, thermophoresis diffusion, and Brownian diffusion, into the energy equation of the proposed model. Additionally, we include the concentration equation of the hybrid nanofluid in the proposed model, considering chemical reactions and diffusion effects. The use of similarity transformation is employed to convert the partial differential equations into a system of ordinary differential equations, which are subsequently solved using the numerical technique.

Chapter 5 presents the concluding remarks and highlights the significant findings obtained from the research conducted in this thesis. This chapter aims to provide a comprehensive summary of the main outcomes and contributions of the study.

The **Bibliography** section includes a comprehensive list of all the references and sources used in the thesis. It acknowledges the contributions of prior research and ensures the academic integrity of the work by properly crediting the original authors and sources.

Chapter 2

Preliminaries

In this chapter, we will elucidate fundamental definitions, essential laws, terminologies, and key concepts necessary for the analysis of nonlinear partial differential equations. These foundational elements are crucial for comprehending the subsequent chapters of this thesis and will provide a solid framework for the development of a comprehensive understanding.

2.1 Foundational Concepts

2.1.1 Fluid

"A substance in the liquid or gas phase is referred to as a fluid. Distinction between a solid and a fluid is made on the basis of the substances ability to resist an applied shear (or tangential) stress that to change its shape. A solid can resist an applied shear stress by deforming, whereas a fluid deforms continuously under the influence of shear stress no matter how small." [48]

2.1.2 Fluid Mechanics

"Fluid mechanics is that branch of science which deals with the behavior of the fluid (liquids or gases) at rest as well as in motion." [49]

2.1.3 Fluid Dynamics

"Fluid dynamics is the study of the motion of liquids, gases and plasma from one place to another." [49]

2.1.4 Viscosity

"Viscosity is defined as the property of a fluid which offers resistance to the movement of one layers of fluid over another adjacent layer of the fluid. When two layers of a fluid, a distance 'dy' apart, move one over the other at different velocities, say u and $u + du$ as shown in the viscosity together with relative velocity causes a shear stress acting between the fluid layers."

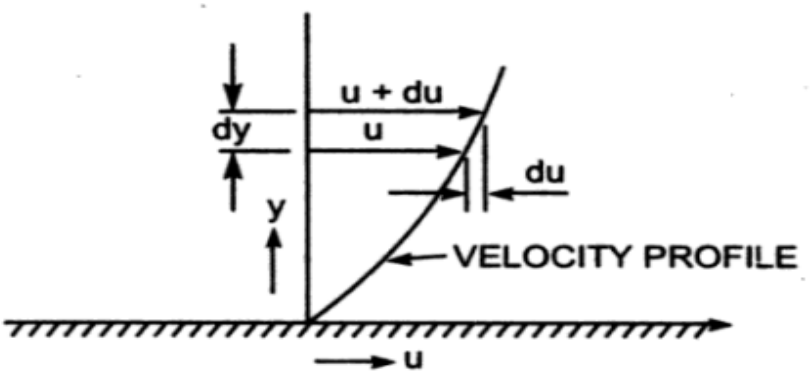

FIGURE 2.1: Velocity variation near a solid surface.

"The top layer causes a shear stress on the adjacent lower layer while the lower layer causes a shear stress on the adjacent top layer. This shear stress is proportional to the rate of change of velocity with respect to y. it is denoted by symbol τ called Tau. Mathematically,

$$\begin{aligned} \tau &\propto \frac{du}{dy} \\ \Rightarrow \quad \tau &= \mu \frac{du}{dy} \\ \Rightarrow \quad \mu &= \frac{\tau}{\frac{\partial u}{\partial y}} \end{aligned} \tag{2.1}$$

where μ is viscosity coefficient, τ is shear stress and $\frac{\partial u}{\partial y}$ represents the velocity gradient or rate of shear strain." [49]

2.1.5 Kinematic Viscosity

"Kinematic viscosity is defined as the ratio between the dynamic viscosity and density of fluid. It is denoted by the Greek symbol ν, thus mathematically,

$$\nu = \frac{\text{Viscosity}}{\text{Density}} = \frac{\mu}{\rho}$$

where the unit of kinematic viscosity is m^2/sec ." [49]

2.1.6 Magnetohydrodynamics

"Magnetohydrodynamics (MHD) is concerned with the flow of electrically conduct- ing fluids in the presence of magnetic fields, either externally applied or generated within the fluid by inductive action."

2.2 Classification of Fluid

2.2.1 Ideal Fluid

"A fluid which is incompressible and is having no viscosity, is known as an ideal fluid. Ideal fluid is only an imaginary fluid as all the fluids, which exist, have some viscosity." [49]

2.2.2 Real Fluid

"A fluid, which possesses viscosity, is known as a real fluid. All the fluids, in actual practice, are real fluids." [49]

2.2.3 Newtonian Fluid

"A real fluid, in which shear stress is directly, proportional to the rate of shear strain (or velocity gradient), is known as a Newtonian fluid." [49]

2.2.4 Non-Newtonian Fluid

"A real fluid, in which the shear stress is not proportional to the rate of shear strain (or velocity gradient), is known as a Non-Newtonian fluid." [49]

2.2.5 Ideal Plastic Fluid

"A fluid, in which shear stress is more than the yield value and shear stress is proportional to the rate of shear strain (or velocity gradient), is known as ideal plastic fluid." [49]

2.3 Modes of Heat Transfer

2.3.1 Conduction

"The mechanism of heat transfer due to a temperature gradient in a stationary medium is called conduction. The medium may solid or a fluid. A very popular example of conduction heat transfer is that when one end of metallic spoon is dipped into a cup of hot tea, the other end becomes gradually hot. In solids, the conduction of heat is attributed to two effects:

(*i*) the flow of free electrons and

(*ii*) the lattice vibrational waves caused by the vibrational motions of the molecules at relatively fixed positions called a lattice." [50]

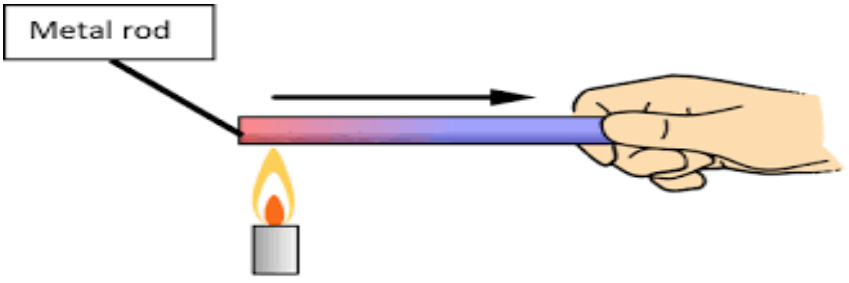

FIGURE 2.2: Example of conduction

As shown in above Figure **??** the simple example of conduction is when you hold one end of an iron rod while the other end is in direct contact with a flame. When a flame is placed at one end of the rod, the atoms at the heated end vibrate faster. The vibrating

atoms at the heated end then force nearby atoms to vibrate as well, creating a chain reaction. The process will continue until the atoms where your hand is placed also vibrate. This is the nature of heat transfer by conduction. This is the transfer of energy from atom to atom or from molecule to molecule.

2.3.2 Convection

"The mode by which heat is transferred between a solid surface and the adjacent fluid in motion when there is a temperature difference between the two is known as convection heat transfer. The temperature of the fluid stream refers either to its bulk or free stream temperature."[50]

Consider a tea kettle which is subjected to heat for boiling water. Here, The water molecules adjacent to the kettle surface get warmer first and then all move upward or relatively cooler portion to carry the heat. In this case, the boiling of water is an example of convection. The heating process of kettle surface is conduction after that the heat is radiated to the air through radiation.

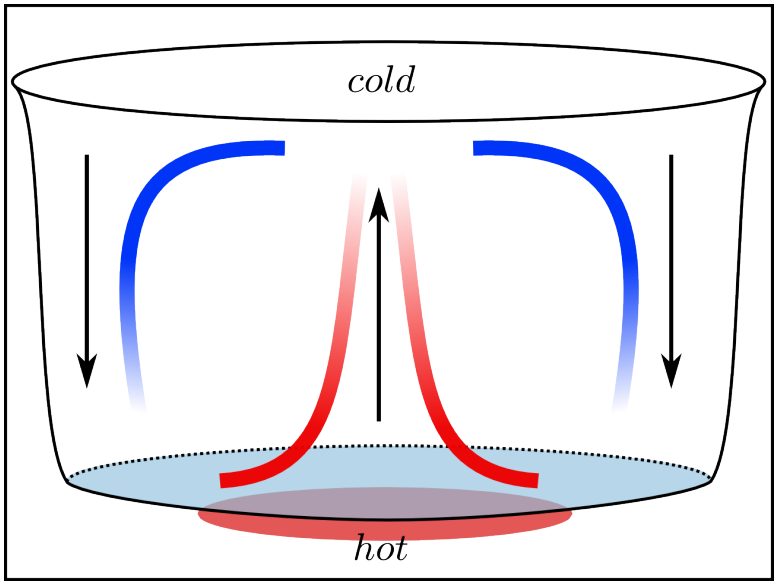

FIGURE 2.3: Example of convection

2.3.3 Forced Convection

"In forced convection, the fluid is forced to flow over a solid surface by external means such as fan, pump or atmospheric wind." [50]

2.3.4 Free Convection

"When the fluid motion is caused by the buoyancy forces that are induced by density differences due to the variation in temperature or species concentration (in case of multicomponent systems) in the fluid, the convection is called natural (or free) convection." [50]

2.3.5 Radiation

"Any substance at a finite temperature emits energy in the form of electromagnetic waves in all directions and at all wavelengths (from a very low one to a very high one). The energy emitted within a specific band of wavelength (0.1–100 μm) is termed thermal radiation. The exchange of such radiant energy between two bodies at different temperatures is defined as heat transfer between the bodies by radiation. We have seen earlier that the heat transfer by conduction or convection requires the presence of a medium. But the radiation heat transfer does not necessarily require a medium, rather it occurs most efficiently in a vacuum." [50]

One of the most important sources of energy is the Sun. Cosmic radiation emitted by the Sun is a mixture of electromagnetic waves; from infrared to ultraviolet. In addition, it also emits visible light. Most of the solar radiation emitted is absorbed by the atmosphere. However, the portion not absorbed by the atmosphere will reach the earth. Humans are exposed to this part of the radiation almost all times.

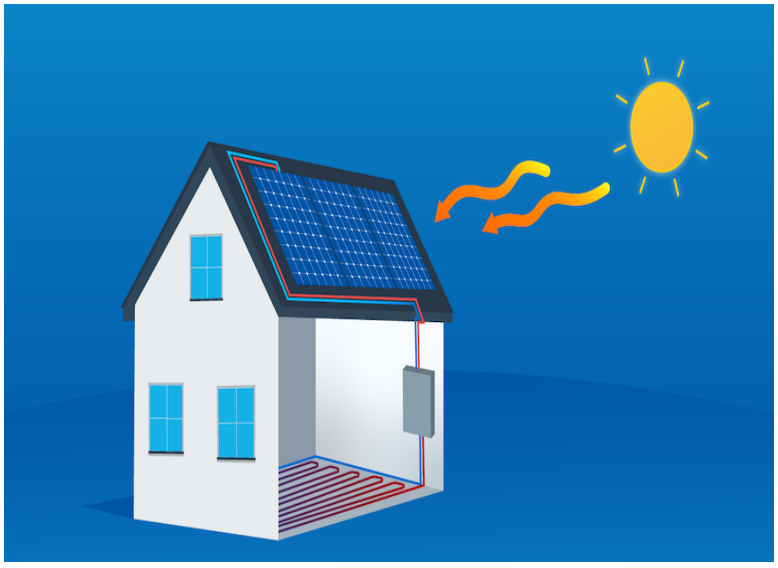

FIGURE 2.4: Example of radiation

2.4 Different Flow Classifications

2.4.1 Steady and Unsteady Flows

"Steady flow is defined as that type of flow in which the fluid characteristics like velocity, pressure, density, etc., at a point do not change with time. Thus for steady flow, mathematically, we have

$$\left(\frac{\partial V}{\partial t}\right)_{x_o,y_o,z_o} = 0, \quad \left(\frac{\partial p}{\partial t}\right)_{x_o,y_o,z_o} = 0, \quad \left(\frac{\partial \rho}{\partial t}\right)_{x_o,y_o,z_o} = 0$$

where (x_o, y_o, z_o) is fixed point in fluid field." [49]

" Unsteady flow is that type of flow, in which the velocity, pressure or density at a point changes with respect to time. thus, mathematically, for unsteady flow

$$\left(\frac{\partial V}{\partial t}\right)_{x_o,y_o,z_o} \neq 0, \quad \left(\frac{\partial p}{\partial t}\right)_{x_o,y_o,z_o} \neq 0 \text{ etc." [49]}$$

2.4.2 Uniform and Non-uniform Flow

"Uniform flow is defined as the type of flow in which the velocity at any given time does not change with respect to space (i.e., length of direction of the flow). Mathematically, for uniform flow

$$\left(\frac{\partial V}{\partial s}\right)_{r=\text{constant}} = 0$$

where ∂V= Change of velocity

∂s= Length of flow in the direction S.

Non-uniform flow is the type of flow in which the velocity at any given time changes with respect to space. Thus, mathematically, for non-uniform flow

$$\left(\frac{\partial V}{\partial s}\right)_{r=\text{constant}} \neq 0." \text{ [49]}$$

2.4.3 Laminar and Turbulent Flows

"Laminar flow is defined as that type of flow in which the fluid particles move along well-defined paths or stream line and all the stream-lines are straight and parallel. Thus the particles move in lamines or layers gliding smoothly over the adjacent layer. This

type of flow is also called stream-line flow or viscus flow." [49]
"Turbulent flow is that type of flow in which the fluid particles move in a zig-zag way. due to the movement of fluid particles in a zig-zag way, the eddies formulation takes place which are responsible for high energy loss." [49]

2.4.4 Compressible and Incompressible Flows

"Compressible flow is that type of flow in which the density for the fluid changes from point to point or in other words the density (ρ) is not constant for the fluid. Thus, mathematically, for compressible flow

$$\rho \neq \text{constant}$$

Incompressible flow is that type of flow in which the density is constant for the fluid flow. Liquids are generally incompressible while gases are compressible. Mathematically, for incompressible flow

$$\rho = \text{constant.}" \text{ [49]}$$

2.4.5 Rotational and Irrotational Flows

"Rotational flow is that type of flow in which the fluid particles while flowing along stream-lines, also rotate about their own axis. And if the fluid particles while flowing along stream-lines, do not rotate about their own axis then that type of flow is called irrotational flow." [49]

2.4.6 Inviscous Flow

"A flow in which viscosity of the fluid is equal to zero is known as inviscous (inviscid) flow."

2.5 Porous Material

"A solid containing holes or voids, either connected or non-connected, dispersed within

it in either a regular or random manner known as porous material provided that holes occur relatively frequently within the solid"[51].

"Pores are either interconnected or non-interconnected. A fluid can flow through a porous material only if at least some of the pores are interconnected"[51]. Some natural porous materials are beach sand, limestone, sandstone, wood, loaf of bread and human lung etc.

2.5.1 Porosity

"The porosity of a porous material is the fraction of the bulk volume of the material occupied by voids. The symbol usually employed for this parameter is ϕ. Thus

$$\phi = \frac{V_P}{V_B} = \frac{\text{Volume of pores}}{\text{Bulk volume}}$$

Bulk volume, which is a dimensionless quantity. Since that portion of the bulk volume not occupied by pores is occupied by the solid grains or matrix of the material, it follows that

$$1 - \phi = \frac{V_S}{V_B} = \frac{\text{Volume of solids}}{\text{Bulk volume}}."[51]$$

2.5.2 Permeability

"Permeability is the property of a porous material which characterizes the ease with which a fluid may be made to ow through the material by an applied pressure gradient. Permeability is the fluid conductivity of the porous material".

"If horizontal linear ow of an incompressible fluid is established through a sample of porous material of length L in the direction of flow, and cross sectional area A, then the permeability K of the material is defined as

$$K = \frac{q\mu}{A\left(\frac{\delta P}{L}\right)}$$

Here q is the fluid flow rate in volume per unit time, μ is the viscosity of the fluid and δP is the applied pressure difference across the length of the specimen"[51].

2.6 Conservation Laws

2.6.1 Law of Conservation of Mass

"The principle of conservation of mass can be stated as the time rate of change of mass in a fixed volume is equal to the net rate of ow of mass across the surface. The mathematical statement of the principle results in the following equation, known as the continuity (of mass) equation

$$\frac{\partial \rho}{\partial t} + \delta.\left(\rho V\right), \tag{2.2}$$

where ρ is the density (kg/m^3) of the medium, V the velocity vector (ms^{-1}), and δ is the nabla or del operator. The continuity equation in (2.2) is in conservation (or divergence) form since it can be derived directly from an integral statement of mass conservation. By introducing the material derivative or Eulerian derivative operator $\frac{D}{Dt}$

$$\frac{D}{Dt} = \frac{\partial}{\partial t} + V.\delta, \tag{2.3}$$

the continuity equation (2.2) can be expressed in the alternate, non-conservation (or advective) form

$$\frac{\partial \rho}{\partial t} + V.\delta\rho + \rho\delta.V = \frac{D\rho}{Dt} + \rho\delta.V \tag{2.4}$$

For steady-state conditions the continuity equation becomes

$$\delta.\left(\rho V\right) = 0. \tag{2.5}$$

When the density changes following a fluid particle are negligible, the continuum is termed incompressible and we have $\frac{D\rho}{Dt}$. The continuity equation (2.4) the becomes

$$\delta.V = 0, \tag{2.6}$$

which is often referred to as the incompressibility condition or incompressibility constraint" [52].

2.6.2 Equation of Momentum

"The principle of conservation of linear momentum (or Newton's Second Law of motion) states that the time rate of change of linear momentum of a given set of particles is equal to the vector sum of all the external forces acting on the particles of the set, provided

Newton's Third Law of action and reaction governs the internal forces. Newton's Second Law can be written as

$$\frac{\partial}{\partial t}(\rho V) + \delta.(\rho V \otimes V) = \delta.\sigma + \rho f, \tag{2.7}$$

where $\otimes$ is the tensor (or dyadic) product of two vectors, σ is the Cauchy stress tensor (N/m^2) and f is the body force vector, measured per unit mass and normally taken to be the gravity vector. Equation (2.7) describes the motion of a continuous medium, and in fluid mechanics they are also known as the Navier equations. The form of the momentum equation shown in (2.7) is the conservation (divergence) form that is most often utilized for compressible flows. This equation may be simplified to a form more commonly used with incompressible flows. Expanding the

first two derivatives and collecting terms

$$\rho\left(\frac{\partial V}{\partial t} + V\delta.V\right) + V\left(\frac{\partial \rho}{\partial t} + \delta.\rho V\right) = \delta.\sigma + \rho f \tag{2.8}$$

The second term in parentheses is the continuity equation (2.2) and neglecting this term allows (2.8) to reduce to the non-conservation (advective) form

$$\rho\left(\frac{DV}{Dt}\right) = \delta.\sigma + \rho f \tag{2.9}$$

where the material derivative (2.3) has been employed.

The principle of conservation of angular momentum can be stated as the time rate of change of the total moment of momentum of a given set of particles is equal to the vector sum of the moments of the external forces acting on the system. In the absence of distributed couples, the principle leads to the symmetry of the stress tensor:

$$\sigma = (\sigma)^T \tag{2.10}$$

where the superscript T denotes the transpose of the enclosed quantity" [52].

2.6.3 Law of Conservation of Energy

"The law of conservation of energy (or the First Law of Thermodynamics) states that the time rate of change of the total energy is equal to the sum of the rate of work done

by applied forces and the change of heat content per unit time. In the general case, the First Law of Thermodynamics can be expressed in conservation form as

$$\frac{\partial \rho e^t}{\partial t} + \delta.\rho v e^t = -\delta.q + \delta.(\sigma.v) + Q + \rho f.v, \tag{2.11}$$

where $e^t = e + 1/2v.v$ is the total energy (J/m^3), e is the internal energy, q is he heat flux vector (W/m^2) and Q is the internal heat generation (W/m^3)" [52].

2.6.4 Newton's Law of Viscosity

"It states that the shear stress (τ) on a fluid element layer is proportional to the rate of shear strain. The constant of proportionally is called coefficient of viscosity. Mathematically, it is expressed as

$$\tau = \mu \frac{\partial u}{\partial y}."$$

2.7 Dimensionless Parameters

2.7.1 Reynolds Number (Re)

"It is the most significant dimensionless number which is used to identify the different flow behaviors like laminar or turbulent flow. Mathematically, it is expressed as

$$Re = \frac{LU}{\nu}$$

where U denotes the free stream velocity, L is the characteristic length and ν stands for kinematic viscosity." [53]

2.7.2 Nusselt Number (Nu)

"It is the relationship between the convective to the conductive heat transfer through the boundary of the surface. Mathematically, it is defined as

$$Nu = \frac{hL}{k}$$

where h stands for convective heat transfer, L stands for characteristic length and k stands for thermal conductivity." [53]

2.7.3 Prandtl Number (Pr)

"The ratio of kinematic diffusivity to heat the diffusivity is said to be Prandtl number. It is denoted by Pr. Mathematically, it can be written as

$$\begin{aligned} Pr &= \frac{\nu}{\alpha} \\ \Rightarrow \quad &= \frac{\mu c_p}{\rho k} \end{aligned}$$

where μ and α denote the momentum diffusivity or kinetic diffusivity and thermal diffusivity respectively." [53]

2.7.4 Skin Friction Coefficient (Cf_x)

"The skin friction coefficient is typically defined as

$$Cf = \frac{2\tau_w}{\rho U_w^2}$$

where τ_w is the local wall shear stress, ρ is the fluid density and U_w is the free stream velocity (usually taken outside the boundary layer or at the inlet)." [53]

2.7.5 Sherwood Number (Sh_x)

"It is a non-dimensional quantity which describes the ratio of the mass transport by convection to the transfer of mass by diffusion. Mathematically,

$$Sh = \frac{kL}{D},$$

here L is characteristics length, D is the mass diffusivity and k is the mass transfer coefficient." [53]

2.7.6 Thermophoresis Parameter

"In a temperature gradient, small particles are pushed towards the lower temper- ature because of the asymmetry of molecular impacts." [53]

2.7.7 Eckert Number

"It is a dimensionless number used in continuum mechanics. It describes the relation between flows and the boundary layer enthalpy difference and it is used for characterized heat dissipation. Mathematically,

$$Ec = \frac{u^2}{c_p \delta T}." [53]$$

2.8 Shooting Method

To elaborate the shooting method, take into account the subsequent nonlinear boundary value problem.

$$\left.\begin{aligned} h''(\zeta) - h(\zeta) + h^2(\zeta) = 0 \\ h'(0) = 0, \quad h(b) = 0. \end{aligned}\right\} \tag{2.12}$$

To reduce the order of the above BVP, introduce the following notations:

$$h(\zeta) = l_1, \quad h'(\zeta) = l_1' = l_2. \tag{2.13}$$

The system of first order ODEs that results form the conversion of (2.12) is as follows:

$$l_1' = l_2, \qquad l_1(0) = 0. \tag{2.14}$$

$$l_2' = l_1^2 - l_1, \qquad l_2(0) = k. \tag{2.15}$$

Where k is the initial condition which will be guessed. The $RK-4$ method will be used to numerically solve the above IVP. Choose missing condition k in such a way that

$$l_1(b,k) = 0. \tag{2.16}$$

The above equation can be solved by using Newton's method with the following iterative scheme:

$$k^{(m+1)} = k^{(m)} - \frac{l_1(b,k)^{(m)}}{\left(\frac{\partial\, l_1(b,k)}{\partial k}\right)^{(m)}} \tag{2.17}$$

To find $\left(\frac{\partial\, l_1(b,k)}{\partial k}\right)^{(m)}$, introduced the following notations:

$$\frac{\partial l_1}{\partial k} = l_3, \quad \frac{\partial l_2}{\partial k} = l_4. \tag{2.18}$$

As a result of these new notations the Newton's iterative scheme, will then get the form

$$k^{(m+1)} = k^{(m)} - \frac{l_1(b,k)^{(m)}}{l_3(b,k)^{(m)}}. \tag{2.19}$$

Now differentiating the system of two first order ODEs (2.14) and (2.15) with respect to k, we get another system f ODEs, as follows:

$$l_3' = l_4, \qquad l_3(0) = 0. \tag{2.20}$$

$$l_4' = 2l_1l_3 - l_3, \qquad l_4(0) = 1. \tag{2.21}$$

Writing all the four ODEs (2.14), (2.15), (2.20) and (2.21) together, following IVP is obtained.

$$\begin{aligned} l_1' &= l_2, & l_1(0) &= 0. \\ l_2' &= l_1^2 - l_1, & l_2(0) &= k. \\ l_3' &= l_4, & l_3(0) &= 0. \\ l_4' &= 2l_1l_3 - l_3, & l_4(0) &= 1. \end{aligned}$$

The above system together will be solved numericaly br $RK-4$ method. The stopping criteria for the Newton's technique is set as

$$|l_1(b,k)| < \epsilon,$$

where $\epsilon > 0$ is an arbitrary small positive number.

Chapter 3

Thermal Characteristics of a Williamson Hybrid Nanofluid Based with Engine Oil Over a Stretched Sheet

3.1 Introduction

In this chapter, we delve into the numerical analysis of the flow of a Williamson hybrid nanofluid ($MoS_2 + ZnO$) over a stretching sheet. This sheet is placed within a porous medium and subjected to both a magnetic field and thermal radiation. To tackle this, we transform the governing nonlinear partial differential equations into a set of dimensionless ordinary differential equations using suitable transformations. These equations are then addressed using the shooting technique in MATLAB. Our focus lies in discussing the numerical solutions for various parameters, notably the velocity profile $f'(\zeta)$ and the temperature profile $\theta(\zeta)$. This chapter provides a thorough exploration of the work previously undertaken by Yahya et al [17].

3.2 Physical Model

We investigate the flow characteristics of a hybrid nanofluid over a stretching sheet, focusing on a two-dimensional and steady boundary layer flow. The coordinate axis along the stretched sheet is denoted by $\tilde{x}$ and that perpendicular to the sheet is $\tilde{y}$. Notably, the wall is considered incompressible ($\widetilde{v}_w = 0$), as depicted in figure 3.1 The steady flow of the hybrid nanofluid is governed by the following equations (3.1)-(3.3) along with the boundary conditions (3.4).

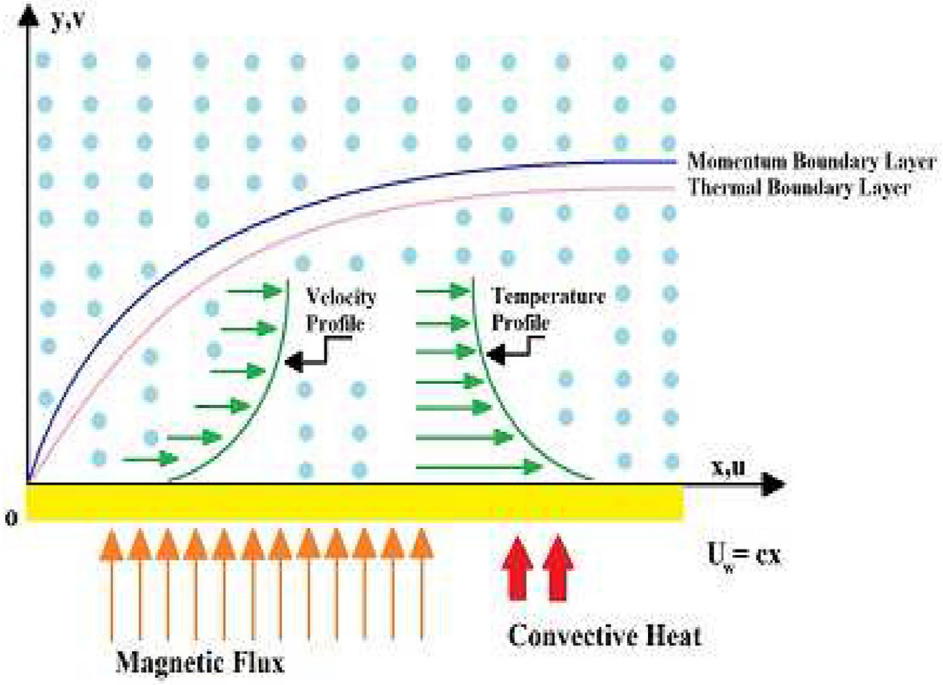

FIGURE 3.1: Flow Pattern Illustration.

Mass conservation equation:

$$\frac{\partial \widetilde{u}}{\partial \widetilde{x}} + \frac{\partial \widetilde{v}}{\partial \widetilde{y}} = 0. \tag{3.1}$$

Momentum equation:

$$\widetilde{u}\frac{\partial \widetilde{u}}{\partial \widetilde{x}} + \widetilde{v}\frac{\partial \widetilde{u}}{\partial \widetilde{y}} + \frac{\widetilde{\sigma}_{hnf}}{\widetilde{\rho}_{hnf}}\widetilde{B}_o^2\widetilde{u} + \frac{\widetilde{\mu}_{hnf}}{\widetilde{\rho}_{hnf}}\frac{\widetilde{u}}{k^*} = \frac{\widetilde{\mu}_{hnf}}{\widetilde{\rho}_{hnf}}\frac{\partial^2 \widetilde{u}}{\partial \widetilde{y}^2} + \sqrt{2}\Gamma\widetilde{\nu}_f\frac{\partial \widetilde{u}}{\partial \widetilde{y}}\frac{\partial^2 \widetilde{u}}{\partial \widetilde{y}^2}. \tag{3.2}$$

Energy equation of hybrid nanofluid:

$$\widetilde{u}\frac{\partial \widetilde{¥}}{\partial \widetilde{x}} + \widetilde{v}\frac{\partial \widetilde{¥}}{\partial \widetilde{y}} = \frac{\widetilde{k}_{hnf}}{(\widetilde{\rho c}_p)_{hnf}}\frac{\partial^2 \widetilde{¥}}{\partial \widetilde{y}^2} + \frac{\widetilde{\mu}_{hnf}}{(\widetilde{\rho c}_p)_{hnf}}\left(\frac{\partial \widetilde{u}}{\partial \widetilde{y}}\right)^2 + \frac{Q_o}{(\widetilde{\rho c}_p)_{hnf}}(\widetilde{¥} - \widetilde{¥}_\infty). \tag{3.3}$$

Boundary condition:

$$\left.\begin{aligned} \widetilde{u} = \widetilde{U}_w = \tilde{a}\tilde{x}, \quad \widetilde{v} = \widetilde{v}_w, \quad -\widetilde{k}_{hnf}\frac{\partial \widetilde{¥}}{\partial \widetilde{y}} = \widetilde{h}_f\big(\widetilde{¥} - \widetilde{¥}_f\big), \quad as \quad \widetilde{y} = 0, \\ \widetilde{u} \longrightarrow 0, \quad \widetilde{¥} \longrightarrow \widetilde{¥}_\infty, \quad as \ \widetilde{y} \longrightarrow \infty. \end{aligned}\right\} \tag{3.4}$$

3.3 Similarity Transformation and Non- Dimensionalization of Mathematical Model

In this section, we present the process of non-dimensionalization for the mathematical model governing the behavior of our hybrid nanofluid. The procedure requires introducing the dimensionless variables and parameters to transform the original equations into a simpler form. By using dimensionless quantities, we gain a deeper insights into the physical phenomena and make the analysis more tractable. The mathematical model will be transformed into a system ODEs using the following similarity transformation:

$$\zeta = \sqrt{\frac{\tilde{a}}{\widetilde{\nu}_f}}\,\widetilde{y}, \quad \widetilde{u} = \tilde{a}\tilde{x}f'(\zeta), \quad \tilde{v} = -\sqrt{\tilde{a}\widetilde{\nu}_f}f(\zeta), \quad \theta(\zeta) = \frac{\widetilde{¥} - \widetilde{¥}_\infty}{\widetilde{¥}_f - \widetilde{¥}_\infty}. \tag{3.5}$$

The mathematical model equations (3.1) - (3.3) and boundary condition (3.4) were transformed into a dimensionless form through a similarity transformation. The following derivative are required to satisfied the mass conservation equation (3.1).

$$\begin{aligned} & \widetilde{u} = \tilde{a}\tilde{x}f'(\zeta) \\ \Rightarrow \quad & \frac{\partial \widetilde{u}}{\partial \widetilde{x}} = \tilde{a}f'(\zeta). \end{aligned} \tag{3.6}$$

$$\begin{aligned} & \widetilde{v} = -\sqrt{\tilde{a}\widetilde{\nu}_f}f(\zeta) \\ \Rightarrow \quad & \frac{\partial \widetilde{v}}{\partial \widetilde{y}} = -\sqrt{\tilde{a}\widetilde{\nu}_f}f'(\zeta).\frac{\partial \zeta}{\partial \widetilde{y}} \\ & = -\sqrt{\tilde{a}\widetilde{\nu}_f}f'(\zeta).\frac{\partial}{\partial \widetilde{y}}\left(\sqrt{\frac{\tilde{a}}{\widetilde{\nu}_f}}\widetilde{y}\right) \qquad (\text{using} \quad (3.5)) \\ & = -\sqrt{\tilde{a}\widetilde{\nu}_f}f'(\zeta)\left(\sqrt{\frac{\tilde{a}}{\widetilde{\nu}_f}}\right) \\ & = \tilde{a}f'(\zeta). \end{aligned} \tag{3.7}$$

Finally, using equations (3.6) and (3.7) in (3.1), we obtain

$$\tilde{a}f'(\zeta) - \tilde{a}f'(\zeta) = 0.$$

Hance equation (3.1) is identically satisfied.

The basic thermo-physical characteristics of nanofluids are obtained from the above literature review. The thermo-physical properties are presented in Table 3.1.

TABLE 3.1: Thermo-physical properties of water base fluid and nanoparticles. [54]

Nanofluid	**Hybrid Nanofluid**
$\tilde{\mu}_{nf} = \frac{\tilde{\mu}_f}{(1-\Phi)^{2.5}}$	$\tilde{\mu}_{nf} = \frac{\tilde{\mu}_f}{(1-\Phi_1)^{2.5}(1-\Phi_2)^{2.5}}$
$\tilde{\rho}_{nf} = \tilde{\rho}_f(1-\Phi) + \Phi(\frac{\tilde{\rho}_s}{\tilde{\rho}_f})$	$\tilde{\rho}_{hnf} = \tilde{\rho}_f(1-\Phi_2)\big((1-\Phi_1) + \Phi_1(\frac{\tilde{\rho}_{s_1}}{\tilde{\rho}_f})\big) + \Phi_2\tilde{\rho}_{s_2}$
$(\tilde{\rho}\tilde{c}_p)_{nf} = (\tilde{\rho}\tilde{c}_p)_f(1-\Phi) + \Phi\frac{(\tilde{\rho}\tilde{c}_p)_s}{(\tilde{\rho}\tilde{c}_p)_f}$	$\frac{(\tilde{\rho}\tilde{c}_p)_{hnf}}{(\tilde{\rho}\tilde{c}_p)_f} = (1-\Phi_2)\big((1-\Phi_1) + \Phi_1\frac{(\tilde{\rho}\tilde{c}_p)_{s_1}}{(\tilde{\rho}\tilde{c}_p)_f}\big) + \Phi_2\frac{(\tilde{\rho}\tilde{c}_p)_{s_2}}{(\tilde{\rho}\tilde{c}_p)_f}$
$\frac{\tilde{K}_{nf}}{\tilde{K}_f} = \frac{\tilde{K}_s+(s_f-1)\tilde{K}_f-(s_f-1)\Phi(\tilde{K}_f-K_s)}{\tilde{K}_s+(s_f-1)\tilde{K}_f+\Phi(\tilde{K}_f-\tilde{K}_s)}$	$\frac{\tilde{K}_{hnf}}{\tilde{K}_{bf}} = \frac{\tilde{K}_{s_2}+(s_f-1)\tilde{K}_{bf}-(s_f-1)\Phi_2(\tilde{K}_{bf}-\tilde{K}_{s_2})}{\tilde{K}_{s_2}+(s_f-1)\tilde{K}_{nf}+\Phi_2(\tilde{K}_{bf}-\tilde{K}_{s_2})}$
	$\frac{\tilde{K}_{nf}}{\tilde{K}_f} = \frac{\tilde{K}_{s_1}+(s_f-1)\tilde{K}_f-(s_f-1)\Phi_1(\tilde{K}_f-\tilde{K}_{s_1})}{\tilde{K}_{s_1}+(s_f-1)\tilde{K}_f+\Phi_1(\tilde{K}_f-\tilde{K}_{s_1})}$
$\widetilde{\sigma}_{nf} = \widetilde{\sigma}_f\left[1 + \frac{3(\sigma-1)\Phi}{(\sigma+2)-(\sigma-1)\Phi}\right]$	$\widetilde{\sigma}_{hnf} = \widetilde{\sigma}_{bf}\left[\frac{\widetilde{\sigma}_{s_2}(1+2\Phi_2)+2\widetilde{\sigma}_{bf}(1-\Phi_2)}{\widetilde{\sigma}_{s_2}(1-\Phi_2)+\widetilde{\sigma}_{bf}(2+\Phi_2)}\right]$
	with $\widetilde{\sigma}_{bf} = \widetilde{\sigma}_f\left[\frac{\widetilde{\sigma}_{s_1}(1+2\Phi_1)+2\widetilde{\sigma}_f(1-\Phi_1)}{\widetilde{\sigma}_{s_1}(1-\Phi_1)+\widetilde{\sigma}_f(2+\Phi_1)}\right]$

Some expression involving the above thermo-physical properties, denoted by $\widetilde{A}_i$ $(i = 1, 2, 3, 4)$, have been defined below. These notations will simplify the dimensionless model to be achieved in the upcoming sections. [17]

$$\widetilde{A}_1 = (1-\phi_1)^{2.5}(1-\phi_2)^{2.5}\left[(1-\phi_2)\left\{(1-\phi_1) + \phi_1\frac{\widetilde{\rho}_{s1}}{\widetilde{\rho}_f}\right\} + \phi_2\frac{\widetilde{\rho}_{s2}}{\widetilde{\rho}_f}\right],$$

$$\widetilde{A}_2 = (1-\phi_2)\left\{(1-\phi_1) + \phi_1\frac{\widetilde{\rho}_{s1}}{\widetilde{\rho}_f} + \phi_2\frac{\widetilde{\rho}_{s2}}{\widetilde{\rho}_f}\right\},$$

$$\widetilde{A}_3 = (1-\phi_2)\left\{(1-\phi_1) + \frac{\left(\widetilde{\rho}\widetilde{C}_p\right)_{s1}}{\left(\widetilde{\rho}\widetilde{C}_p\right)_f}\phi_1\right\} + \frac{\left(\widetilde{\rho}\widetilde{C}_p\right)_{s2}}{\left(\widetilde{\rho}\widetilde{C}_p\right)_f}\phi_2,$$

$$\widetilde{A}_4 = (1-\phi_1)^{2.5}(1-\phi_2)^{2.5}.$$

$$\widetilde{A}_5 = \left[\frac{\widetilde{\sigma}_{s_2}(1+2\Phi_2) + 2\widetilde{\sigma}_{bf}(1-\Phi_2)}{\widetilde{\sigma}_{s_2}(1-\Phi_2) + \widetilde{\sigma}_{bf}(2+\Phi_2)}\right]\left[\frac{\widetilde{\sigma}_{s_1}(1+2\Phi_1) + 2\widetilde{\sigma}_f(1-\Phi_1)}{\widetilde{\sigma}_{s_1}(1-\Phi_1) + \widetilde{\sigma}_f(2+\Phi_1)}\right]$$

3.3.1 Non-Dimensionalization of Momentum Equation

For the momentum equation (3.2), the following derivatives are needed:

$$\frac{\partial \widetilde{u}}{\partial \widetilde{y}} = \frac{\partial}{\partial \widetilde{y}}\left(\tilde{a}\tilde{x}f'(\zeta)\right)$$

$$= \tilde{a}\tilde{x}f''(\zeta)\sqrt{\frac{\tilde{a}}{\widetilde{\nu}_f}}. \tag{3.8}$$

$$\Rightarrow \quad \frac{\partial^2 \widetilde{u}}{\partial \widetilde{y}^2} = \tilde{a}\tilde{x}\sqrt{\frac{\tilde{a}}{\widetilde{\nu}_f}}\, f'''(\zeta).\frac{\partial \zeta}{\partial \widetilde{y}}$$

$$= \frac{\tilde{a}^2\tilde{x}}{\widetilde{\nu}_f} f'''(\zeta). \tag{3.9}$$

Now, we substitute the values of all the partial derivatives (3.6) , (3.8) and (3.9) and velocity components (3.5) into the equation (3.2) to get the following:

$$\left[\left(\tilde{a}\tilde{x}f'(\zeta)\right)\left(\tilde{a}f'(\zeta)\right)\right] + \left[\left(-\sqrt{\tilde{a}\widetilde{\nu}_f}f(\zeta)\right)\left(\tilde{a}\tilde{x}f''(\zeta)\sqrt{\frac{\tilde{a}}{\widetilde{\nu}_f}}\right)\right]$$
$$+ \left[\frac{\widetilde{\sigma}_f \widetilde{A}_5}{\widetilde{\rho}_f \widetilde{A}_2}\widetilde{B}_o^2\left(\tilde{a}\tilde{x}f'(\zeta)\right)\right] + \left[\frac{\widetilde{\mu}_f}{\widetilde{\rho}_f \widetilde{A}_2 \widetilde{A}_4}\frac{\tilde{a}\tilde{x}f'(\zeta)}{k^*}\right] = \left[\frac{\widetilde{\mu}_f}{\widetilde{\rho}_f \widetilde{A}_2 \widetilde{A}_4}\frac{\tilde{a}^2\tilde{x}}{\widetilde{\nu}_f}f'''(\zeta)\right]$$
$$+ \left[\sqrt{2}\Gamma\widetilde{\nu}_f\left(\tilde{a}\tilde{x}f''(\zeta)\sqrt{\frac{\tilde{a}}{\widetilde{\nu}_f}}\right)\left(\frac{\tilde{a}^2\widetilde{x}}{\widetilde{\nu}_f}f'''(\zeta)\right)\right].$$

$$\Rightarrow \quad \tilde{a}^2\tilde{x}\left(f'(\zeta)\right)^2 - \tilde{a}^2\tilde{x}f(\zeta)f''(\zeta) + \frac{\widetilde{\sigma}_f\widetilde{B}_o^2\widetilde{A}_5}{\widetilde{\rho}_f\widetilde{A}_2}\tilde{a}\tilde{x}f'(\zeta) + \frac{\widetilde{\nu}_f\tilde{a}\tilde{x}}{k^*\widetilde{A}_2\widetilde{A}_4}$$
$$= \frac{\tilde{a}^2\tilde{x}}{\widetilde{A}_2\widetilde{A}_4}f'''(\zeta) + \sqrt{2}\Gamma\frac{\tilde{a}^2\tilde{x}^2\tilde{a}^{\frac{3}{2}}}{\widetilde{\nu}_f^{\frac{1}{2}}}f''(\zeta)f'''(\zeta).$$

$$\Rightarrow \quad \left(f'(\zeta)\right)^2 - f(\zeta)f''(\zeta) + \frac{\widetilde{\sigma}_f\widetilde{B}_o^2}{\widetilde{\rho}_f\tilde{a}}\frac{\widetilde{A}_5}{\widetilde{A}_2}f'(\zeta) + \frac{\widetilde{\nu}_f}{\tilde{a}k^*}\frac{1}{\widetilde{A}_2\widetilde{A}_4}f'(\zeta)$$
$$= \frac{1}{\widetilde{A}_2\widetilde{A}_4}f'''(\zeta) + \sqrt{2}\tilde{x}\Gamma\frac{\tilde{a}^{\frac{3}{2}}}{\widetilde{\nu}_f^{\frac{1}{2}}}f''(\zeta)f'''(\zeta).$$

$$\Rightarrow \quad \left(f'(\zeta)\right)^2 - f(\zeta)f''(\zeta) + M\frac{\widetilde{A}_5}{\widetilde{A}_2}f'(\zeta) + \frac{K_p}{\widetilde{A}_2\widetilde{A}_4}f'(\zeta) = \frac{1}{\widetilde{A}_2\widetilde{A}_4}f'''(\zeta) + w_e f''(\zeta)f'''(\zeta).$$

$$\Rightarrow \quad \widetilde{A}_2\widetilde{A}_4\left(\left(f'(\zeta)^2\right) - f(\zeta)f''(\zeta)\right) + M\widetilde{A}_5\widetilde{A}_4 f'(\zeta) + K_p f'(\zeta)$$
$$= f'''(\zeta) + \widetilde{A}_2\widetilde{A}_4 w_e f''(\zeta)f'''(\zeta).$$

$$\Rightarrow \quad \left(1 + w_e\widetilde{A}_1 f''(\zeta)\right)f'''(\zeta) - \widetilde{A}_1\left(\left(f'(\zeta)\right)^2 - f(\zeta)f''(\zeta)\right)$$

$$-\left(M\widetilde{A}_4\widetilde{A}_5 + K_p\right) f'(\zeta) = 0. \tag{3.10}$$

3.3.2 Non-Dimensionalization of Energy Equation

In this section, we discuss the non-dimensionalization process of the energy equation (3.3) for our hybrid nanofluid model.

$$\theta(\zeta) = \frac{\widetilde{\text{¥}} - \widetilde{\text{¥}}_\infty}{\widetilde{\text{¥}}_f - \widetilde{\text{¥}}_\infty}$$

$$\Rightarrow \quad \widetilde{\text{¥}} = \left(\widetilde{\text{¥}}_f - \widetilde{\text{¥}}_\infty\right)\theta(\zeta) + \widetilde{\text{¥}}_\infty. \tag{3.11}$$

$$\Rightarrow \quad \frac{\partial \widetilde{\text{¥}}}{\partial \tilde{x}} = 0. \tag{3.12}$$

$$\Rightarrow \quad \frac{\partial^2 \widetilde{\text{¥}}}{\partial \tilde{x}^2} = 0. \tag{3.13}$$

Now, differentiating equation (3.11) w.r.t $\tilde{y}$, we obtain

$$\frac{\partial \widetilde{\text{¥}}}{\partial \tilde{y}} = \left(\widetilde{\text{¥}}_f - \widetilde{\text{¥}}_\infty\right)\theta'(\zeta).\frac{\partial \zeta}{\partial \tilde{y}}$$

$$\Rightarrow \quad \frac{\partial \widetilde{\text{¥}}}{\partial \tilde{y}} = \left(\widetilde{\text{¥}}_f - \widetilde{\text{¥}}_\infty\right)\sqrt{\frac{\tilde{a}}{\widetilde{\nu}_f}}\theta'(\zeta). \tag{3.14}$$

$$\Rightarrow \quad \frac{\partial^2 \widetilde{\text{¥}}}{\partial \tilde{y}^2} = \frac{\tilde{a}}{\widetilde{\nu}_f}\left(\widetilde{\text{¥}}_f - \widetilde{\text{¥}}_\infty\right)\theta''(\zeta). \tag{3.15}$$

Now, we substitute the partial derivatives (3.8) , (3.11), (3.12) and (3.15) and velocity components $\tilde{u}$ and $\tilde{v}$ from (3.5) into the equation (3.3).

$$\left[\left(-\sqrt{\tilde{a}\widetilde{\nu}_f}f(\zeta)\right)\left(\widetilde{\text{¥}}_f - \widetilde{\text{¥}}_\infty\right)\sqrt{\frac{\tilde{a}}{\widetilde{\nu}_f}}\theta'(\zeta)\right] = \frac{\widetilde{k}_{hnf}}{\left(\widetilde{\rho c}_p\right)_f \widetilde{A}_3}\left(\frac{\tilde{a}}{\widetilde{\nu}_f}\left(\widetilde{\text{¥}}_f - \widetilde{\text{¥}}_\infty\right)\theta''(\zeta)\right)$$
$$+ \frac{\widetilde{\mu}_f}{\left(\widetilde{\rho c}_p\right)_f}\frac{1}{\widetilde{A}_3\widetilde{A}_4}\left(\tilde{a}^2\tilde{x}^2\left(f''(\zeta)\right)^2\frac{\tilde{a}}{\widetilde{\nu}_f}\right) + \frac{\widetilde{Q}_o}{\left(\widetilde{\rho c}_p\right)_f \widetilde{A}_3}\left[\left(\widetilde{\text{¥}}_f - \widetilde{\text{¥}}_\infty\right)\theta(\eta)\right].$$

$$\Rightarrow \quad -\tilde{a}\left(\widetilde{\text{¥}}_f - \widetilde{\text{¥}}_\infty\right)f(\zeta)\theta'(\zeta) = \frac{\widetilde{k}_{hnf}}{\left(\widetilde{\rho c}_p\right)_f \widetilde{A}_3}\frac{\tilde{a}}{\widetilde{\nu}_f}\theta''(\zeta)\frac{\tilde{a}}{\left(\widetilde{\rho c}_p\right)_f \widetilde{A}_3\widetilde{A}_4}\left(\tilde{a}^2\tilde{x}^2\left(f''(\zeta)\right)^2\frac{\tilde{a}}{\widetilde{\nu}_f}\right)$$
$$+ \frac{\widetilde{Q}_o}{\left(\widetilde{\rho c}_p\right)_f \widetilde{A}_3}\left(\widetilde{\text{¥}}_f - \widetilde{\text{¥}}_\infty\right)\theta(\zeta).$$

$$\Rightarrow \quad f(\zeta)\theta'(\zeta) = \frac{\widetilde{k}_{hnf}}{\widetilde{A}_3\widetilde{k}_f}\frac{\widetilde{k}_f}{\left(\widetilde{\rho c_p}\right)_f\widetilde{\nu}_f}\theta''(\zeta) + \frac{\tilde{a}^2\tilde{x}^2}{\left(\widetilde{c}_p\right)f\left(\widetilde{\Yen}_f - \widetilde{\Yen}_\infty\right)}\frac{1}{\widetilde{A}_3\widetilde{A}_4}\left(f''(\zeta)\right)^2 + \frac{\widetilde{Q}_o}{\widetilde{A}_3\tilde{a}\left(\widetilde{\rho c_p}\right)_f}\theta(\zeta).$$

$$\Rightarrow \quad -f(\zeta)\theta'(\zeta) = \frac{\widetilde{k}_{hnf}}{\widetilde{A}_3\widetilde{k}_f Pr}\theta''(\zeta) + \frac{Ec}{\widetilde{A}_3\widetilde{A}_4}\left(f''(\zeta)\right)^2 + \frac{Q}{\widetilde{A}_3}\theta(\zeta).$$

$$\Rightarrow \quad \theta''(\zeta) + \frac{\widetilde{k}_f}{\widetilde{k}_{hnf}}Pr\left[\widetilde{A}_3\left(f(\zeta)\theta'(\zeta) + \frac{Ec}{\widetilde{A}_4}\left(f''(\zeta)\right)^2 + Q\theta(\zeta)\right)\right] = 0. \tag{3.16}$$

3.3.3 Non-Dimensionalization of Boundary Condition

The corresponding BCs are transformed into non-dimensional form through the following procedure.

- $\widetilde{u} = \widetilde{U}_w(\tilde{x}), \qquad at \quad \tilde{y} = 0.$

  $\Rightarrow \quad \tilde{a}xf'(\zeta) = \tilde{a}\tilde{x}, \qquad at \quad \zeta = 0.$

  $\Rightarrow \quad f'(\zeta) = 1, \qquad at \quad \zeta = 0.$

- $\widetilde{v} = \widetilde{v}_w, \qquad at \quad y = 0.$

  $\Rightarrow \quad -\sqrt{\tilde{a}\widetilde{\nu}_f}f(\zeta) = -\sqrt{\tilde{a}\widetilde{\nu}_f}S, \qquad at \quad \zeta = 0.$

  $\Rightarrow \quad f(\zeta) = S, \qquad at \quad \zeta = 0.$

- $-\widetilde{k}_{hnf}\frac{\partial\widetilde{\Yen}}{\partial\widetilde{y}} = \widetilde{h}_f\left(\widetilde{\Yen} - \widetilde{\Yen}_f\right), \qquad at \quad \widetilde{y} = 0.$

  $\Rightarrow \quad -\widetilde{k}_{hnf}\left[\left(\widetilde{\Yen}_f - \widetilde{\Yen}_\infty\right)\sqrt{\frac{\tilde{a}}{\widetilde{\nu}_f}}\theta'(\zeta)\right] = \widetilde{h}_f\left[\widetilde{\Yen}_\infty + \left(\widetilde{\Yen}_f - \widetilde{\Yen}_\infty\right)\theta(\zeta) - \widetilde{\Yen}_f\right], \quad at \quad \zeta = 0.$

  $\Rightarrow \quad \widetilde{k}_{hnf}\left[\left(\widetilde{\Yen}_f - \widetilde{\Yen}_\infty\right)\sqrt{\frac{\tilde{a}}{\widetilde{\nu}_f}}\theta'(\zeta)\right] = \widetilde{h}_f\left[\left(\widetilde{\Yen}_f - \widetilde{\Yen}_\infty\right) - \left(\widetilde{\Yen}_f - \widetilde{\Yen}_\infty\right)\theta(\zeta)\right], \quad at \quad \zeta = 0.$

  $\Rightarrow \quad \frac{\widetilde{k}_{hnf}}{\widetilde{k}_f}\theta'(\zeta) = \frac{\widetilde{h}_f}{\widetilde{k}_f}\sqrt{\frac{\widetilde{\nu}_f}{\tilde{a}}}\left(1 - \theta(\zeta)\right), \qquad at \quad \zeta = 0.$

  $\Rightarrow \quad \frac{\widetilde{k}_{hnf}}{\widetilde{k}_f}\theta'(\zeta) = B_i\left(1 - \theta(\zeta)\right), \qquad at \quad \zeta = 0.$

- $\widetilde{u} \longrightarrow 0, \qquad as \quad \tilde{y} \longrightarrow \infty.$

  $\Rightarrow \quad \tilde{a}\tilde{x}f'(\zeta) \longrightarrow 0, \qquad as \quad \zeta \longrightarrow \infty.$

$$\Rightarrow \quad f'(\zeta) \longrightarrow 0, \qquad as \quad \zeta \longrightarrow \infty.$$

- $$\widetilde{¥} \longrightarrow \widetilde{¥}_{\infty}, \qquad as \quad \widetilde{y} \longrightarrow \infty.$$

$$\Rightarrow \quad \widetilde{¥}_{\infty} + \big(\widetilde{¥}_f - \widetilde{¥}_{\infty}\big)\theta(\zeta) \longrightarrow \widetilde{¥}_{\infty}, \qquad as \quad \zeta \longrightarrow \infty.$$

$$\Rightarrow \quad \big(\widetilde{¥}_f - \widetilde{¥}_{\infty}\big)\theta(\zeta) \longrightarrow 0, \qquad as \quad \zeta \longrightarrow \infty.$$

$$\Rightarrow \quad \theta(\zeta) \longrightarrow 0, \qquad as \quad \zeta \longrightarrow \infty.$$

3.3.4 Non-Dimensionalization of Physical Quantities

The dimensionless physical quantities section of this thesis focuses on two important parameters: the skin fraction and the Nusselt number. This section provides an introduction to these dimensionless quantities and their mathematical calculation.

Skin fraction:

$$\begin{aligned}
C_f &= \frac{\widetilde{\tau}_w}{\widetilde{\rho}_f \widetilde{U}_w^2}, \qquad \left(\widetilde{\tau}_w = \widetilde{\mu}_{hnf}\left[\frac{\partial \widetilde{u}}{\partial \widetilde{y}} + \frac{\Gamma}{\sqrt{2}}\left(\frac{\partial \widetilde{u}}{\partial \widetilde{y}}\right)^2\right], \quad \widetilde{\mu}_{hnf} = \frac{\widetilde{\mu}_f}{\widetilde{A}_4}\right) \\
&= \frac{\frac{\tilde{\mu}_f}{\widetilde{A}_4}\left[\tilde{a}\tilde{x} f''(\zeta)\sqrt{\frac{\tilde{a}}{\widetilde{\nu}_f}} + \frac{\Gamma}{\sqrt{2}}\frac{\tilde{a}^3\tilde{x}^2}{\widetilde{\nu}_f}\big(f''(\zeta)\big)^2\right]}{\widetilde{\rho}_f \tilde{a}_2 \tilde{x}^2}, \\
&= \frac{\widetilde{\nu}_f \tilde{a}\tilde{x}\left[f''(\zeta)\sqrt{\frac{\tilde{a}}{\widetilde{\nu}_f}} + \frac{\Gamma}{\sqrt{2}}\frac{\tilde{a}^2\tilde{x}}{\widetilde{\nu}_f}\big(f''(\zeta)\big)^2\right]}{\widetilde{A}_4 \tilde{a}^2 \tilde{x}^2} \\
&= \frac{\widetilde{\nu}_f\left[f''(\zeta)\sqrt{\frac{\tilde{a}}{\widetilde{\nu}_f}} + \frac{\Gamma\sqrt{2}}{\sqrt{2}\sqrt{2}}\frac{\tilde{x}\tilde{a}^2\sqrt{\tilde{a}}}{\tilde{a}\widetilde{\nu}_f}\right]}{\widetilde{A}_4 \tilde{a}\tilde{x}} \\
&= \frac{\widetilde{\nu}_f\sqrt{\frac{\tilde{a}}{\widetilde{\nu}_f}}\left[f''(\zeta) + \frac{\Gamma\sqrt{2}\tilde{x}\tilde{a}^{\frac{3}{2}}}{2\widetilde{\nu}_f^{\frac{1}{2}}\big(f''(\zeta)\big)^2}\right]}{\widetilde{A}_4 \tilde{a}\tilde{x}} \\
&= \frac{\sqrt{\widetilde{\nu}_f \tilde{a}}\left[f''(\zeta) + \frac{w_e}{2}\big(f''(\zeta)\big)^2\right]}{\widetilde{A}_4 \tilde{a}\tilde{x}}.
\end{aligned}$$

$$\Rightarrow \quad \big(R_e\big)^{\frac{1}{2}} C_f = \frac{\left[f''(0) + \frac{w_e}{2}\big(f''(0)\big)^2\right]}{\widetilde{A}_4}, \tag{3.17}$$

where the Reynolds number (Re) is defined as $\big(Re\big)^{\frac{1}{2}} = \sqrt{\frac{\tilde{a}}{\widetilde{\nu}_f}}\tilde{x}$.

Nusslt number:

$$Nu = \frac{\tilde{x}\widetilde{q}_w}{\widetilde{k}_f\left(\widetilde{¥}_f - \widetilde{¥}_{\infty}\right)}$$

$$= \frac{\tilde{x}\tilde{K}_{hnf}\frac{\partial\widetilde{\Upsilon}}{\partial\widetilde{y}}}{\widetilde{k}_f\left(\widetilde{\Upsilon}_f - \widetilde{\Upsilon}_\infty\right)}, \qquad \left(\tilde{q}_w = \tilde{K}_{hnf}\frac{\partial\widetilde{\Upsilon}}{\partial\widetilde{y}}\right)$$

$$= \frac{\tilde{K}_{hnf}\tilde{x}\sqrt{\frac{\tilde{a}}{\widetilde{\nu}_f}}\left(\widetilde{\Upsilon}_f - \widetilde{\Upsilon}_\infty\right)\theta'(\zeta)}{\widetilde{K}_f\left(\widetilde{\Upsilon}_f - \widetilde{\Upsilon}_\infty\right)}$$

$$= \sqrt{\frac{\tilde{a}}{\widetilde{\nu}_f}}\tilde{x}\left(\frac{\widetilde{K}_{hnf}}{\widetilde{K}_f}\theta'(\zeta)\right).$$

$$\Rightarrow \quad Re^{-1/2}Nu_{\tilde{x}} = \frac{\widetilde{K}_{hnf}}{\widetilde{K}_f}\theta'(\zeta). \tag{3.18}$$

3.4 Solution Framework

In order to solve the ODE (3.10), the shooting method has been used. The following notation has been considered.

$$f(\zeta) = \widetilde{Y}_1, \qquad f'(\zeta) = \widetilde{Y}_1' = \widetilde{Y}_2, \qquad f''(\zeta) = \widetilde{Y}_2' = \widetilde{Y}_3.$$

The following system of first order ODEs is created for the momentum equation:

$$\begin{aligned}
&\widetilde{Y}_1' = \widetilde{Y}_2, && \widetilde{Y}_1(0) = S,\\
&\widetilde{Y}_2' = \widetilde{Y}_3, && \widetilde{Y}_2(0) = 1,\\
&\widetilde{Y}_3' = \frac{\left[\widetilde{A}_1\left((\widetilde{Y}_2)^2 - \widetilde{Y}_1\widetilde{Y}_3\right) + \left(M\widetilde{A}_4\widetilde{A}_5 + K_p\right)\widetilde{Y}_2\right]}{\left(1 + we\widetilde{A}_1\widetilde{Y}_3\right)}, && \widetilde{Y}_3(0) = l.
\end{aligned}$$

To utilize the Runge-Kutta 4th order (RK4) method for the numerical solution of the above IVP, the missing condition l within the system of equations need to be carefully chosen. The missing condition l is to be chosen such that

$$\widetilde{Y}_2\big(\zeta_\infty, l\big) = 0.$$

Newton's method will be used to find l. This method has the following iterative scheme:

$$l^{(n+1)} = l^{(n)} - \frac{\widetilde{Y}_2\big(\zeta_\infty, l^{(n)}\big)}{\left(\frac{\partial}{\partial s}\widetilde{Y}_2\big(\zeta_\infty, l\big)\right)^{(n)}}.$$

We further introduce the following notations:

$$\frac{\partial \widetilde{Y}_1}{\partial l} = \widetilde{Y}_4, \qquad \frac{\partial \widetilde{Y}_2}{\partial l} = \widetilde{Y}_5, \qquad \frac{\partial \widetilde{Y}_3}{\partial l} = \widetilde{Y}_6.$$

As a result these new notations, the Newton's iterative scheme gets the form:

$$l^{(n+1)} = l^{(n)} - \frac{\widetilde{Y}_2\big(\zeta_\infty, l^{(n)}\big)}{\widetilde{Y}_5\big(\zeta_\infty, l^{(n)}\big)}.$$

Now differentiating the most recently presented system of three first order ODEs with respect to l, we get another system of ODEs, as follows:

$$\begin{aligned}
&\widetilde{Y}_4' = \widetilde{Y}_5, && \widetilde{Y}_1(0) = 0,\\
&\widetilde{Y}_5' = \widetilde{Y}_6, && \widetilde{Y}_2(0) = 0,\\
&\widetilde{Y}_6' = \frac{\Big[\widetilde{A}_1\big(2\widetilde{Y}_2\widetilde{Y}_5 - \widetilde{Y}_4\widetilde{Y}_3 - \widetilde{Y}_1\widetilde{Y}_6\big) + \big(M\widetilde{A}_4\widetilde{A}_5 + K_p\big)\widetilde{Y}_5\Big]}{\big(1 + We\widetilde{A}_1\widetilde{Y}_3\big)}\\
&\qquad - \left[\frac{We\widetilde{A}_1\widetilde{Y}_6}{\big(1 + We\widetilde{A}_1\widetilde{Y}_3\big)}\right]\widetilde{Y}_3', && \widetilde{Y}_6(0) = 1.
\end{aligned}$$

The stopping criteria for the Newton's techniques is set as.

$$\Big|\widetilde{Y}_2\big(\zeta_\infty, l\big)\Big| < \epsilon,$$

where $\epsilon > 0$ is an arbitrarily small positive number. From now onward, ϵ has been taken as 10^{-6}.

Now, to solve the energy equation numerically by using shooting method, f and f'' will be taken as a known functions. The notations below are used for the implementation of the shooting method.

$$\theta = \widetilde{Z}_1, \qquad \theta' = \widetilde{Z}_1' = \widetilde{Z}_2'.$$

The energy equation can be formulated as the following system of first-order coupled ODEs:

$$\begin{aligned}
&\widetilde{Z}_1' = \widetilde{Z}_2, && \widetilde{Z}_1(0) = m,\\
&\widetilde{Z}_2' = \frac{\widetilde{k}_f}{\widetilde{k}_{hnf}} Pr\left[\widetilde{A}_3 f \widetilde{Z}_2 + \frac{Ec}{\widetilde{A}_4}(f'')^2 + Q\widetilde{Z}_1\right], && \widetilde{Z}_2(0) = \frac{\widetilde{k}_f}{\widetilde{k}_{hnf}} B_i\,(1 - m)\,.
\end{aligned}$$

To utilize the Runge-Kutta 4th order (RK4) method for numerical solution of the above-mentioned initial value problem, the condition m within the system of equations needs to be carefully chosen. The missing condition m is to be chosen such that:

$$\widetilde{Z}_1\big(\zeta_\infty, m\big) = 0.$$

Newton's method will be used to find m with the following iterative scheme:

$$m^{(n+1)} = m^{(n)} - \frac{\widetilde{Z}_1\big(\zeta_\infty, m^{(n)}\big)}{\Big(\frac{\partial}{\partial \widetilde{m}}\widetilde{Z}_1\big(\zeta_\infty, m\big)\Big)^{(n)}}.$$

We further introduce the following notations.

$$\frac{\partial \widetilde{Z}_1}{\partial m} = \widetilde{Z}_3, \qquad \frac{\partial \widetilde{Z}_2}{\partial m} = \widetilde{Z}_4.$$

As a result of these new notations, the Newton's iterative scheme gets the form:

$$m^{(n+1)} = m^{(n)} - \frac{\widetilde{Z}_1\big(\zeta_\infty, m^{(n)}\big)}{\widetilde{Z}_3\big(\zeta_\infty, m^{(n)}\big)}.$$

Now differentiating the system of two first order ODEs with respect to m, we get another system of ODEs, as follows:

$$\begin{aligned} &\widetilde{Z}_3' = \widetilde{Z}_4, && \widetilde{Z}_3(0) = 1, \\ &\widetilde{Z}_4' = \frac{\widetilde{k}_f}{\widetilde{k}_{hnf}} Pr\Big[\widetilde{A}_3 f \widetilde{Z}_4 + Q\widetilde{Z}_3\Big], && \widetilde{Z}_4(0) = -\frac{\widetilde{k}_f}{\widetilde{k}_{hnf}} B_i. \end{aligned}$$

The stopping criteria for the Newton's technique is set as:

$$\Big|\widetilde{Z}_1\big(\zeta_\infty, m\big)\Big| < \epsilon,$$

where $\epsilon > 0$ is an arbitrarily small positive number. From now onward, ϵ has been taken as 10^{-6}.

3.5 Result Interpretation

This section aims to evaluate the physical characteristics of velocity and energy profiles concerning the variations in several significant physical constants, such as magnetic field strength (M), porosity parameter (Kp), Weissenberg number (We), Prandtl number (Pr), Eckert number (Ec), heat source (Q), Biot number (Bi), and suction parameter

(S). The evaluation is conducted by utilizing graphical representations of velocity profiles and temperature profiles. Furthermore, by modifying the values of dimensionless parameters, the effects of these parameters on physical quantities such as skin friction and Nusselt number are examined and presented in tabular form.

The graphical representations of velocity and temperature profiles provide visual insights into the behavior of the system as the physical constants vary. By observing the trends in these profiles, a better understanding of the system's physical characteristics and energy distribution can be obtained. The graphical representations allow for the analysis of how changes in M, Kp, We, Pr, Ec, Q, Bi, and S affect the velocity and energy profiles.

3.5.1 Analysis of Computational Results

Table 3.2 presents the results of the skin friction coefficient and local Nusselt number for the $ZnO + MoS_2$ / Engine oil hybrid nanofluid, considering different inputs of M, Kp, We, and S. The findings reveal that an increase in the values of M and Kp leads to higher absolute values of local skin friction coefficients, indicating a decrease in the fluid velocity. This decrease is a consequence of the opposing forces arising from electro-magnetic interaction and the porosity of the medium. Conversely, the magnitude of skin friction coefficient decreases as the Williamson fluid parameter (We) and mass transpiration parameter (S) increase.

TABLE 3.2: The result of the skin friction coefficients $C_f\sqrt{Re_x}$ and the local Nusselt number $\frac{Nu_x}{\sqrt{Re_x}}$ for values of M, K_p, W_e and S parameters when $Pr = 20$, $Ec = 0.1$, $Q = 0.01$ and $Bi = 0.5$.

M	K_p	We	S	$C_f\sqrt{Re_x}$	$\frac{Nu_x}{\sqrt{Re_x}}$
0.2	0.5	0.2	0.5	-1.738269	-0.449249
0.5				-1.846976	-0.442512
0.8				-1.947539	-0.436031
1.2				-2.071454	-0.427692
	0.1			-1.579986	-0.458581
	0.3			-1.661680	-0.453834
	0.5			-1.738269	-0.449249
	0.7			-1.810506	-0.444802
		0.1		-1.773112	-0.454571
		0.2		-1.738269	-0.449249
		0.3		-1.709905	-0.440248
			0.2	-1.535328	-0.437185
			0.5	-1.738269	-0.449249
			0.7	-1.886997	-0.453356
			1.0	-2.130804	-0.456621

Moreover, Table 3.3 provides details on the absolute value of the Nusselt number as it relates to the Prandtl number (Pr). The results indicate that Nusselt number increases with higher values of Pr, reflecting enhanced heat transfer. Furthermore, it is observed that Nusselt number decreases reciprocally with the Eckert number (Ec) and the heat source parameter (Q).

TABLE 3.3: The result of the local Nusselt number $\frac{Nu_x}{\sqrt{Re_x}}$ for values of Pr, Q, Ec and Bi parameters when $M = 0.2$,$K_p = 0.5$, $We = 0.2$ and $S = 0.5$.

Pr	Q	Ec	B_i	$\frac{Nu_x}{\sqrt{Re_x}}$
20	0.01	0.1	0.5	0.437577
30				0.441587
40				0.437577
50				0.435096
	0.02			0.448963
	0.05			0.448091
	0.07			0.447496
	1.00			0.399591
		0.2		0.376089
		0.3		0.302929
		0.4		0.229769
		0.5		0.156609
			0.3	0.264802
			0.5	0.449249
			0.7	0.640429
			0.9	0.838718

3.5.2 Velocity Profile

Figures 3.2 to 3.6 provide insights into the nature of the velocity profile, denoted as $f'(\zeta)$, with respect to various physical parameters. Specifically, Figure 3.2 and 3.3 illustrate the effects of the magnetic force (M) and porosity parameter (K_p) on the dimensionless velocity $f'(\zeta)$. It is evident that both the nanofluids, namely MoS_2/Engine oil and

$MoS_2 + ZnO$/Engine oil, experience a significant decrease in flow velocity as the values of these two parameters (M and K_p) increase.

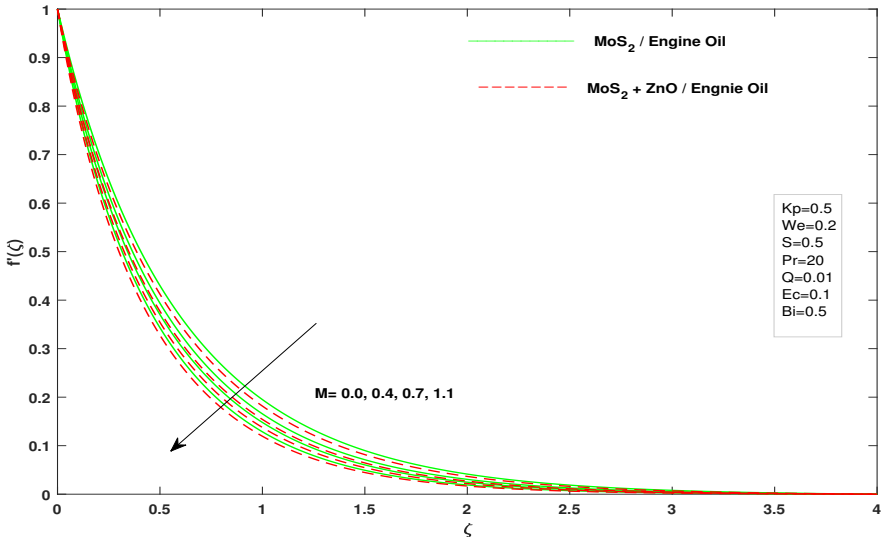

FIGURE 3.2: Influence of M on velocity profile $f'(\zeta)$

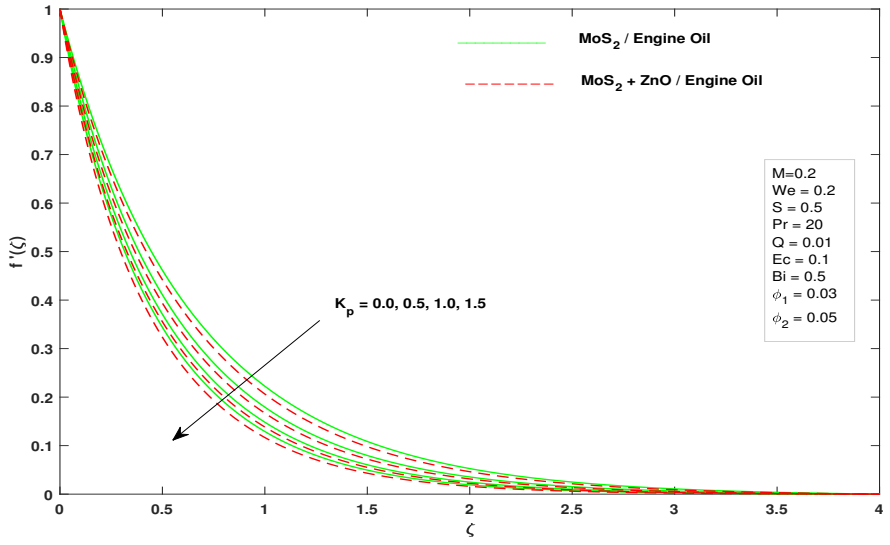

FIGURE 3.3: The velocity profile $f'(\zeta)$ for different value of kp

Physically, a higher value of the parameter M indicates a larger Lorentz force, which acts in opposition to the flow. Similarly, an increase in the value of K_p corresponds to a decrease in porosity and an increase in flow resistance within the medium.

Figures 3.4 and 3.5 illustrate significant findings regarding the impact of the Weissenberg number (We) and suction parameter (S) on the velocity profile f'(ζ). The

analysis reveals that variations in both We and S result in a reduction in fluid velocity. The Weissenberg number, which represents the ratio of relaxation time to the specific process time, plays a crucial role in shaping the velocity profile. Higher We values correspond to shorter specific process times, leading to decreased flow velocity and boundary layer thickness. Elevated We values introduce additional resistance, hampering the flow velocity.

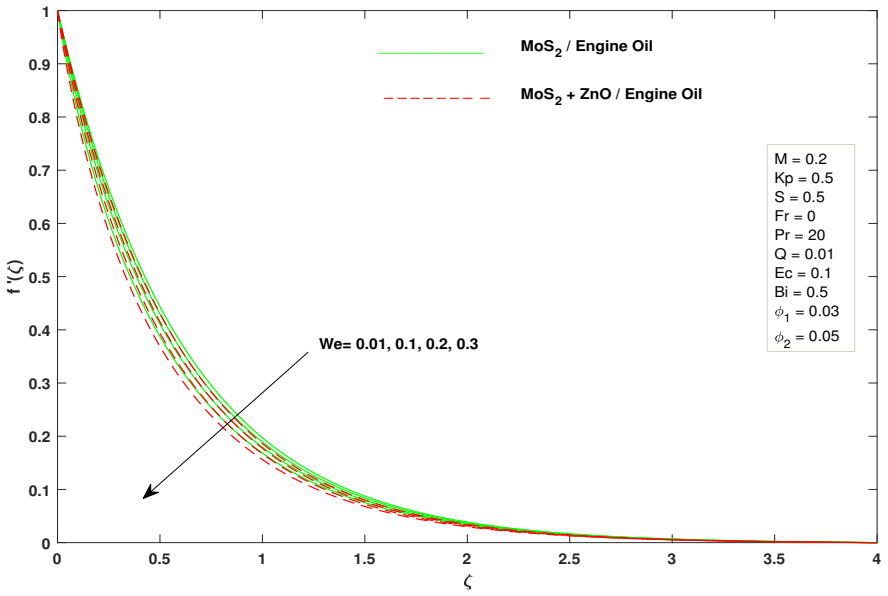

FIGURE 3.4: Influence of We on velocity profile $f'(\zeta)$

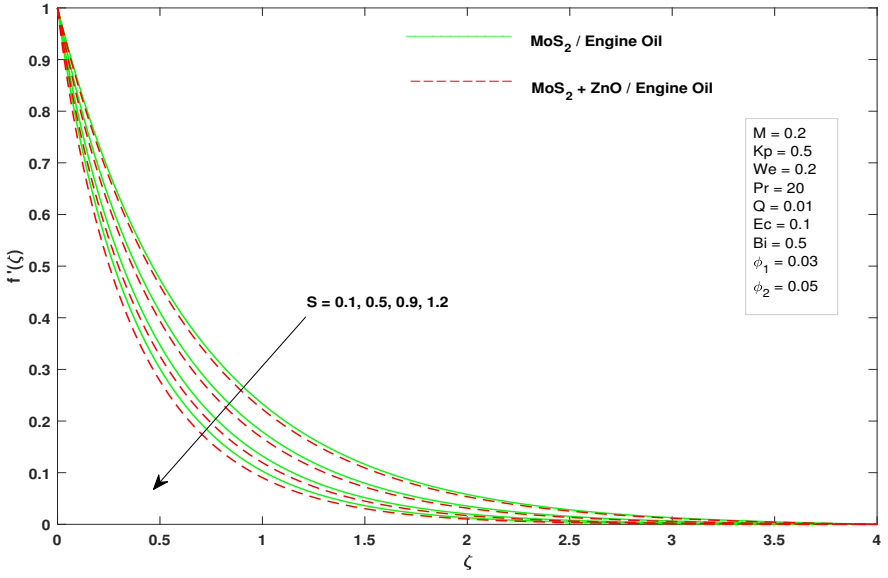

FIGURE 3.5: Influence of S on velocity profile $f'(\zeta)$

The suction parameter (S) also holds a key role in influencing fluid flow characteristics. Increasing suction ($S > 0$) leads to a more pronounced reduction in flow speed. This effect is attributed to mass transfer phenomena occurring at the suction area of the wall. Suction generates flow motion counteracting the primary flow, resulting in an overall decrease in velocity throughout the system. Figure 3.6 presents an important finding that highlights the relationship between the volume fraction ϕ_1 and fluid velocity. The results indicate a significant enhancement in fluid velocity as the volume fraction ϕ_1 of nanoparticles increases. When nanoparticles are added to the base fluid, their presence reduces the overall average heat absorbing capacity. As a result, the velocity profile of the fluid rises due to this alteration in heat absorption characteristics.

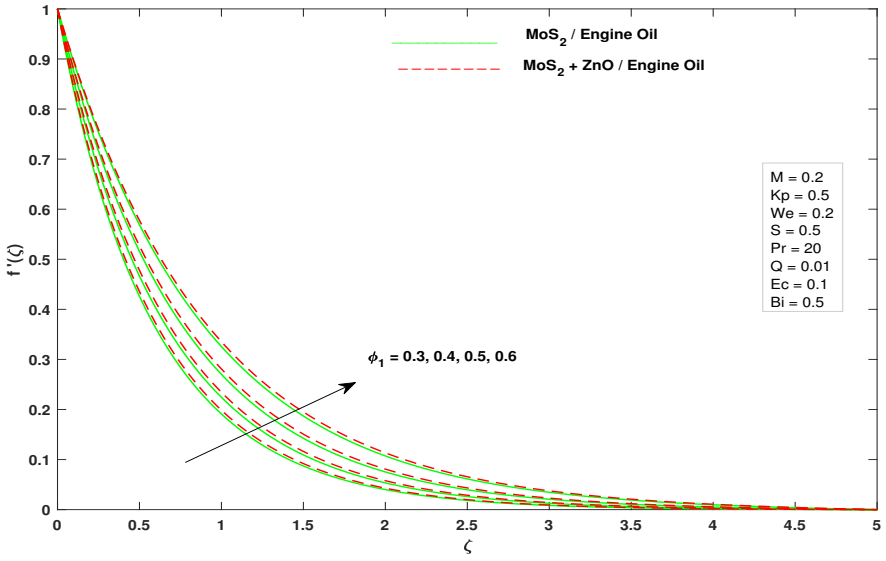

FIGURE 3.6: Effects of ϕ_1 on velocity profile $f'(\zeta)$

3.5.3 Temperature Profile

Figures 3.7 to 3.11 present the characteristics of the energy profile $\theta(\zeta)$ with respect to various parameters, including the Prandtl number (Pr), heat source (Q), Eckert number (Ec), Biot number (Bi), and volume fraction (ϕ_1). Figure 3.7 and 3.8 illustrate the temperature fluctuations of the fluid (both nano-and hybrid nanofluids) with varying values of Pr and Q. It is observed that the fluid temperature decreases with increasing Pr, which can be attributed to a decrease in the thermal diffusivity as Pr increases. Additionally, it is noted that the presence of a higher heat source ($Q > 0$) leads to an

increase in the fluid temperature.

Figures 3.9 and 3.10 depict the relationship between the temperature of the fluid and the Eckert number (Ec) and Biot number (Bi). A higher Ec value represents the conversion of mechanical energy to heat energy through thermal dissipation. It is evident that an increase in Ec results in an increment in fluid temperature. Similarly, the Biot number shows a direct proportionality to temperature, with higher Bi values corresponding to greater convective heating along the sheet, leading to an increased temperature gradient. As a result, the thickness of the boundary layer and the temperature exhibit an increasing trend with the Bi. Furthermore, it is observed that the temperature of hybrid nanofluid is higher as compared to that of nanofluid. This can be attributed to the enhanced thermal conductivities exhibited by hybrid nanofluid. These observations further support the hypothesis that hybrid nanofluid possess superior thermal efficiency in terms of heat transport. The findings from Figure 3.11 indicate a positive correlation between the temperature and the volume fraction ϕ_1 of MoS_2 in the hybrid nanofluid. This relationship can be attributed to the enhanced thermal conductivity resulting from the higher volume fraction. Consequently, the increased thermal conductivity contributes to a rise on temperature within the nanofluid.

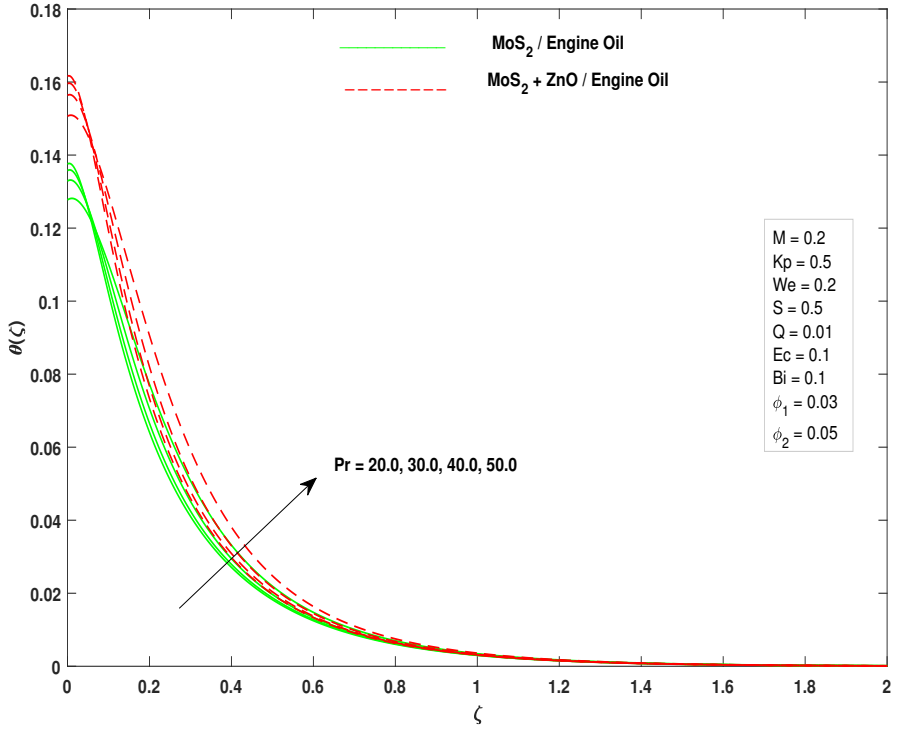

FIGURE 3.7: Influence of Pr on temperature profile $\theta(\zeta)$

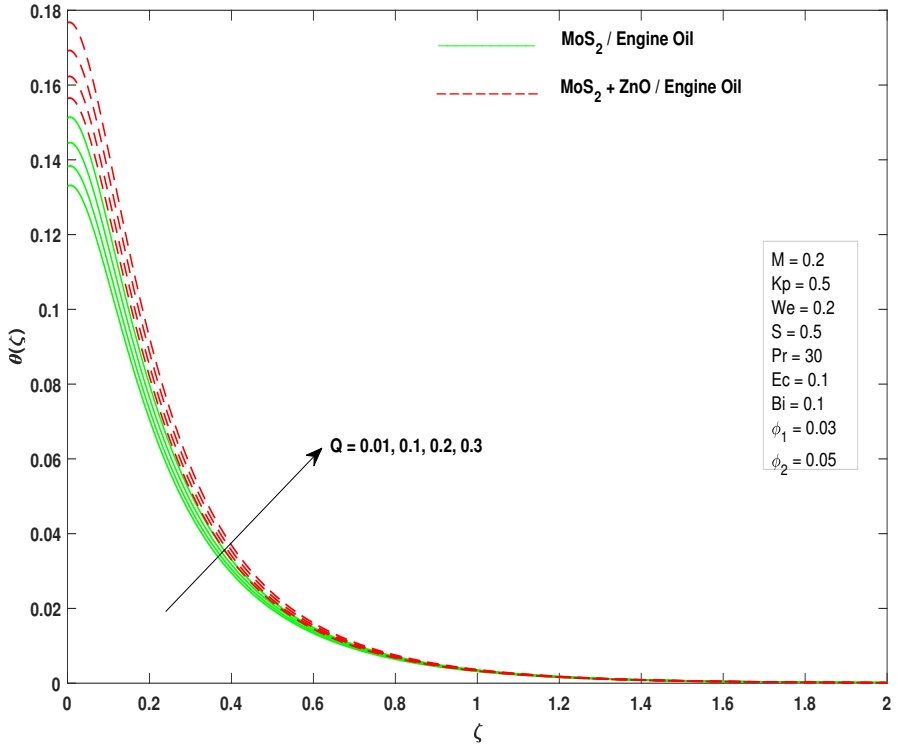

FIGURE 3.8: Influence of Q on temperature profile $\theta(\zeta)$

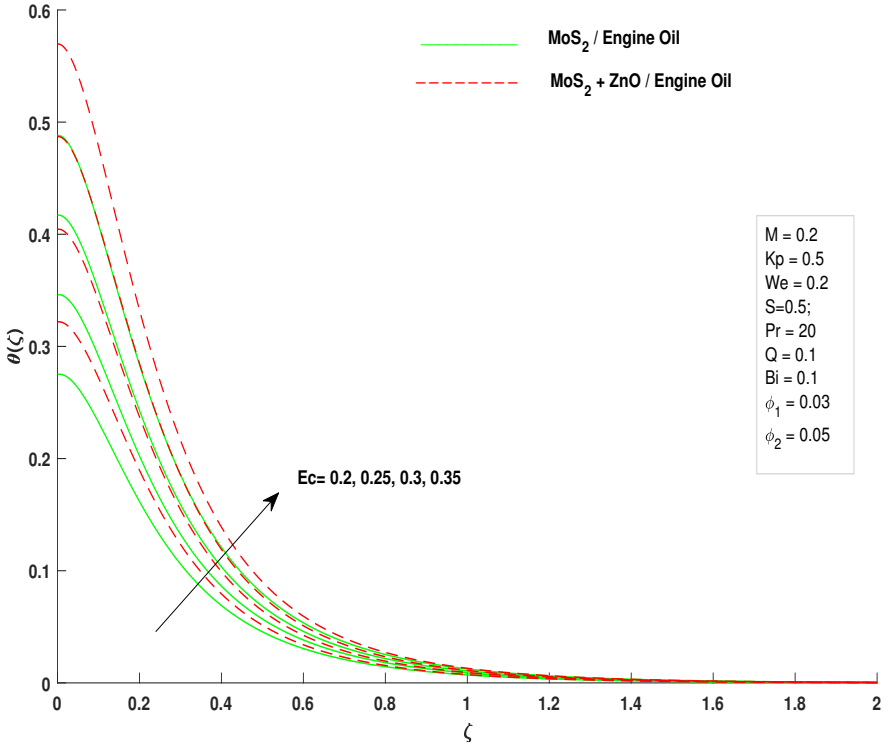

FIGURE 3.9: Influence of Ec on temperature profile $\theta(\zeta)$

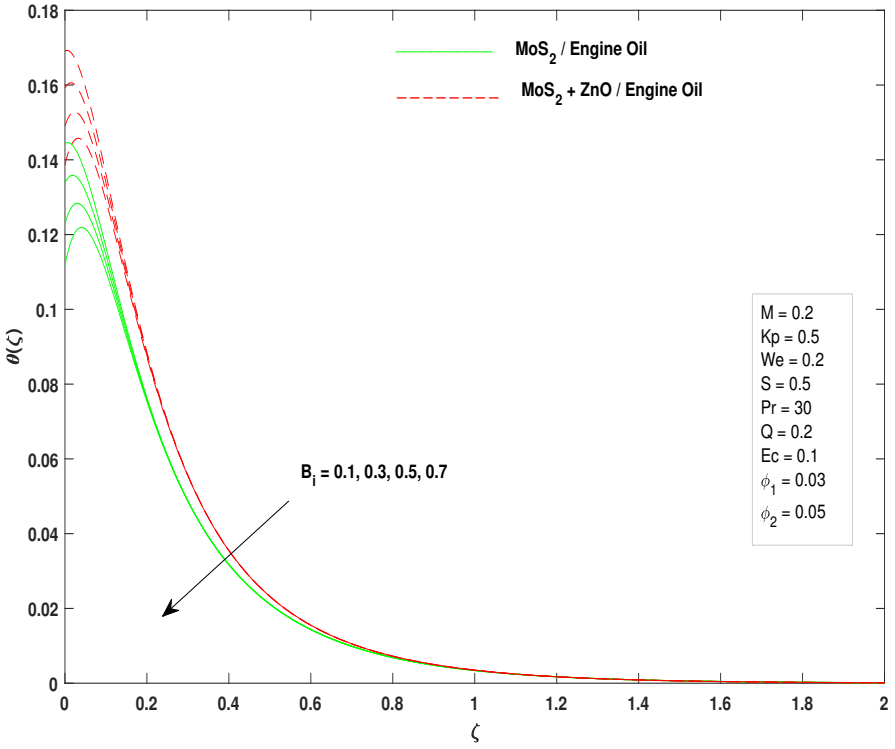

FIGURE 3.10: Influence of Bi on temperature profile $\theta(\zeta)$

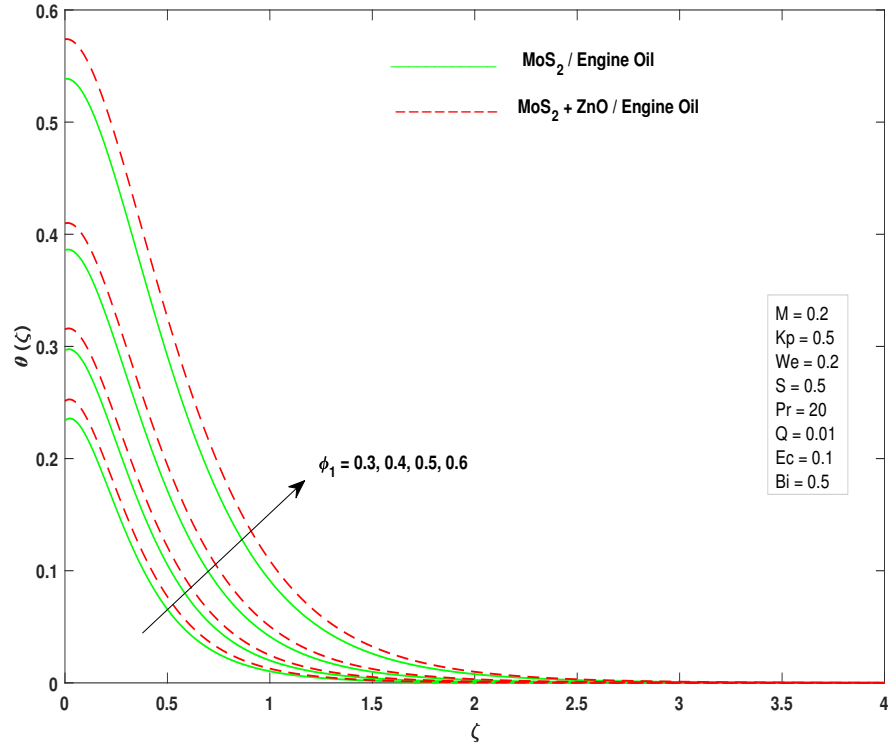

FIGURE 3.11: Effects of ϕ_1 on temperature profile $\theta(\zeta)$

Chapter 4

A Hybrid Williamson Nanofluid Flow: An Investigation Involving Cattaneo-Christov Model, Magnetic Field, Diffusion, Forchheimer Flow, and Chemical Reaction.

4.1 Introduction

In this chapter, the Williamson fluid model, discussed in Chapter 3 [17] , has been modified by incorporating Cattaneo-Christov heat flux, magnetic field, thermal radiation, and diffusion, in the energy equation. In addition, the Forchheimer flow in the momentum equation has been incorporated. Further a concentration equation for a new water-based hybrid nanofluid ($MoS_2 + GO$), has been incorporated. The consideration of these multiple effects allows us to explore their collective influence on the Williamson fluid flow over a stretching sheet. Through comprehensive numerical simulations and analysis, the intricate interplay of these effects and their combined impact on the overall

flow behavior has been investigated. The results of this study offer valuable insights into the behavior of the Williamson fluid under various physical conditions, providing a deeper understanding of the considered fluid flow.

4.2 Mathematical Modeling

This investigation focuses on the flow characteristics of a Williamson hybrid nano-fluid over a stretching sheet, assuming a two-dimensional and steady boundary layer flow. The coordinate axis along the stretched sheet is denoted by $\tilde{x}$ and that perpendicular to the sheet is $\tilde{y}$. Notably, the wall is considered incompressible

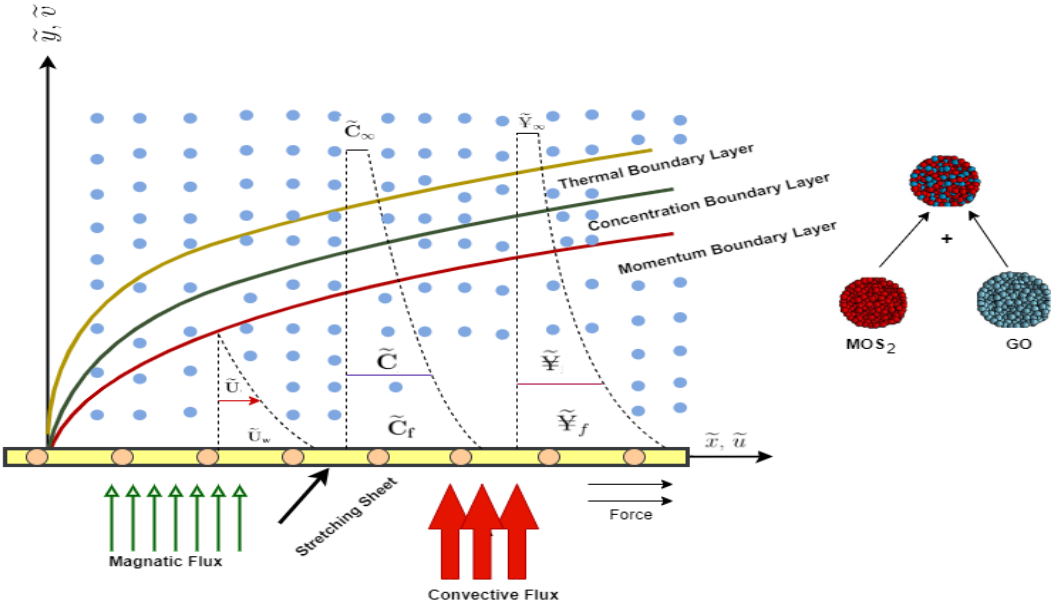

FIGURE 4.1: Flow Diagram

($\widetilde{v}_w = 0$), as depicted in figure 4.1. To observe mass diffusion and heat transfer, the interface of the applied magnetization field with dynamic viscosity and a porous medium are used. The flow phenomenon has been assumed to occur with some crucial assumptions like the Brownian diffusion, thermophysical diffusion, Cattaneo-Christov heat flux, heat generation/absorption and Forchheimer flow with a surface velocity of $\widetilde{U}_w(x) = \tilde{a}x$ ($\tilde{a} > 0$, constant). A uniform transverse magnetic field of strength $\widetilde{B}_o$ is applied parallel to y-axis. The temperature and concentration near the surface are $\widetilde{\Upsilon}_f$ and $\widetilde{C}_f$, while the constant ambient temperature and concentration of the hybrid nanofluid are $\widetilde{\Upsilon}_\infty$ and $\widetilde{C}_\infty$, respectively.

The continuity, momentum, energy and concentration equations governing the above stated problem under the usual boundary layer approximations are expressed through the upcoming equations [2, 17, 20].

Mass conservation:

$$\frac{\partial \widetilde{u}}{\partial \widetilde{x}} + \frac{\partial \widetilde{v}}{\partial \widetilde{y}} = 0. \tag{4.1}$$

Momentum Equation:

$$\widetilde{u}\frac{\partial \widetilde{u}}{\partial \widetilde{x}} + \widetilde{v}\frac{\partial \widetilde{u}}{\partial \widetilde{y}} + \frac{\widetilde{\sigma}_{hnf}}{\widetilde{\rho}_{hnf}} B_o^2 \widetilde{u} + \frac{\widetilde{\mu}_{hnf}}{\widetilde{\rho}_{hnf}} \frac{\widetilde{u}}{k^*} + \frac{C_b}{\tilde{x}\sqrt{K}} \widetilde{u}^2 = \frac{\widetilde{\mu}_{hnf}}{\widetilde{\rho}_{hnf}} \frac{\partial^2 \widetilde{u}}{\partial \widetilde{y}^2} + \sqrt{2}\Gamma \widetilde{\nu}_f \frac{\partial \widetilde{u}}{\partial \widetilde{y}} \frac{\partial^2 \widetilde{u}}{\partial \widetilde{y}^2}. \tag{4.2}$$

Energy Equation:

$$\begin{aligned} \widetilde{u}\frac{\partial \widetilde{\Upsilon}}{\partial \widetilde{x}} + \widetilde{v}\frac{\partial \widetilde{\Upsilon}}{\partial \widetilde{y}} + \frac{1}{(\widetilde{\rho}\widetilde{c}_p)_{hnf}} \frac{\partial \tilde{q}_r}{\partial \widetilde{y}} + \lambda_T \Bigg[\widetilde{u}\frac{\partial \widetilde{u}}{\partial \widetilde{x}} + \widetilde{v}\frac{\partial \widetilde{v}}{\partial \widetilde{y}} \frac{\partial \widetilde{\Upsilon}}{\partial \widetilde{y}} + 2\widetilde{u}\widetilde{v}\frac{\partial^2 \widetilde{\Upsilon}}{\partial \widetilde{x}\partial \widetilde{y}} + \widetilde{u}\frac{\partial \widetilde{v}}{\partial \widetilde{x}} \frac{\partial \widetilde{\Upsilon}}{\partial \widetilde{y}} \\ + \widetilde{v}\frac{\partial \widetilde{u}}{\partial \widetilde{y}} \frac{\partial \widetilde{\Upsilon}}{\partial \widetilde{x}} + \widetilde{u}^2 \frac{\partial^2 \widetilde{\Upsilon}}{\partial \widetilde{x}^2} + \widetilde{v}^2 \frac{\partial^2 \widetilde{\Upsilon}}{\partial \widetilde{y}^2} \Bigg] = \frac{\widetilde{K}_{hnf}}{(\widetilde{\rho}\widetilde{c}_p)_{hnf}} \frac{\partial^2 \widetilde{\Upsilon}}{\partial \widetilde{y}^2} + \frac{\widetilde{\mu}_{hnf}}{(\widetilde{\rho}\widetilde{c}_p)_{hnf}} \left(\frac{\partial \widetilde{u}}{\partial \widetilde{y}}\right)^2 \\ + \frac{Q_o}{(\widetilde{\rho}\widetilde{c}_p)_{hnf}} + \frac{\widetilde{\sigma}_{hnf} B_o^2}{(\rho c_p)_{hnf}} \widetilde{u}^2 + \frac{(\widetilde{\rho}\widetilde{c}_p)_p}{(\widetilde{\rho}\widetilde{c}_p)_{hnf}} \left[\frac{\widetilde{D}_{\widetilde{\Upsilon}}}{\widetilde{\Upsilon}_\infty} \left(\frac{\partial \widetilde{\Upsilon}}{\partial \widetilde{y}}\right)^2 + \widetilde{D}_B \left(\frac{\partial \widetilde{C}}{\partial \widetilde{y}} \frac{\partial \widetilde{\Upsilon}}{\partial \widetilde{y}}\right) \right]. \end{aligned} \tag{4.3}$$

Concentration Equation:

$$\widetilde{u}\frac{\partial \widetilde{C}}{\partial \widetilde{x}} + \widetilde{v}\frac{\partial \widetilde{C}}{\partial \widetilde{y}} + R^*\left(\widetilde{C} - \widetilde{C}_\infty\right) = \frac{\widetilde{D}_{\widetilde{\Upsilon}}}{\widetilde{\Upsilon}_\infty} \frac{\partial^2 \widetilde{\Upsilon}}{\partial \widetilde{y}^2} + \widetilde{D}_B \frac{\partial^2 \widetilde{C}}{\partial \widetilde{y}^2}. \tag{4.4}$$

Boundary Conditions:

The boundary conditions corresponding to the current fluidic problem are as follows [2]:

$$\left.\begin{aligned} &\widetilde{u} = \widetilde{U}_w = \tilde{a}x, \;\; \widetilde{v} = 0, \;\; \widetilde{\Upsilon} = \widetilde{\Upsilon}_\infty, \;\; \widetilde{D}_B \frac{\partial \widetilde{C}}{\partial \widetilde{y}} + \frac{\widetilde{D}_{\widetilde{\Upsilon}}}{\widetilde{\Upsilon}_\infty} \frac{\partial \widetilde{\Upsilon}}{\partial \widetilde{y}} = 0, \quad at \quad \widetilde{y} = 0, \\ &\widetilde{u} \longrightarrow 0, \quad \widetilde{\Upsilon} \longrightarrow \widetilde{\Upsilon}_\infty, \quad \widetilde{C} \longrightarrow \widetilde{C}_\infty \quad as \;\; \widetilde{y} \longrightarrow \infty. \end{aligned}\right\} \tag{4.5}$$

The radiation heat flux $\tilde{q}_r$ can be expressed as:

$$\tilde{q}_r = -\frac{4\tilde{\sigma}^*}{3\tilde{k}^*} \frac{\partial \widetilde{\Upsilon}^4}{\partial \widetilde{y}}. \tag{4.6}$$

The Stefan-Boltzman constant is denoted by $\tilde{\sigma}^*$, and the absorption coefficient is represented by $\tilde{k}^*$. In the case of a small temperature difference, the Taylor series expansion can be utilized to express the temperature $\widetilde{\Upsilon}^4$ around $\widetilde{\Upsilon}_\infty$, as follows

$$\widetilde{\Upsilon}^4 = \widetilde{\Upsilon}_\infty^4 + 4\widetilde{\Upsilon}_\infty^3\left(\widetilde{\Upsilon} - \widetilde{\Upsilon}_\infty\right) + 6\widetilde{\Upsilon}_\infty^2\left(\widetilde{\Upsilon} - \widetilde{\Upsilon}_\infty\right)^2 + ...$$

The higher-order terms are neglected, resulting in the following expression:

$$\begin{aligned}\widetilde{¥}^4 &= \widetilde{¥}_\infty^4 + 4\widetilde{¥}_\infty^3\left(\widetilde{¥} - \widetilde{¥}_\infty\right)\\ &= \widetilde{¥}_\infty^4 + 4\widetilde{¥}_\infty^3\widetilde{¥} - 4\widetilde{¥}_\infty^4\\ &= 4\widetilde{¥}_\infty^3\widetilde{¥} - 3\widetilde{¥}_\infty^4.\end{aligned}$$

Substituting the above expression into equation (4.6), we obtain

$$\begin{aligned}\tilde{q_r} &= -\frac{4\tilde{\sigma}^*}{3\tilde{k}^*}\frac{\partial}{\partial\tilde{y}}\left(4\widetilde{¥}_\infty^3\widetilde{¥} - 3\widetilde{¥}_\infty^4\right)\\ &= -\frac{16\tilde{\sigma}^*\widetilde{¥}_\infty^3}{3\tilde{k}^*}\frac{\partial\widetilde{¥}}{\partial\tilde{y}}.\end{aligned} \tag{4.7}$$

4.2.1 Formulation and Thermo-physical Characteristics

To provide a clear comparison, the valuable thermo-physical characteristics of both the HNF and the NF are presented in Table 4.1.

TABLE 4.1: Thermo-physical characteristics related to present model [54]

.

Physical Properties	MoS_2	GO	H_2O
$\widetilde{\rho}\left(kg.m^{-3}\right)$	5060	1800	997.1
$\widetilde{c_p}\left(J(kg.^ok)\right)$	397.21	717	4179
$\widetilde{k}\left(W(m.^ok)\right)$	904.4	5000	0.613
$\widetilde{\sigma}\left(\Omega.m\right)$	2.09×10^4	6.30×10^7	0.005
Pr	6.2		

The formulation of different thermo-physical properties for both nanofluid and hybrid nanofluid are articulated in Table 3.1.

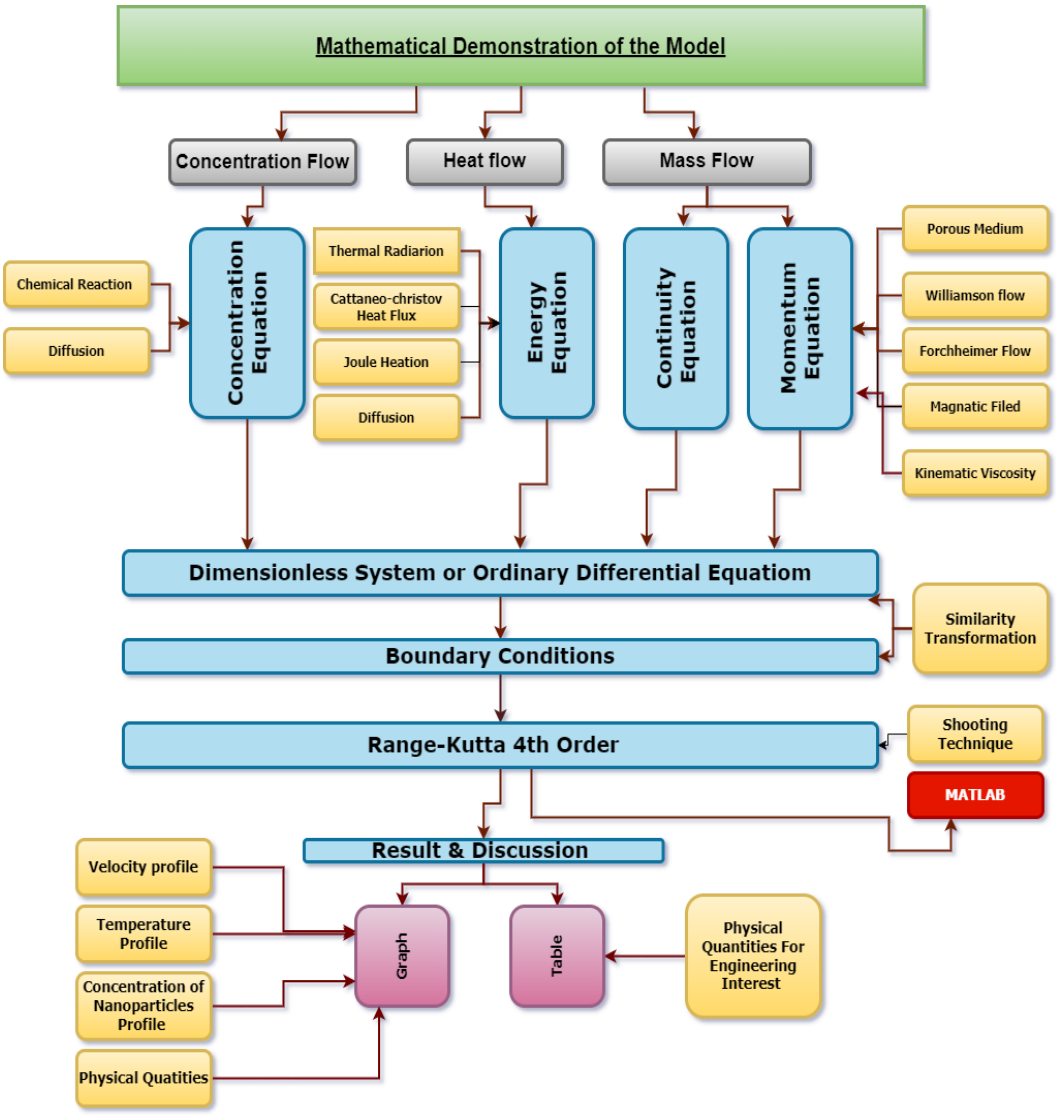

FIGURE 4.2: Mathematical model's flow structure

4.3 Similarity Transformation and Non- Dimensionalization of Mathematical Model

In this section, we present the process of non-dimensionalization for the mathematical model governing the behavior of our hybrid nanofluid. The procedure required introducing the dimensionless variables and parameters to transform the original equations into a simpler form. By using dimensionless quantities, we gain a deeper insight into the physical phenomena and make the analysis more tractable. The mathematical model will be transformed into a system of ordinary differential equations (ODEs) using the following similarity transformation (Figure 4.2):

$$\left.\begin{aligned} &\zeta = \sqrt{\frac{\tilde{a}}{\widetilde{\nu}_f}}\,\tilde{y}, \quad \tilde{u} = \tilde{a}\tilde{x}f'(\zeta), \quad \tilde{v} = -\sqrt{\tilde{a}\widetilde{\nu}_f}f(\zeta), \\ &\theta(\zeta) = \frac{\widetilde{¥} - \widetilde{¥}_\infty}{\widetilde{¥}_f - \widetilde{¥}_\infty}, \quad \phi(\zeta) = \frac{\widetilde{C} - \widetilde{C}_\infty}{\widetilde{C}_f - \widetilde{C}_\infty}. \end{aligned}\right\} \tag{4.8}$$

The symbol ζ represents the similarity variable. The velocity components in the x and y directions are denoted by $\tilde{u}$ and $\tilde{v}$, respectively, while $\theta(\zeta)$ and $\phi(\zeta)$ stand for the dimensionless temperature and concentration profiles. Different parameters used in the upcoming ODEs and their BCs, have been listed in TABLE 4.2.

TABLE 4.2: Different Dimensionless parameters used in governing ODEs

Symbols	**Name**	**Appearance**
M	Magnetic field	$M = \frac{\tilde{\sigma}_f \tilde{B}_o^2}{\tilde{\rho}_f \tilde{a}}$
Kp	Porosity medium	$Kp = \frac{\widetilde{\nu}_f}{\tilde{a}k^*}$
We	Non-Newtonian Williamson	$We = x\sqrt{2}\Gamma\frac{\tilde{a}^{3/2}}{\widetilde{\nu}_f^{1/2}}$
Pr	Prandtl number	$Pr = \frac{\widetilde{\nu}_f\left(\widetilde{\rho c_p}\right)_f}{\tilde{K}_f}$
Ec	Eckert number	$Ec = \frac{\tilde{a}^2\tilde{x}^2}{\left(\widetilde{c_p}\right)_f\left(\widetilde{¥}_f - \widetilde{¥}_\infty\right)}$
Q	Heat source	$Q = \frac{Q_o}{\tilde{a}\left(\widetilde{\rho c_p}\right)_f}$
Ω	Time Relaxation	$\Omega = \tilde{a}\lambda_T$
R	Non-linear thermal radiation	$R = \frac{16\tilde{\sigma}^*\widetilde{¥}_\infty^3}{3\widetilde{K}_f\widetilde{K}^*}$
Nb	Brownian motion parameter	$Nb = \frac{\left(\tilde{\rho}\widetilde{c_p}\right)_p\widetilde{D}_B\left(\widetilde{C}_f - \widetilde{C}_\infty\right)}{\widetilde{\nu}_f\left(\widetilde{\rho c_p}\right)_f}$
Nt	Thermophoresis parameter	$Nt = \frac{\left(\tilde{\rho}\widetilde{c_p}\right)_p\widetilde{D}_{¥}\left(\widetilde{¥}_f - \widetilde{¥}_\infty\right)}{\left(\tilde{\rho}\widetilde{c_p}\right)_f\widetilde{\nu}_f\widetilde{¥}_\infty}$
Le	Lewis number	$Le = \frac{\widetilde{\nu}_f}{\widetilde{D}_B}$
γ	Chemical reaction	$\gamma = \frac{R^*}{\tilde{a}}$

4.3.1 Non-Dimensionalization of Momentum Equation

In this subsection, we transform the governing momentum equation (4.2) into a non-dimensional form. For this purpose, we substitute all the partial derivatives (3.6) , (3.8) and (3.9) and velocity components from expression (3.5) into the equation (4.2) to get the following:

$$\left[\left(\widetilde{a}\tilde{x}f''(\zeta)\right)\left(\widetilde{a}f'(\zeta)\right)\right]+\left[\left(-\sqrt{\widetilde{a}\widetilde{\nu}_f}f(\zeta)\right)\left(\widetilde{a}\tilde{x}f''(\zeta)\sqrt{\frac{\widetilde{a}}{\widetilde{\nu}_f}}\right)\right]$$
$$+\left[\frac{\widetilde{\sigma}_f\widetilde{A}_5}{\widetilde{\rho}_f\widetilde{A}_2}\widetilde{B}_o^2\left(\widetilde{a}\tilde{x}f'(\zeta)\right)\right]+\left[\frac{\widetilde{\mu}_f}{\widetilde{\rho}_f\widetilde{A}_2\widetilde{A}_4}\frac{\widetilde{a}\tilde{x}f''(\zeta)}{k^*}\right]+\left[\frac{C_b}{x\sqrt{K}}\widetilde{a}^2\tilde{x}^2\big(f'(\zeta)\big)^2\right]$$
$$=\left[\frac{\widetilde{\mu}_f}{\widetilde{\rho}_f\widetilde{A}_2\widetilde{A}_4}\frac{\widetilde{a}^2\tilde{x}}{\widetilde{\nu}_f}f'''(\zeta)\right]+\left[\sqrt{2}\Gamma\widetilde{\nu}_f\left(\widetilde{a}\tilde{x}f''(\zeta)\sqrt{\frac{\widetilde{a}}{\widetilde{\nu}_f}}\right)\left(\frac{\widetilde{a}^2\tilde{x}}{\widetilde{\nu}_f}f'''(\zeta)\right)\right].$$

$$\Rightarrow\quad \widetilde{a}^2x\big(f'(\zeta)\big)^2-\widetilde{a}^2xf(\zeta)f''(\zeta)+\frac{\widetilde{\sigma}_fB_o^2\widetilde{A}_5}{\widetilde{\rho}_f\widetilde{A}_2}\widetilde{a}\tilde{x}f''(\zeta)+\frac{\widetilde{\nu}_f\widetilde{a}\tilde{x}}{k^*\widetilde{A}_2\widetilde{A}_4}+\frac{C_b}{\sqrt{K}}\widetilde{a}^2\tilde{x}\big(f'(\zeta)\big)^2$$
$$=\frac{\widetilde{a}^2x}{\widetilde{A}_2\widetilde{A}_4}f'''(\zeta)+\sqrt{2}\Gamma\frac{\widetilde{a}^2\tilde{x}^2\widetilde{a}^{\frac{3}{2}}}{\widetilde{\nu}_f^{\frac{1}{2}}}f''(\zeta)f'''(\zeta).$$

$$\Rightarrow\quad \big(f'(\zeta)\big)^2-f(\zeta)f''(\zeta)+\frac{\widetilde{\sigma}_fB_o^2}{\widetilde{\rho}_f\widetilde{a}}\frac{\widetilde{A}_5}{\widetilde{A}_2}f'(\zeta)+\frac{\widetilde{\nu}_f}{\widetilde{a}k^*}\frac{1}{\widetilde{A}_2\widetilde{A}_4}f'(\zeta)+\frac{C_b}{\sqrt{K}}(f'(\zeta))^2$$
$$=\frac{1}{\widetilde{A}_2\widetilde{A}_4}f'''(\zeta)+\sqrt{2}\tilde{x}\Gamma\frac{\widetilde{a}^{\frac{3}{2}}}{\widetilde{\nu}_f^{\frac{1}{2}}}f''(\zeta)f'''(\zeta).$$

$$\Rightarrow\quad \big(f'(\zeta)\big)^2-f(\zeta)f''(\zeta)+M\frac{\widetilde{A}_5}{\widetilde{A}_2}f'(\zeta)+\frac{K_p}{\widetilde{A}_2\widetilde{A}_4}f'(\zeta)+F_r\big(f'(\zeta)\big)^2$$
$$=\frac{1}{\widetilde{A}_2\widetilde{A}_4}f'''(\zeta)+w_ef''(\zeta)f'''(\zeta).$$

$$\Rightarrow\quad \widetilde{A}_2\widetilde{A}_4\Big(\big(f'(\zeta)^2\big)-f(\zeta)f''(\zeta)\Big)+M\widetilde{A}_5\widetilde{A}_4f'(\zeta)+K_pf'(\zeta)+\widetilde{A}_2\widetilde{A}_4F_r\big(f'(\zeta)\big)^2$$
$$=f'''(\zeta)+\widetilde{A}_2\widetilde{A}_4wef''(\zeta)f'''(\zeta).$$

$$\Rightarrow\quad \Big(1+w_e\widetilde{A}_1f''(\zeta)\Big)f'''(\zeta)-\widetilde{A}_1\Big(\big(f'(\zeta)\big)^2-f(\zeta)f''(\zeta)+F_r\big(f'(\zeta)\big)^2\Big)$$
$$-\Big(M\widetilde{A}_4\widetilde{A}_5+K_p\Big)f'(\zeta)=0. \tag{4.9}$$

4.3.2 Non-Dimensionalization of Energy Equation

In this section, we discuss the non-dimensionalization process of the energy equation (4.3) for our hybrid nanofluid model. For this equation, the following derivatives are also required.

$$\frac{\partial^2\widetilde{\Upsilon}}{\partial\tilde{x}\partial\tilde{y}}=0. \qquad \text{(using (3.12))} \tag{4.10}$$

$$\tilde{q_r} = -\frac{16\tilde{\sigma}^*\widetilde{¥}_\infty^3}{3\tilde{k}^*}\frac{\partial\widetilde{¥}}{\partial\tilde{y}}.$$

$$\Rightarrow \quad \frac{\partial\tilde{q_r}}{\partial\tilde{y}} = -\frac{16\tilde{\sigma}^*\widetilde{¥}_\infty^3}{3\tilde{k}^*}\frac{\partial^2\widetilde{¥}}{\partial\tilde{y}^2}$$

$$= -\frac{16\widetilde{\sigma}^*\widetilde{¥}_\infty^3}{3\widetilde{k}^*}\frac{\tilde{a}}{\widetilde{\nu}_f}\left(\widetilde{¥}_f - \widetilde{¥}_\infty\right)\theta''(\zeta). \tag{4.11}$$

$$\phi(\zeta) = \frac{\widetilde{C} - \widetilde{C}_\infty}{\widetilde{C}_f - \widetilde{C}_\infty}.$$

$$\Rightarrow \quad \widetilde{C} = \left(\widetilde{C}_f - \widetilde{C}_\infty\right)\phi(\zeta) + \widetilde{C}_\infty. \tag{4.12}$$

$$\Rightarrow \quad \frac{\partial\widetilde{C}}{\partial\tilde{y}} = \left(\widetilde{C}_f - \widetilde{C}_\infty\right)\phi'(\zeta)\frac{\partial\zeta}{\partial\tilde{y}}$$

$$= \left(\widetilde{C}_f - \widetilde{C}_\infty\right)\sqrt{\frac{\tilde{a}}{\widetilde{\nu}_f}}\phi'(\zeta). \tag{4.13}$$

Substituting (3.5) - (3.15) and (4.11)- (4.13), the dimensionless governing equation for energy (4.3), can be expressed as:

$$\begin{aligned}
&\left[\left(-\sqrt{\tilde{a}\widetilde{\nu}_f}\right)\left(\widetilde{¥}_f - \widetilde{¥}_\infty\right)\sqrt{\frac{\tilde{a}}{\widetilde{\nu}_f}}\theta'(\zeta)\right] + \left[\frac{1}{\left(\widetilde{\rho}\widetilde{c}_p\right)_f\widetilde{A}_3}\left(\frac{-16\sigma^*\widetilde{¥}_\infty^3}{3k^*}\right)\left(\frac{\tilde{a}}{\widetilde{\nu}_f}\left(\widetilde{¥}_f - \widetilde{¥}_\infty\right)\theta''(\zeta)\right)\right] \\
&+ \lambda_T\left[\left(\left(-cf'(\zeta)\right)\left(-\sqrt{\tilde{a}\widetilde{\nu}_f}f(\zeta)\right)\left(\widetilde{¥}_f - \widetilde{¥}_\infty\right)\sqrt{\frac{\tilde{a}}{\widetilde{\nu}_f}}\theta'(\zeta)\right)\right. \\
&\left.+ \left(\tilde{a}\widetilde{\nu}_f\left(f(\zeta)\right)^2\right)\left(\frac{\tilde{a}}{\widetilde{\nu}_f}\left(\widetilde{¥}_f - \widetilde{¥}_\infty\right)\theta''(\zeta)\right)\right] \\
&= \frac{\widetilde{K}_{hnf}}{\left(\widetilde{\rho}\widetilde{c}_p\right)_f\widetilde{A}_3}\left(\frac{\tilde{a}}{\widetilde{\nu}_f}\left(\widetilde{¥}_f - \widetilde{¥}_\infty\right)\theta''(\zeta)\right) + \frac{\widetilde{\mu}_f}{\left(\widetilde{\rho}\widetilde{c}_p\right)_f\widetilde{A}_3\widetilde{A}_4}\left(\tilde{a}^2\tilde{x}^2\left(f''(\zeta)\right)^2\frac{\tilde{a}}{\widetilde{\nu}_f}\right) \\
&+ \frac{Q_o}{\left(\widetilde{\rho}\widetilde{c}_p\right)_f\widetilde{A}_3}\left[\left(\widetilde{¥}_f - \widetilde{¥}_\infty\right)\right] + \frac{\widetilde{\sigma}_f\widetilde{A}_5B_o^2}{\left(\widetilde{\rho}\widetilde{c}_p\right)_f\widetilde{A}_3}\tilde{a}^2x^2\left(f'(\zeta)\right)^2 + \frac{\left(\tilde{\rho}\tilde{c_p}\right)_p}{\left(\tilde{\rho}\tilde{c_p}\right)_f\widetilde{A}_3}\left[\frac{\widetilde{D}_{¥}}{\widetilde{¥}_\infty}\left(\widetilde{¥}_f - \widetilde{¥}_\infty\right)^2\frac{\tilde{a}}{\widetilde{\nu}_f}\right. \\
&\left.\left(\theta'(\zeta)\right)^2 + \widetilde{D}_B\frac{\tilde{a}}{\widetilde{\nu}_f}\left(\widetilde{C}_f - \widetilde{C}_\infty\right)\left(\widetilde{¥}_f - \widetilde{¥}_\infty\right)\phi'(\zeta)\theta'(\zeta)\right]. \\
\Rightarrow\ &-\tilde{a}\left(\widetilde{¥}_f - \widetilde{¥}_\infty\right)f(\zeta)\theta'(\zeta) - \frac{16\sigma^*\widetilde{¥}_\infty^3}{3\left(\rho c_p\right)_f k^*\widetilde{A}_3\widetilde{\nu}_f}\tilde{a}\left(\widetilde{¥}_f - \widetilde{¥}_\infty\right)\theta''(\zeta) \\
&+ \lambda_T\left[\tilde{a}^2\left(\widetilde{¥}_f - \widetilde{¥}_\infty\right)f(\zeta)f'(\zeta)\theta'(\zeta) + \tilde{a}^2\left(\widetilde{¥}_f - \widetilde{¥}_\infty\right)\left(f(\zeta)\right)^2\theta''(\zeta)\right]
\end{aligned}$$

$$= \frac{\widetilde{K}_{hnf}}{(\widetilde{\rho}\widetilde{c}_p)_f \widetilde{A}_3}\frac{\widetilde{a}}{\widetilde{\nu}_f}\theta''(\zeta)\frac{\widetilde{a}}{(\rho c_p)_f \widetilde{A}_3\widetilde{A}_4}\left(\widetilde{a}^2x^2\big(f''(\zeta)\big)^2\frac{\widetilde{a}}{\widetilde{\nu}_f}\right) + \frac{Q_o}{(\widetilde{\rho}\widetilde{c}_p)_f\widetilde{A}_3}\big(\widetilde{\Upsilon}_f - \widetilde{\Upsilon}_\infty\big)\theta(\zeta)$$
$$+ \frac{\widetilde{\sigma}_f B_o^2\widetilde{A}_5}{(\widetilde{\rho}\widetilde{c}_p)_f\widetilde{A}_3}\widetilde{a}^2x^2\big(f'(\zeta)\big)^2 + \frac{1}{\widetilde{A}_3}\Bigg[\frac{(\widetilde{\rho}\widetilde{c}_p)_p\widetilde{D}_{\widetilde{\Upsilon}}}{(\widetilde{\rho}\widetilde{c}_p)_f\widetilde{\Upsilon}_\infty\widetilde{\nu}_f}\widetilde{a}\big(\widetilde{\Upsilon}_f - \widetilde{\Upsilon}_\infty\big)^2$$
$$+ \frac{(\widetilde{\rho}\widetilde{c}_p)_p}{(\widetilde{\rho}\widetilde{c}_p)_f}\frac{\widetilde{D}_B}{\widetilde{\nu}_f}\big(\widetilde{C}_f - \widetilde{C}_\infty\big)\widetilde{a}\big(\widetilde{\Upsilon}_f - \widetilde{\Upsilon}_\infty\big)\theta'(\zeta)\phi'(\zeta)\Bigg].$$

$$\Rightarrow -f(\zeta)\theta'(\zeta) - \frac{16\widetilde{\sigma}^*\widetilde{\Upsilon}_\infty^3}{\widetilde{A}_3 3\widetilde{K}_f}\frac{\widetilde{K}_f}{\widetilde{\nu}_f(\widetilde{\rho}\widetilde{c}_p)_f}\theta''(\zeta) + \widetilde{a}\lambda_T\Big[f(\zeta)f'(\zeta)\theta'(\zeta) + \big(f(\zeta)\big)^2\theta''(\zeta)\Big]$$
$$= \frac{\widetilde{K}_{hnf}}{\widetilde{A}_3\widetilde{K}_f}\frac{\widetilde{K}_f}{(\widetilde{\rho}\widetilde{c}_p)_f\widetilde{\nu}_f}\theta''(\zeta) + \frac{\widetilde{a}^2x^2}{(\widetilde{c}_p)_f(\widetilde{\Upsilon}_f - \widetilde{\Upsilon}_\infty)}\frac{1}{\widetilde{A}_3\widetilde{A}_4}\big(f''(\zeta)\big)^2 + \frac{Q_o}{\widetilde{A}_3\widetilde{a}(\rho c_p)_f}\theta(\zeta)$$
$$+ \frac{\widetilde{A}_5\widetilde{\sigma}_f B_o^2}{\widetilde{A}_3\widetilde{\rho}_f\widetilde{a}}\frac{\widetilde{a}^2x^2}{(c_p)_f(\widetilde{\Upsilon}_f - \widetilde{\Upsilon}_\infty)}\big(f'(\zeta)\big)^2 + \frac{1}{\widetilde{A}_3}\Bigg[\frac{(\widetilde{\rho}\widetilde{c}_p)_p\widetilde{D}_{\widetilde{\Upsilon}}(\widetilde{\Upsilon}_f - \widetilde{\Upsilon}_\infty)}{(\widetilde{\rho}\widetilde{c}_p)_f\widetilde{\nu}_f\widetilde{\Upsilon}_\infty}\big(\theta'(\zeta)\big)^2$$
$$+ \frac{(\widetilde{\rho}\widetilde{c}_p)_p\widetilde{D}_B(\widetilde{C}_f - \widetilde{C}_\infty)}{(\widetilde{\rho}\widetilde{c}_p)_f\widetilde{\nu}_f}\theta'(\zeta)\phi'(\zeta)\Bigg].$$

$$\Rightarrow -f(\zeta)\theta'(\zeta) - \frac{R}{\widetilde{A}_3 Pr}\theta''(\zeta) + \Omega\Big[f(\zeta)f'(\zeta)\theta'(\zeta) + \big(f(\zeta)\big)^2\theta''(\zeta)\Big]$$
$$= \frac{\widetilde{K}_{hnf}}{\widetilde{A}_3\widetilde{K}_f Pr}\theta''(\zeta) + \frac{Ec}{\widetilde{A}_3\widetilde{A}_4}\big(f''(\zeta)\big)^2 + \frac{Q}{\widetilde{A}_3}\theta(\zeta) + \frac{\widetilde{A}_5}{\widetilde{A}_3}MEc\big(f'(\zeta)\big)^2$$
$$+ \frac{1}{\widetilde{A}_3}\Big[Nt\big(\theta'(\zeta)\big)^2 + Nb\theta'(\zeta)\phi'(\zeta)\Big].$$

$$\Rightarrow \left(\frac{\widetilde{K}_{hnf}}{\widetilde{K}_f} + R + \Omega\widetilde{A}_3 Pr\big(f(\zeta)\big)^2\right)\theta''(\zeta) + Pr\Big[\widetilde{A}_3\big(f(\zeta)\theta'(\zeta) - \Omega f(\zeta)f'(\zeta)\theta'(\zeta)\big)$$
$$+ \frac{Ec}{\widetilde{A}_4}\big(f''(\zeta)\big)^2 + Q\theta(\zeta) + MEc\widetilde{A}_5\big(f'(\zeta)\big)^2 + Nt\big(\theta'(\zeta)\big)^2 + Nb\theta'(\zeta)\phi'(\zeta)\Big] = 0. \tag{4.14}$$

4.3.3 Non-Dimensionalization of Concentration Equation

Here, we focus on the non-dimensionalization process specifically applied to the concentration equation (4.4) in our hybrid nanofluid model. For this purpose, the following derivatives are also required.

$$\frac{\partial^2\widetilde{C}}{\partial\widetilde{y}^2} = \left(\widetilde{C}_f - \widetilde{C}_\infty\right)\frac{\tilde{a}}{\widetilde{\nu}_f}. \qquad \text{(using (4.13))} \tag{4.15}$$

$$\frac{\partial\widetilde{C}}{\partial\widetilde{x}} = 0. \qquad \text{(using (4.12))} \tag{4.16}$$

Substituting equation (3.15) , (4.13),(4.15) and (4.16) into concentration equation (4.4), it gets the following form :

$$\left((\widetilde{C}_f-\widetilde{C}_\infty)\sqrt{\frac{\widetilde{a}}{\widetilde{\nu}_f}}\phi'(\zeta)\right)\left(-\sqrt{\widetilde{C}\widetilde{\nu}_f}f(\zeta)\right)+R^*\left(\widetilde{C}_\infty+(\widetilde{C}_f-\widetilde{C}_\infty)\phi(\zeta)-\widetilde{C}_\infty\right)$$
$$=\frac{\widetilde{D}_{\widetilde{¥}}}{\widetilde{¥}_\infty}\left(\frac{\widetilde{a}}{\widetilde{\nu}_f}(\widetilde{¥}_f-\widetilde{¥}_\infty)\theta''(\zeta)\right)+\widetilde{D}_B\left((\widetilde{C}_f-\widetilde{C}_\infty)\phi''(\zeta)\frac{\widetilde{a}}{\widetilde{\nu}_f}\right).$$

$$\Rightarrow\quad -(\widetilde{C}_f-\widetilde{C}_\infty)\widetilde{a}f(\zeta)\phi'(\zeta)+R^*(\widetilde{C}_f-\widetilde{C}_\infty)\phi(\zeta)$$
$$=\frac{(\widetilde{\rho}\widetilde{c}_p)_p(\widetilde{\rho}\widetilde{c}_p)_f}{(\widetilde{\rho}\widetilde{c}_p)_p(\widetilde{\rho}\widetilde{c}_p)_f}\frac{\widetilde{D}_{\widetilde{¥}}\widetilde{a}}{\widetilde{¥}_\infty\widetilde{\nu}_f}(\widetilde{¥}_f-\widetilde{¥}_\infty)\theta''(\zeta)+\frac{\widetilde{D}_B(\widetilde{C}_f-\widetilde{C}_\infty)\widetilde{a}}{\widetilde{\nu}_f}\phi''(\zeta).$$

$$\Rightarrow\quad -f(\zeta)\phi'(\zeta)+\gamma\phi(\zeta)=\left(\frac{Nt}{Nb}\right)\frac{1}{Le}\theta''(\zeta)+\frac{1}{Le}\phi''(\zeta).$$

$$\Rightarrow\quad \phi''(\zeta)+Lef(\zeta)\phi'(\zeta)-Le\gamma\phi(\zeta)-\left(\frac{Nt}{Nb}\right)\theta''(\zeta)=0. \tag{4.17}$$

4.3.4 Dimensionless form of Boundary Conditions

The corresponding BCs are transformed into the non-dimensional form through the following procedure:

- $\widetilde{u}=U_w(\tilde{x}),$ *at* $\tilde{y}=0.$

  $\Rightarrow\ \widetilde{a}\tilde{x}f'(\zeta)=\widetilde{a}x,$ *at* $\zeta=0.$

  $\Rightarrow\ \widetilde{a}\tilde{x}f'(\zeta)=\widetilde{a}x,$ *at* $\zeta=0,$

  $\Rightarrow\ f'(\zeta)=1,$ *at* $\zeta=0.$

- $\widetilde{v}=0,$ *at* $\tilde{y}=0.$

  $\Rightarrow\ -\sqrt{\widetilde{a}\widetilde{\nu}_f}f(\zeta)=0,$ *at* $\zeta=0.$

  $\Rightarrow\ f(\zeta)=0,$ *at* $\zeta=0.$

- $\widetilde{D}_B\frac{\partial\widetilde{C}}{\partial\widetilde{y}}+\frac{\widetilde{D}_{\widetilde{¥}}}{\widetilde{¥}_\infty}\frac{\partial\widetilde{¥}}{\partial\widetilde{y}}=0$ *at* $\widetilde{y}=0.$

  $\Rightarrow\ \widetilde{D}_B\frac{\tilde{a}}{\widetilde{\nu}_f}\left(\widetilde{C}_f-\widetilde{C}_\infty\right)\phi'(\zeta)+\frac{\widetilde{D}_{\widetilde{¥}}}{\widetilde{¥}_\infty}\left(\widetilde{¥}_f-\widetilde{¥}_\infty\right)\frac{\tilde{a}}{\widetilde{\nu}_f}\phi'(\zeta)=0,$ *at* $\zeta=0.$

$$\Rightarrow \quad \widetilde{D}_B\left(\widetilde{C}_f-\widetilde{C}_\infty\right)\phi'(\zeta)+\frac{\widetilde{D}_{\widetilde{\text{¥}}}}{\widetilde{\text{¥}}_\infty}\left(\widetilde{\text{¥}}_f-\widetilde{\text{¥}}_\infty\right)\phi'(\zeta)=0, \qquad at \quad \zeta=0.$$

$$\Rightarrow \quad Nb\phi'(\zeta)+Nt\theta'(\zeta)=0, \qquad at \quad \zeta=0.$$

- $\widetilde{u}\longrightarrow 0, \qquad as \quad \tilde{y}\longrightarrow\infty.$

$$\Rightarrow \quad \widetilde{a}\tilde{x}f'(\zeta)\longrightarrow 0, \qquad as \quad \zeta\longrightarrow\infty.$$

$$\Rightarrow \quad f'(\zeta)\longrightarrow 0, \qquad as \quad \zeta\longrightarrow\infty.$$

- $\widetilde{\text{¥}}\longrightarrow\widetilde{\text{¥}}_\infty, \qquad as \quad \tilde{y}\longrightarrow\infty.$

$$\Rightarrow \quad \widetilde{\text{¥}}_\infty+\left(\widetilde{\text{¥}}_f-\widetilde{\text{¥}}_\infty\right)\theta(\zeta)\longrightarrow\widetilde{\text{¥}}_\infty, \qquad as \quad \zeta\longrightarrow\infty.$$

$$\Rightarrow \quad \left(\widetilde{\text{¥}}_f-\widetilde{\text{¥}}_\infty\right)\theta(\zeta)\longrightarrow 0, \qquad as \quad \zeta\longrightarrow\infty.$$

$$\Rightarrow \quad \theta(\zeta)\longrightarrow 0, \qquad as \quad \zeta\longrightarrow\infty.$$

- $\widetilde{C}\longrightarrow\widetilde{C}_\infty, \qquad as \quad \tilde{y}\longrightarrow\infty.$

$$\Rightarrow \quad \left(\widetilde{C}_f-\widetilde{C}_\infty\right)\phi'(\zeta)+\widetilde{C}_\infty\longrightarrow\widetilde{C}_\infty, \qquad as \quad \zeta\longrightarrow\infty.$$

$$\Rightarrow \quad \left(\widetilde{C}_f-\widetilde{C}_\infty\right)\phi'(\zeta)\longrightarrow\widetilde{C}_\infty, \qquad as \quad \zeta\longrightarrow\infty.$$

$$\Rightarrow \quad \phi'(\zeta)\longrightarrow 0, \qquad as \quad \zeta\longrightarrow\infty.$$

4.4 Solution Framework

The numerical solutions are computed using the shooting method, which involves the utilization of the fourth-order Runge-Kutta technique. The computational procedure of the shooting method, is elaborated and depicted in Figure 4.3. In order to solve the ODE (4.9), the following notations have been considered, as an initial step:

$$f(\zeta)=\widetilde{Y}_1, \qquad f'(\zeta)=\widetilde{Y}_1'=\widetilde{Y}_2, \qquad f''(\zeta)=\widetilde{Y}_2'=\widetilde{Y}_3.$$

The following system of first order ODEs has been obtained to replace the momentum equation:

$$\widetilde{Y}_1' = \widetilde{Y}_2, \qquad \widetilde{Y}_1(0) = 0,$$

$$\widetilde{Y}_2' = \widetilde{Y}_3, \qquad \widetilde{Y}_2(0) = 1,$$

$$\widetilde{Y}_3' = \frac{\left[\widetilde{A}_1\left(\left(\widetilde{Y}_2\right)^2 - \widetilde{Y}_1\widetilde{Y}_3 + F_r\left(\widetilde{Y}_2\right)^2\right) + \left(M\widetilde{A}_4\widetilde{A}_5 + K_p\right)\widetilde{Y}_2\right]}{\left(1 + we\widetilde{A}_1\widetilde{Y}_3\right)}, \qquad \widetilde{Y}_3(0) = s_1.$$

To utilize the Runge-Kutta 4th order (RK4) method for the numerical solution of the mentioned initial value problem, the condition s_1 within the system of equations need to be carefully chosen. The missing condition s_1 is to be chosen such that

$$\widetilde{Y}_2\left(\zeta_\infty, s_1\right) = 0.$$

Newton's method will be used to further refine the selection of s_1. This method has the following iterative scheme:

$${s_1}^{(m+1)} = s_1^{(m)} - \frac{\widetilde{Y}_2\left(\zeta_\infty, s_1^{(m)}\right)}{\left(\frac{\partial}{\partial s_1}\widetilde{Y}_2\left(\zeta_\infty, s_1\right)\right)^{(m)}}.$$

We further introduce the following notations:

$$\frac{\partial\widetilde{Y}_1}{\partial s_1} = \widetilde{Y}_4, \qquad \frac{\partial\widetilde{Y}_2}{\partial s_1} = \widetilde{Y}_5, \qquad \frac{\partial\widetilde{Y}_3}{\partial s_1} = \widetilde{Y}_6.$$

As a result these of new notations, the Newton's iterative scheme gets the form:

$${s_1}^{(m+1)} = s_1^{(m)} - \frac{\widetilde{Y}_2\left(\zeta_\infty, s_1^{(m)}\right)}{\widetilde{Y}_5\left(\zeta_\infty, s_1\right)}.$$

Now differentiating the above system of three first order ODEs with respect to s_1, we get another system of ODEs, as follows:

$$\widetilde{Y}_4' = \widetilde{Y}_5, \qquad \widetilde{Y}_4(0) = 0,$$

$$\widetilde{Y}_5' = \widetilde{Y}_6, \qquad \widetilde{Y}_5(0) = 0,$$

$$\widetilde{Y}_6' = \frac{\tilde{A}_1\left(2\widetilde{Y}_2\widetilde{Y}_5 - \widetilde{Y}_1\widetilde{Y}_6 - \widetilde{Y}_4\widetilde{Y}_3 - 2\widetilde{Y}_2\widetilde{Y}_5 Fr\right) + \left(M\widetilde{A}_4\widetilde{A}_5 + K_p\right)\widetilde{Y}_5}{\left(1 + We\widetilde{A}_1\widetilde{Y}_3\right)},$$

$$- \frac{We\widetilde{A}_1\widetilde{Y}_6}{\left(1 + We\widetilde{A}_1\widetilde{Y}_3\right)}\widetilde{Y}_3', \qquad \widetilde{Y}_6(0) = 1.$$

The stopping criteria for the Newton's technique is set as:

$$\left|\widetilde{Y}_2\left(\zeta_\infty, s_1\right)\right| < \epsilon,$$

where $\epsilon > 0$ is an arbitrarily small positive number. From now onward, ϵ has been taken as 10^{-6}.

Now, to solve equations (4.14) and (4.17) numerically by using shooting method, assume f, f' and f'' as known functions. The notations below have been used for the implementation of the shooting method:

$$\theta'(\zeta) = \widetilde{Z}_1, \qquad \theta'(\zeta) = \widetilde{Z}_1' = \widetilde{Z}_2, \qquad \phi(\zeta) = \widetilde{Z}_3, \qquad \phi'(\zeta) = \widetilde{Z}_3' = \widetilde{Z}_4.$$

and

$$b_1 = \left[\frac{\widetilde{K}_{hnf}}{\widetilde{K}_f} + R - \Omega \widetilde{A}_3 Pr\big(f(\zeta)\big)^2\right].$$

The system of equations (4.14) and (4.17), can be represented in the form of the following first-order coupled ODEs:

$$\begin{aligned}
&\widetilde{Z}_1' = \widetilde{Z}_2, && \widetilde{Z}_1(0) = 1,\\
&\widetilde{Z}_2' = \frac{-Pr}{b_1}\Big[\widetilde{A}_3\big(f(\zeta)\widetilde{Z}_2 - \Omega f f' \widetilde{Z}_2\big) + \frac{Ec}{\widetilde{A}_4}\big(f''\big)^2 + MEc\widetilde{A}_5\big(f'\big)^2\\
&\qquad + Q\widetilde{Z}_1 + Nt\big(\widetilde{Z}_2\big)^2 + Nb\widetilde{Z}_2\widetilde{Z}_4\Big], && \widetilde{Z}_2(0) = \tilde{p},\\
&\widetilde{Z}_3' = \widetilde{Z}_4, && \widetilde{Z}_3(0) = \tilde{q},\\
&\widetilde{Z}_4' = Le\gamma\widetilde{Z}_3 - Lef\widetilde{Z}_4 - \left(\frac{Nt}{Nb}\right)\widetilde{Z}_2', && \widetilde{Z}_4(0) = -\frac{Nt}{Nb}\tilde{p}.
\end{aligned}$$

To utilize the Runge-Kutta 4th order method for numerical solution of the above mentioned initial value problem, the conditions $\tilde{p}$ and $\tilde{q}$ within the system of equations need to be carefully chosen. The missing conditions $\widetilde{p}$ and $\widetilde{q}$ in the above system of equations must be selected in such a way, that

$$\widetilde{Z}_1\big(\zeta_\infty, \tilde{p}, \tilde{q}\big) = 0, \qquad \widetilde{Z}_3\big(\zeta_\infty, \tilde{p}, \tilde{q}\big) = 0.$$

To solve the aforementioned system of algebraic equations, we employ Newton's method, which follows the following scheme.

$$\begin{bmatrix}\tilde{p}\\ \tilde{q}\end{bmatrix}^{(n+1)} = \begin{bmatrix}\tilde{p}\\ \tilde{q}\end{bmatrix}^{(n)} - \left(\begin{bmatrix}\frac{\partial \widetilde{Z}_1}{\partial \tilde{p}} & \frac{\partial \widetilde{Z}_1}{\partial \tilde{q}}\\ \frac{\partial \widetilde{Z}_3}{\partial \tilde{p}} & \frac{\partial \widetilde{Z}_3}{\partial \tilde{q}}\end{bmatrix}^{-1}\begin{bmatrix}\widetilde{Z}_1\\ \widetilde{Z}_3\end{bmatrix}\right)^{(n)}.$$

To proceed further the following new notations, have been introduced:

$$\frac{\partial \widetilde{Z}_1}{\partial \tilde{p}} = \widetilde{Z}_5, \quad \frac{\partial \widetilde{Z}_2}{\partial \tilde{p}} = \widetilde{Z}_6, \quad \frac{\partial \widetilde{Z}_3}{\partial \tilde{p}} = \widetilde{Z}_7, \quad \frac{\partial \widetilde{Z}_4}{\partial \tilde{p}} = \widetilde{Z}_8,$$
$$\frac{\partial \widetilde{Z}_1}{\partial \tilde{q}} = \widetilde{Z}_9, \quad \frac{\partial \widetilde{Z}_2}{\partial \tilde{q}} = \widetilde{Z}_{10}, \quad \frac{\partial \widetilde{Z}_3}{\partial \tilde{q}} = \widetilde{Z}_{11}, \quad \frac{\partial \widetilde{Z}_4}{\partial \tilde{q}} = \widetilde{Z}_{12}.$$

As a result of these new notations, the Newton's iterative scheme takes the following form:

$$\begin{bmatrix}\tilde{p}\\ \tilde{q}\end{bmatrix}^{(n+1)} = \begin{bmatrix}\tilde{p}\\ \tilde{q}\end{bmatrix}^{(n)} - \left(\begin{bmatrix}\widetilde{Z}_5 & \widetilde{Z}_9\\ \widetilde{Z}_7 & \widetilde{Z}_1 1\end{bmatrix}^{-1}\begin{bmatrix}\widetilde{Z}_1\\ \widetilde{Z}_3\end{bmatrix}\right)^{(n)}. \tag{4.18}$$

Now differentiating the system of four first order ODEs with respect to $\tilde{p}$ and $\tilde{q}$ we obtain another system of ODEs as follows.

$$\begin{aligned}
&\widetilde{Z}_5' = \widetilde{Z}_6, && \widetilde{Z}_5(0) = 0,\\
&\widetilde{Z}_6' = -\frac{Pr}{b_1}\Big[\widetilde{A}_3\big(f\widetilde{Z}_6 - \Omega f f'\widetilde{Z}_6\big) + Q\widetilde{Z}_5 + 2Nt\widetilde{Z}_2\widetilde{Z}_6,\\
&\qquad + Nb\widetilde{Z}_2\widetilde{Z}_8 + + Nb\widetilde{Z}_6\widetilde{Z}_4\Big], && \widetilde{Z}_6(0) = 1,\\
&\widetilde{Z}_7' = \widetilde{Z}_8, && \widetilde{Z}_7(0) = 0,\\
&\widetilde{Z}_8' = Le\gamma\widetilde{Z}_7 - Lef\widetilde{Z}_8 - \left(\frac{Nt}{Nb}\right)\widetilde{Z}_6', && \widetilde{Z}_8(0) = -\frac{Nt}{Nb},\\
&\widetilde{Z}_9' = \widetilde{Z}_{10}, && \widetilde{Z}_9(0) = 0,\\
&\widetilde{Z}_{10}' = -\frac{Pr}{b1}\Big[\widetilde{A}_3\big(f\widetilde{Z}_{10} - \Omega f f'\widetilde{Z}_{10}\big) + Q\widetilde{Z}_9 + 2Nt\widetilde{Z}_2\widetilde{Z}_{10},\\
&\qquad + Nb\widetilde{Z}_2\widetilde{Z}_{12} + Nb\widetilde{Z}_{10}\widetilde{Z}_4\Big], && \widetilde{Z}_{10}(0) = 0,\\
&\widetilde{Z}_{11}' = \widetilde{Z}_{12}, && \widetilde{Z}_{11}(0) = 1,\\
&\widetilde{Z}_{12}' = Le\gamma\widetilde{Z}_{11} - Lef\widetilde{Z}_{12} - \left(\frac{Nt}{Nb}\right)\widetilde{Z}_{10}', && \widetilde{Z}_{12}(0) = 0.
\end{aligned}$$

The set stopping criteria for Newton's technique are as follows.

$$max\left\{\left|\widetilde{Z}_1\big(\zeta_\infty, \tilde{p}, \tilde{q}\big)\right|, \left|\widetilde{Z}_3\big(\zeta_\infty, \tilde{p}, \tilde{q}\big)\right|\right\} < \epsilon.$$

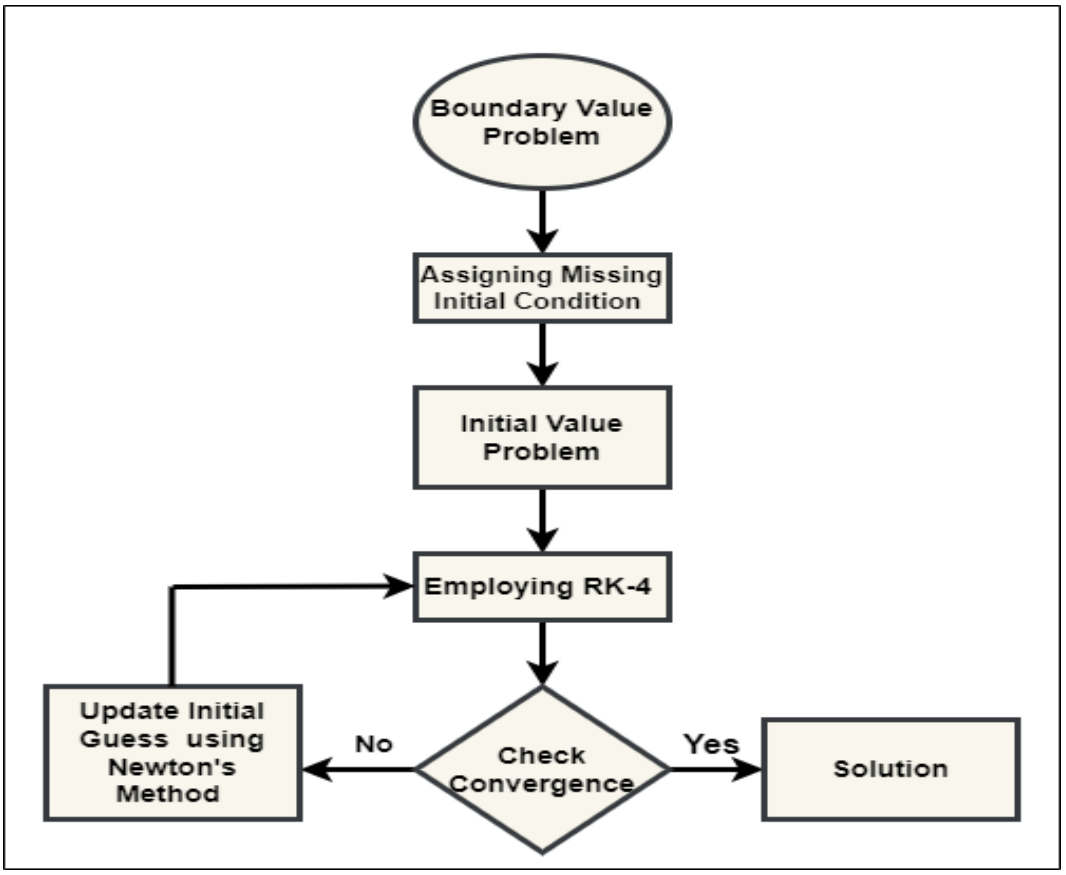

FIGURE 4.3: The shooting method's methodological framework

4.5 Result Interpretation

After transforming the governing PDEs describing the fluid flow into a system of ODEs, several crucial parameters emerge. The impact of these physical parameters on the velocity $f'(\zeta)$, temperature $\theta(\zeta)$, and concentration of nanoparticle $\phi(\zeta)$ distributions is thoroughly investigated through the use of graphical representations. The significance and interpretations the impact of each parameter in this study are discussed in detail, and the study's results are comprehensively presented.

4.5.1 Analysis of Computational Result

Here an investigation is carried out to highlight the impact of various physical parameters on the coefficient of skin friction, the local Nusselt number and local Sherwood number. An increment in the magnetic field coefficient, Forchheimer number and Darcy

number reduces the coefficient of skin friction, while the local Nusselt number decreases with higher values of the nonlinear thermal radiation parameter, heat generation/absorption parameter, and temperature ratio parameter. The skin friction is observed to vary prominently for the magnetic field coefficient, Darcy number, and non-Newtonian Williamson and Forchheimer parameter.

TABLE 4.3: The numerical result of the physical quantities like skin fraction $\left(C_f\sqrt{Re_x}\right)$,local Nusselt number $\left(Re_x^{-1/2}Nu_x\right)$ and Sherwood number $\left(Re_x^{-1/2}Sh_x\right)$ for values of M, K_p, W_e and S parameters when $Pr = 6.2$, $Q = -0.1$, $Nb = Ec = 0.2$, $Nt = 0.5$, $Le = 2$, $\gamma = 0.4$ and $\Omega = 0.3$.

M	K_p	We	Fr	$-f''(0)$	$Re^{1/2}Cf_x$	$-\theta'(0)$	$Re_x^{-1/2}Nu_x$	$Re_x^{-1/2}Sh_x$
0.2	0.5	0.2	0.4	1.512624	-1.617169	0.532864	0.693639	-1.332159
0.4				1.605807	-1.697944	0.457554	0.595607	-1.143886
0.6				1.695904	-1.773963	0.387058	0.503841	-0.967645
0.8				1.783426	-1.845852	0.320672	0.417425	-0.801680
	0.1			1.320918	-1.444111	0.617194	0.803414	-1.542986
	0.3			1.418916	-1.533733	0.573801	0.746928	-1.434504
	0.5			1.512624	-1.617169	0.532864	0.693639	-1.332159
	0.7			1.602826	-1.695393	0.494040	0.643101	-1.235080
		0.1		1.430725	-1.673294	0.554481	0.721778	-1.386202
		0.2		1.512624	-1.617169	0.532864	0.693639	-1.332160
		0.3		1.629234	-1.550726	0.506087	0.658783	-1.265218
		0.4		1.835800	-1.463424	0.469708	0.611427	-1.174269
			0.2	1.456906	-1.567825	0.548996	0.714639	-1.372490
			0.4	1.512624	-1.617169	0.532864	0.693639	-1.332159
			0.6	1.567228	-1.664768	0.517126	0.673153	-1.292816
			0.8	1.620827	-1.710759	0.501756	0.653145	-1.254389

TABLE 4.4: The numerical result of embedded parameters on local Nusselt and Sherwood number, respectively. when $M = We = 0.2$, $Fr = 0.4$ and $Kp = 0.5$.

R	Nb	Nt	Pr	Le	Q	Ec	γ	Ω	$-\theta'(0)$	$Re_x^{-1/2}Nu_x$	$Re_x^{-1/2}Sh_x$
1.2	0.2	0.5	6.2	2	-0.1	0.2	0.4	0.3	0.532864	0.693638	-1.332159
0.1									0.610153	0.794247	-1.525381
0.5									0.5812802	0.756663	-1.453201
0.9									0.5527918	0.719580	-1.381980
	0.1								0.532864	0.693639	-2.664318
	0.3								0.532864	0.693639	-0.888106
	0.5								0.532864	0.693639	-0.532864
	0.7								0.532864	0.693639	-0.380617
		0.1							0.661177	0.860666	-0.330588
		0.3							0.596069	0.775949	-0.894144
		0.5							0.532864	0.693639	-1.332159
		0.7							0.472089	0.614527	-1.652312
			5						0.497208	0.647225	-1.243020
			6						0.527576	0.686755	-1.318939
			7						0.551825	0.718321	-1.379563
			8						0.573121	0.743680	-1.428303
				1					0.586778	0.763820	-1.466944
				2					0.532864	0.693639	-1.332159
				3					0.498335	0.648693	-1.245839
				4					0.474025	0.616047	-1.185061
					-0.3				0.794713	1.034493	-1.986782
					-0.1				0.532864	0.693639	-1.332159
					0.1				0.173135	0.225372	-0.432836
					0.2				-0.103405	-0.134605	0.258513
						0.1			0.732032	0.952900	-1.830081
						0.2			0.532864	0.693639	-1.332159
						0.3			0.333015	0.433492	-0.832537
						0.4			0.132476	0.172446	-0.331189
							0.3		0.5411360	0.704406	-1.352839
							0.4		0.532864	0.963639	-1.33259
							0.5		0.524898	0.683269	-1.312244
							0.6		0.517344	0.673437	-1.293361
								0.1	0.522487	0.680131	-1.306217
								0.2	0.527516	0.686677	-1.318789
								0.3	0.532864	0.693639	-1.332159
								0.4	0.538565	0.701060	-1.346413

4.5.2 Velocity Profile

Understanding the velocity distributions is essential for a deeper view of the fluid flow and its related characteristics. The external forces acting upon the flowing fluids, are expected to affect fluid's motion. One such external force is the magnetic field.

In Figure 4.4, the impact of the magnetic field parameter (M) on the velocity profile $f'(\zeta)$ is depicted. The results show a negative effect for both fluids, indicating an inverse relationship between the magnetic field strength and the velocity distribution. As the magnetic parameter values increase, the velocity of both fluids decreases. This phenomenon occurs because when a moving fluid, whether it is a MoS_2/H_2O or $MoS_2 + GO/H_2O$ fluid, is influenced by the magnetic field, the fluid particles experience stimulation, resulting in a counter force that hinders and reduces the fluid's motion. This counter force, known as the Lorentz force, acts perpendicular to both the velocity vector and the magnetic field vector, leading to a resistance in the flow.

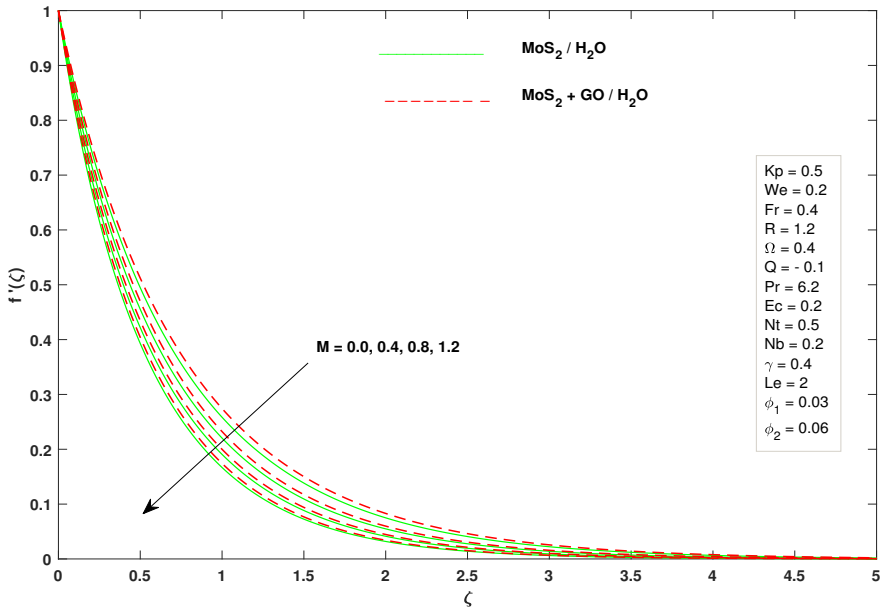

FIGURE 4.4: Effect of M on $f'(\zeta)$

The results from Figure 4.5 clearly reveal a similar trend for both fluids. As the value of the non-Newtonian Williamson parameter We increases, a significant decrement in the velocity $f'(\zeta)$ can be seen.

This behavior can be attributed to the non-Newtonian characteristics of fluid, where the influence of the Williamson parameter We on their flow behavior becomes evident.

With an increasing Williamson parameter, the resistance to flow within each fluid intensifies, leading to a higher internal friction and deformation. Consequently, the fluid particles experience a greater hindrance, resulting in a reduction in their respective velocities. Physically, this response can be explained by the non-linear relationship between shear stress and velocity gradient of the non-Newtonian fluids. The non-Newtonian Williamson parameter governs the extent of this non-linearity, and its elevation leads to more constrained flow, subsequently decreasing the velocity of both the fluids.

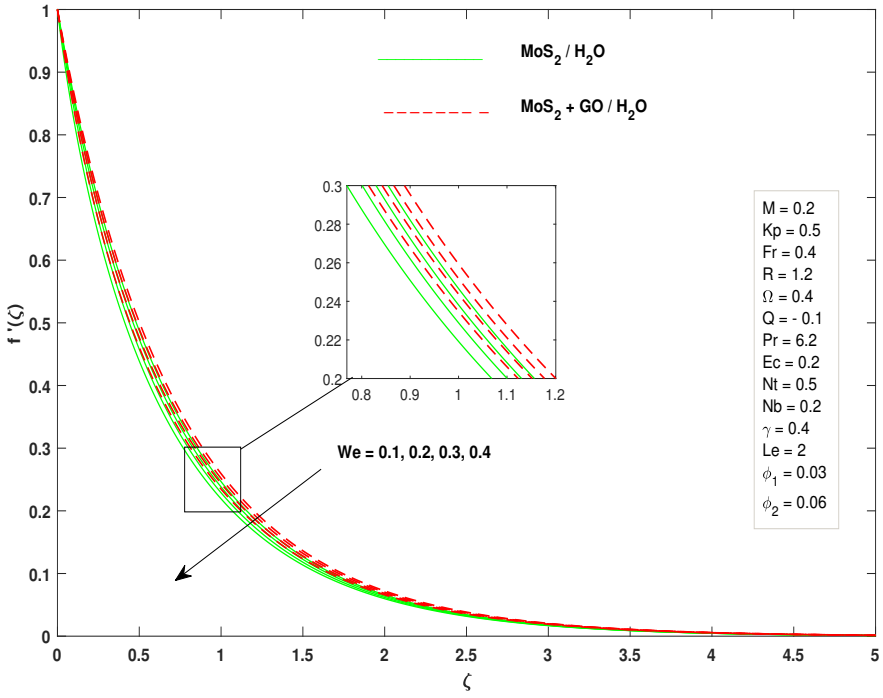

FIGURE 4.5: Effect of We on $f'(\zeta)$

In Figure 4.6, the impact of the Forchheimer parameter (Fr) on the velocity distribution is depicted. The findings demonstrate that as the value of Fr increases, the fluid's velocity profiles are significantly reduced. This behavior arises due to the direct relationship between the inertia coefficient and the drag coefficient. Higher Fr values lead to an increase in the drag coefficient, resulting in an elevated resistive force within the fluid. As a consequence, the fluid experiences greater hindrance to its movement, leading to a decline in the velocity. The influence of increasing Fr values is particularly notable in relation to the thermal boundary layer. As Fr increases, the thermal boundary layer thickens, effectively impeding the fluid's passage. This phenomenon restricts the fluid flow, making it less facile.

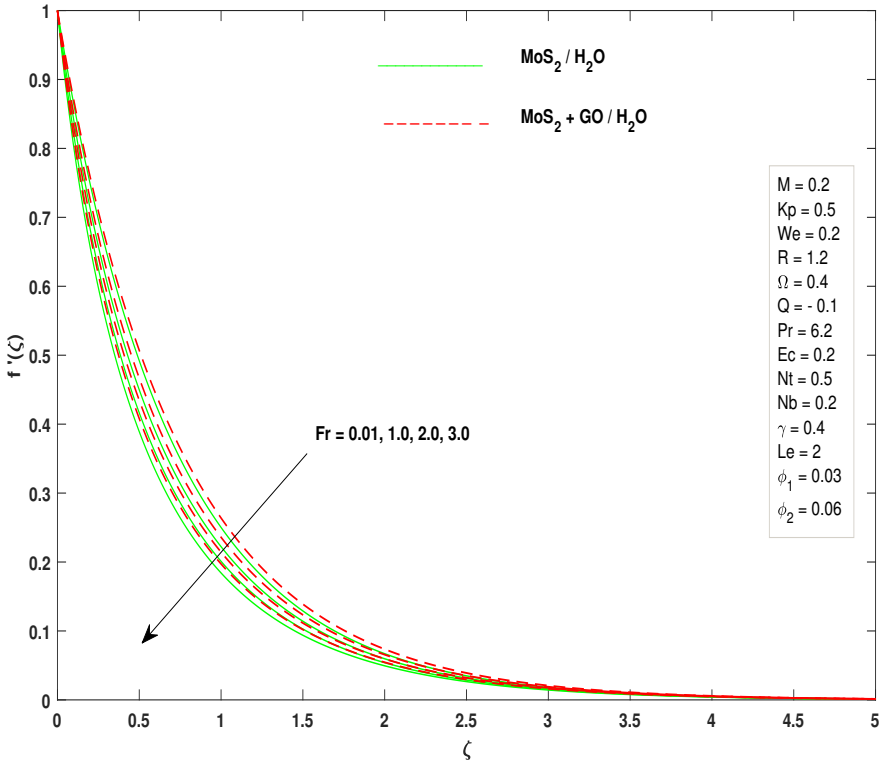

FIGURE 4.6: Effect of Fr on $f'(\zeta)$

To investigate the impact of the porosity parameter Kp on the velocity distribution, we refer to Figure 4.7. The results from Figure 4.7 clearly demonstrate that the velocity distribution experiences a depressive trend when influenced by higher values of the porosity parameter. The physical explanation lies in the nature of a porous medium, which contains a network of small voids or pores that impede the fluid's motion as it flows through the medium. The porosity parameter is directly related to the fluid's permeability through the porous medium. As the porosity parameter increases, the resistance offered by the porous medium to the fluid's movement becomes greater. As a consequence, with larger values of the porosity parameter, the fluid experiences a higher resistance both from the porous medium and its inherent viscosity. This combined effect results in a notable decrease in the fluid's velocity within the porous medium. The impact of the volume fraction ϕ_1 of MoS_2 on the velocity profile $f'(\zeta)$ is illustrated in Figure 4.8. Here, it becomes evident that as ϕ_1 increases, the velocity of the fluid decreases. This phenomenon can be attributed to the corresponding increase in viscosity with rising ϕ_1. Consequently, heightened viscosity exerts a decelerating effect on the flow.

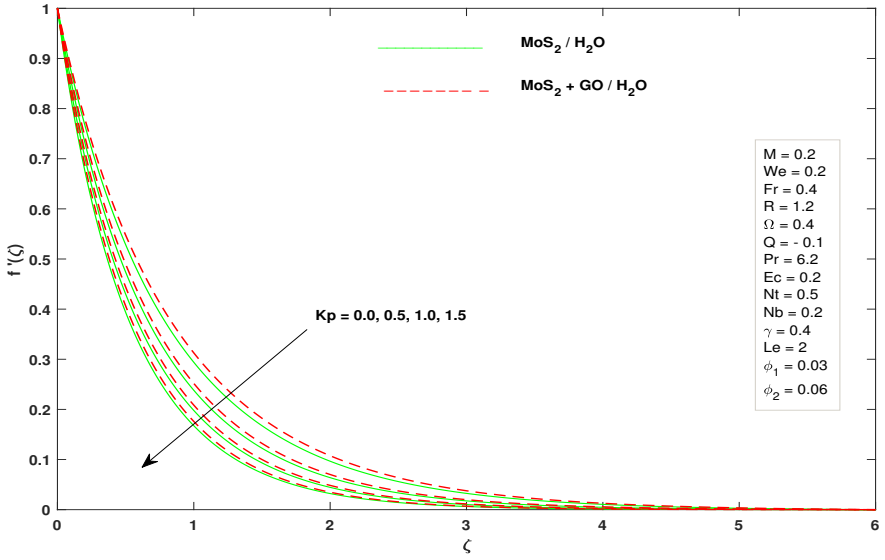

FIGURE 4.7: Effect of Kp on $f'(\zeta)$

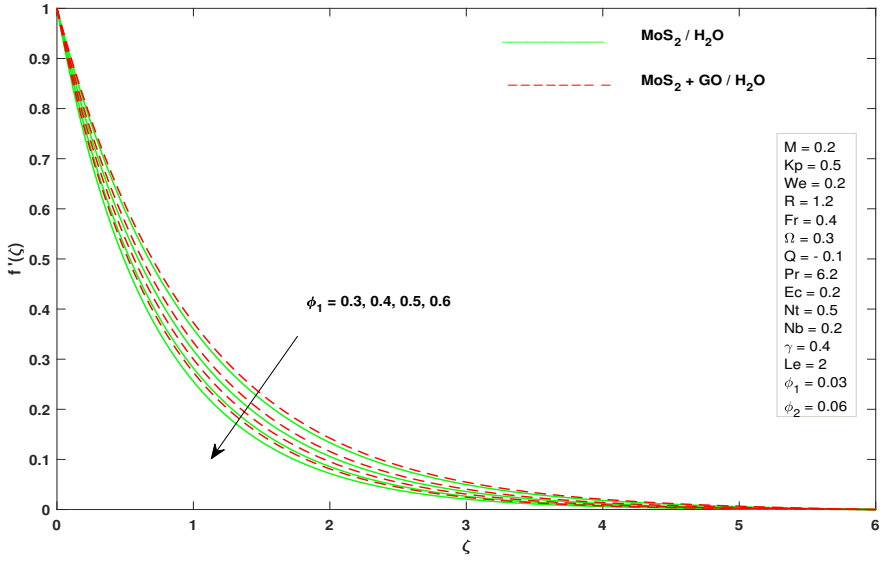

FIGURE 4.8: Effect of ϕ_1 on $f'(\zeta)$

4.5.3 Temperature Profile

Here we examine the influence of several physical parameters on the temperature distribution, denoted as $\theta(\zeta)$, for two different fluids. In Figures 4.9 and 4.10, we study the effect of the magnetic field coefficient (M) and the porosity parameter (Kp) on the temperature distribution for both fluids.

For both fluids, an augmentation in the porosity parameter (Kp) leads to elevate the temperature and the boundary layer. The higher resistance of the porous medium impedes fluid flow, intensifying the internal friction and heat generation, leading to a higher temperatures. Similarly, an increase in the magnetic field coefficient (M) leads to elevate fluid temperature. The intensified magnetic forces restrict fluid movement, increasing internal friction and heat generation, resulting in a higher temperature.

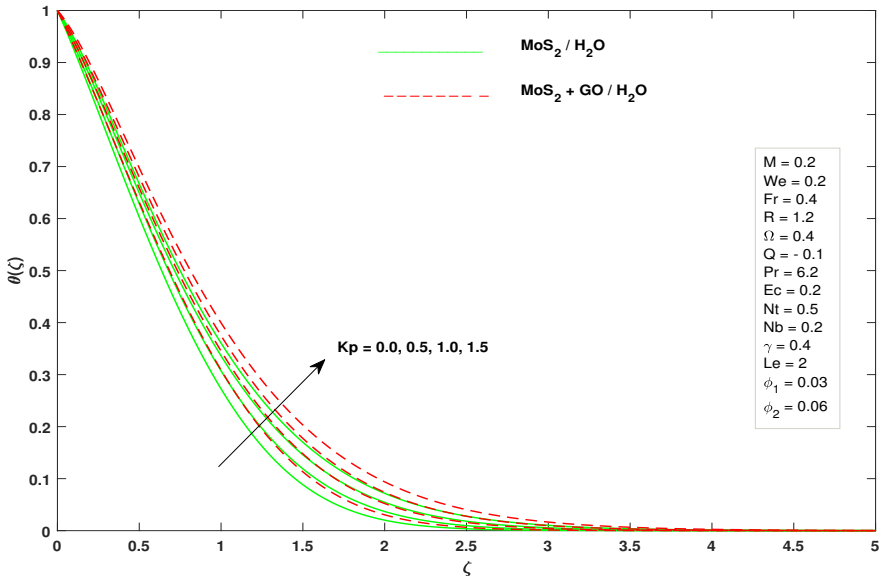

FIGURE 4.9: Effect of Kp on profile $\theta(\zeta)$

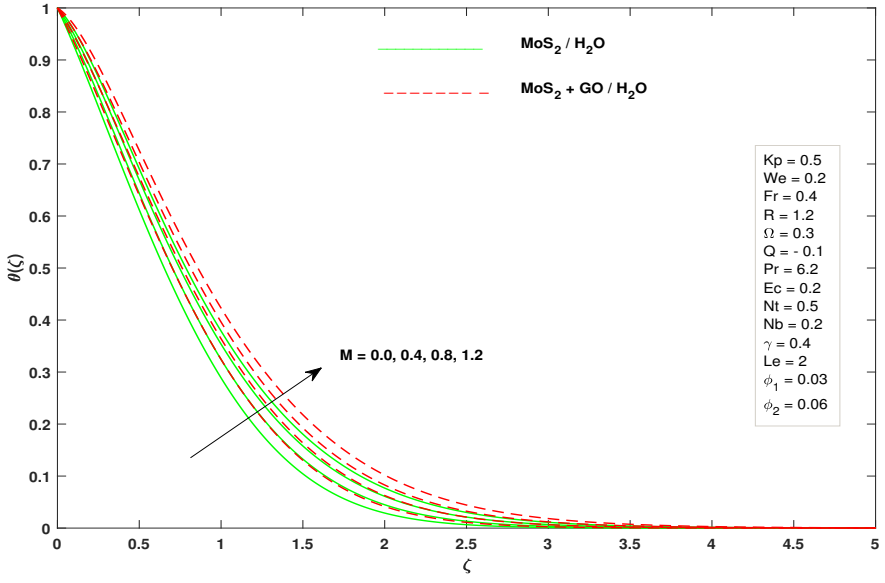

FIGURE 4.10: Effect of Kp on profile $\theta(\zeta)$

Figure 4.11 illustrates the relationship between the non-Newtonian Williamson parameter We and the fluid's temperature distribution $\theta(\zeta)$. Notably, an increase in We leads to a rise in the fluid's temperature for both fluids. This can be attributed to the intensified resistance and deformation experienced by non-Newtonian fluids as the We parameter increases, resulting in a greater heat generation within the fluid and subsequently a higher temperatures.

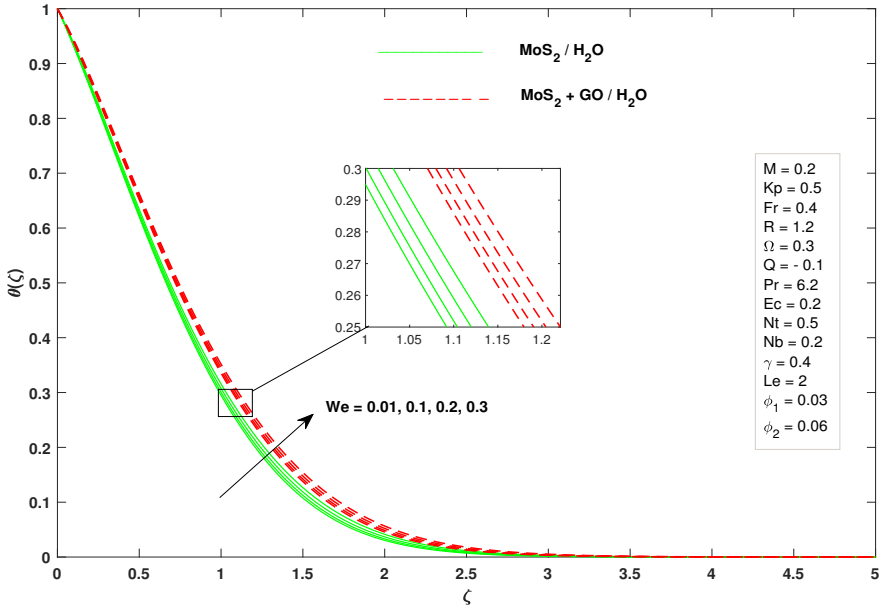

FIGURE 4.11: Effect of We on profile $\theta(\zeta)$

In Figure 4.12, we observe a correlation between the Forchheimer parameter Fr and the temperature distribution for both fluids. The results clearly demonstrate that as Fr increases, the temperature of the fluid also rises. This effect is attributed to the increased drag coefficient and resistance force experienced by the fluid with larger Fr values, leading to heighten the heat generation and higher fluid temperature.

Figure 4.13 presents the effect of the nonlinear thermal radiation parameter R on the temperature distribution. Remarkably, higher values of this parameter lead to an enhancement in the heat transfer within the fluids, stimulating their thermal behavior. Physically, the positive effect of the nonlinear thermal radiation parameter on the fluid's temperature is based on three key factors. Firstly, it promotes heat transfer across the boundary layer, resulting in a systematic temperature rise. Secondly, it facilitates the absorption of thermal energy by nanoparticles in the fluid, thus improving the thermal diffusion due to the nanoparticles enhanced thermal conductivity. Thirdly, it augments

the thermal transfer mechanisms within the fluids, encompassing both conduction and heat transfer by load.

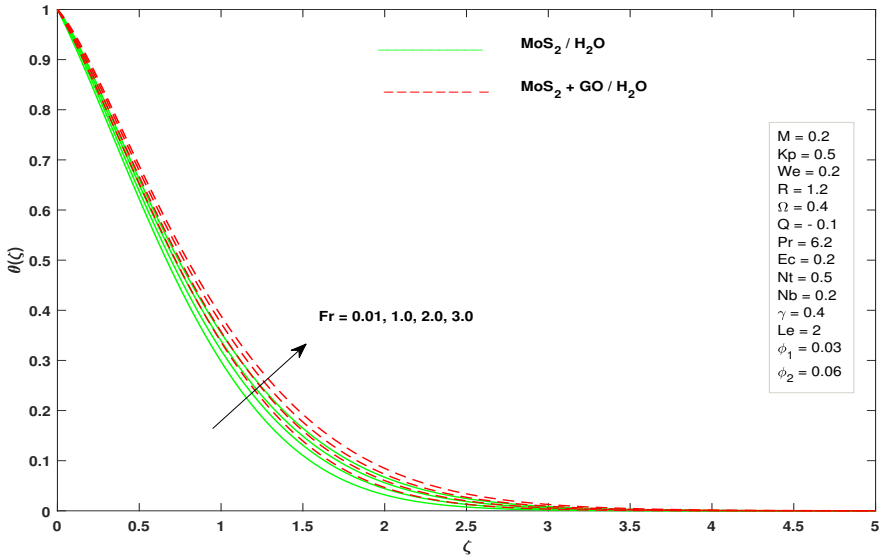

FIGURE 4.12: Effect of Fr on profile $\theta(\zeta)$

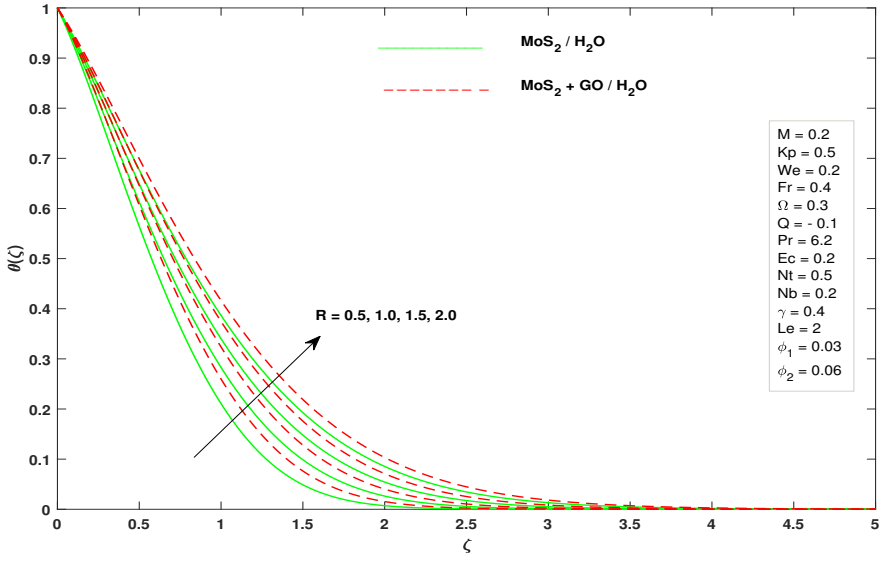

FIGURE 4.13: Effect of R on profile $\theta(\zeta)$

Moving forward, Figure 4.14 depicts the impact of the heat generation/absorption parameter Q on the temperature distribution for both fluids. The results reveal a significant enhancement in the temperature distribution with increasing values of this parameter. In case of heat generation ($S > 0$), there is an overall improvement in the heat transfer and thermal distribution, leading to increase the fluid temperature and a thicker

boundary layer. Conversely, in case of heat absorption ($S < 0$), an opposite effect is experienced. Notably, transitioning from heat absorption to heat generation enhances the thermal diffusion and the thickness of the boundary layer.

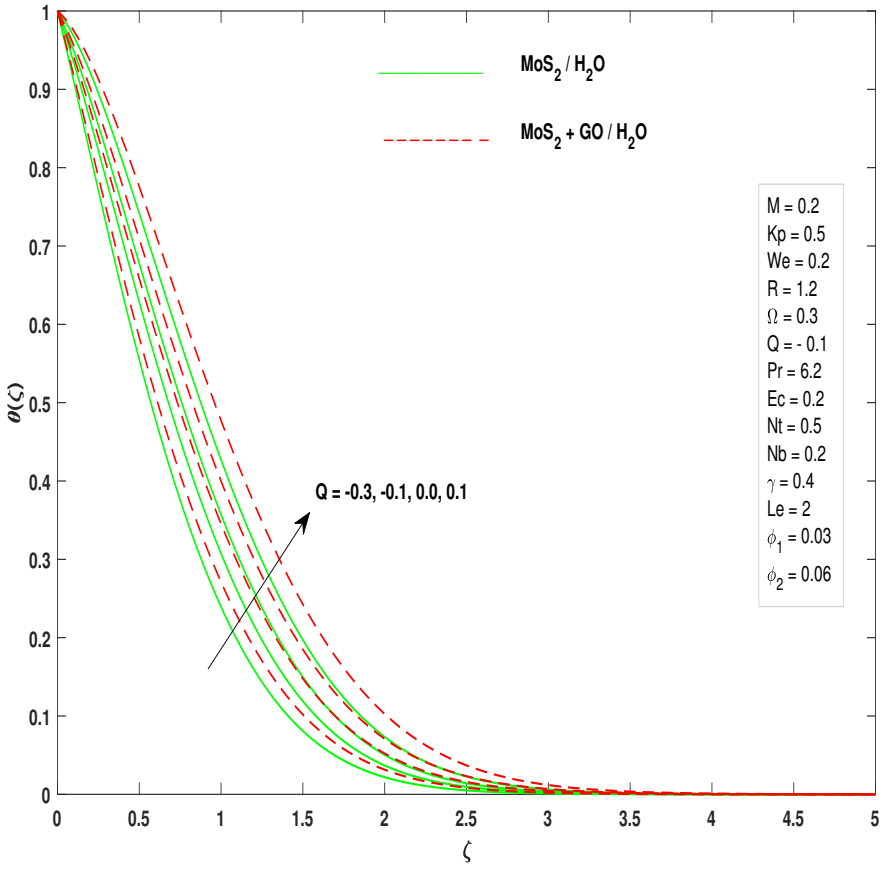

FIGURE 4.14: Effect of Q on profile $\theta(\zeta)$

Figure 4.15 explores the relationship between the Prandtl number Pr and the temperature distribution for both fluids. Larger Prandtl number values ($Pr > 1$) indicate that momentum diffusion prevails over thermal diffusion, resulting in a fall in the fluid's temperature and the thickness of the boundary layer.

In Figure 4.16, we observe that increasing the Eckert number (Ec) leads to higher fluid temperatures for both the nanofluid and the hybrid nanofluid. Physically, the effect of the Eckert number on the temperature distribution can be understood through the fluid's energy conversion. With higher Ec values, the fluid's kinetic energy dominates, and the excessive kinetic energy is converted into thermal energy. This process leads to increase the heat generation within the fluid, subsequently raising the fluid's temperature.

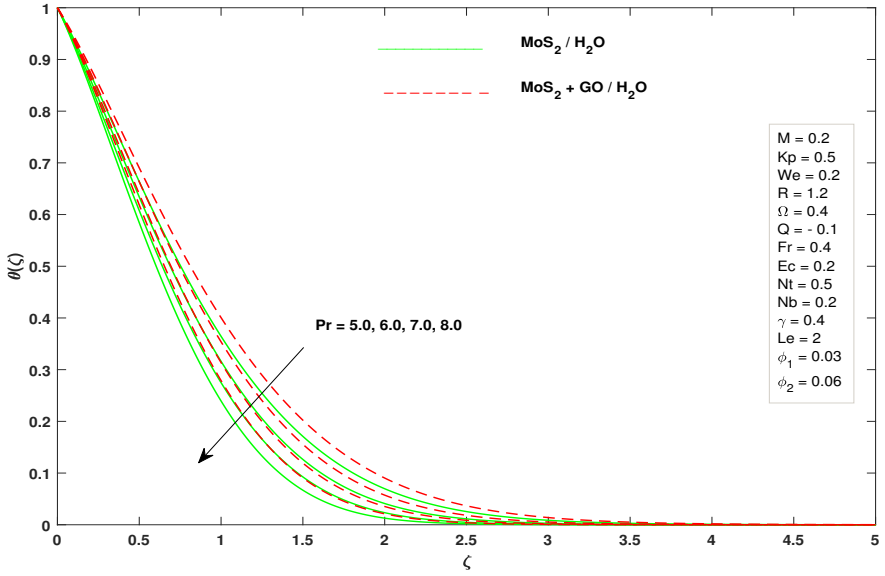

FIGURE 4.15: Effect of Pr on profile $\theta(\zeta)$

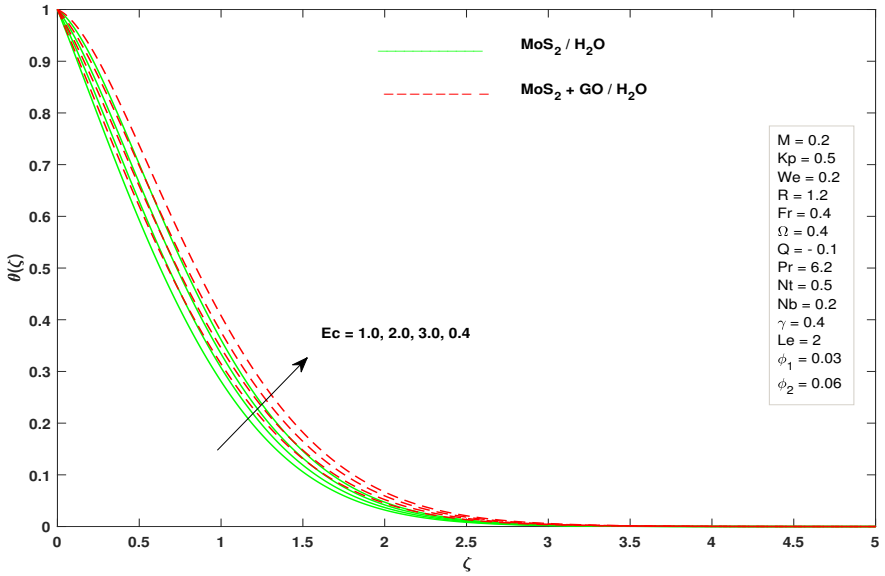

FIGURE 4.16: Effect of Ec on profile $\theta(\zeta)$

The impact of the thermophoresis parameter Nt on the temperature distribution has been noticed through figure 4.17. An increase in Nt values directly enhances the fluid's temperature distribution. This effect is attributed to the process of thermal potential difference, where fluid particles absorb heat energy, leading to their movement from hotter to colder regions and enhancing the convection mechanism. This process effectively raises the fluid's temperature and increases the thickness of its boundary layer.

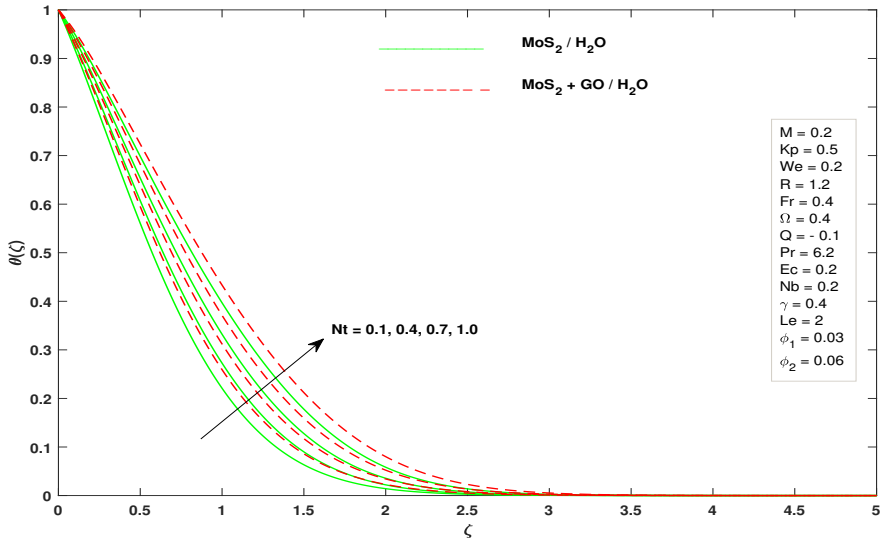

FIGURE 4.17: Effect of Nt on profile $\theta(\zeta)$

Figure 4.18 explores the impact of the time relaxation parameter Ω on the temperature distribution. Interestingly, an increase in Ω results in a decrease in the temperature of both the fluids. This can be explained by the fluid's longer response time to changes in external forces with larger Ω values, leading to slower adjustments in temperature and subsequently lower overall temperatures.

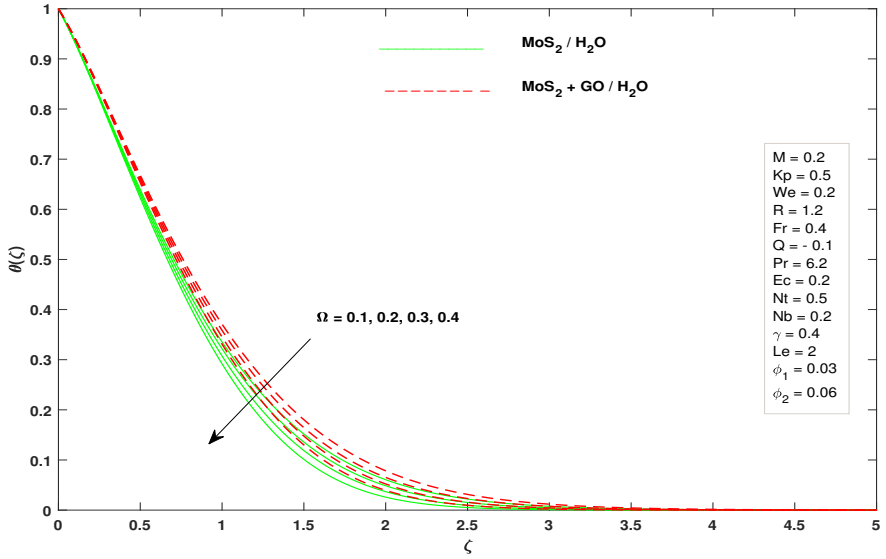

FIGURE 4.18: Effect of Ω on profile $\theta(\zeta)$

In Figures 4.19 and 4.20, we observe that increasing the chemical reaction parameter (γ) and the Lewis number (Le) leads to rise the fluid's temperatures for both the fluids. The

rise in γ intensifies the heat generation through chemical reactions, while an increase in Le enhances thermal diffusion within the fluid, resulting in elevated temperatures.

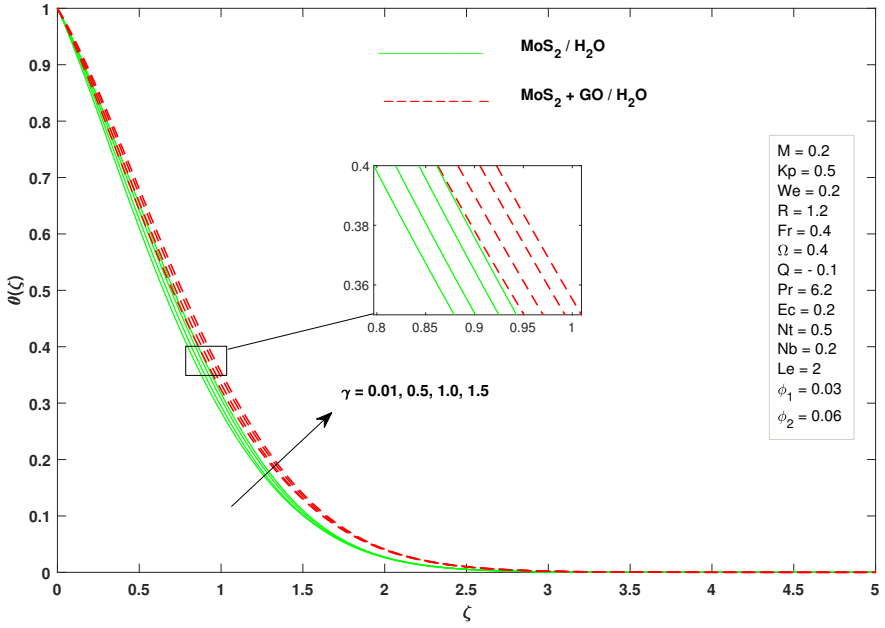

FIGURE 4.19: Effect of γ on profile $\theta(\zeta)$

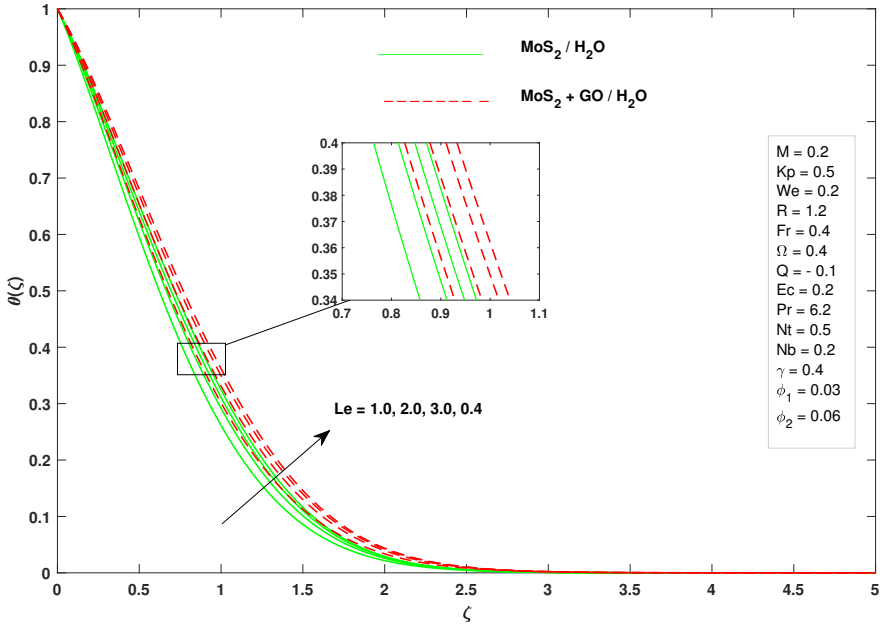

FIGURE 4.20: Effect of Le on profile $\theta(\zeta)$

Figure 4.21 delves into the influence of ϕ_1 on the temperature profile. In this case, as ϕ_1 increases, the temperature of the fluid rises. This temperature elevation can be

attributed to the concurrent increase in thermal conductivity associated with higher ϕ_1 values. As a result, the augmented thermal conductivity leads to an increase in temperature within the fluid.

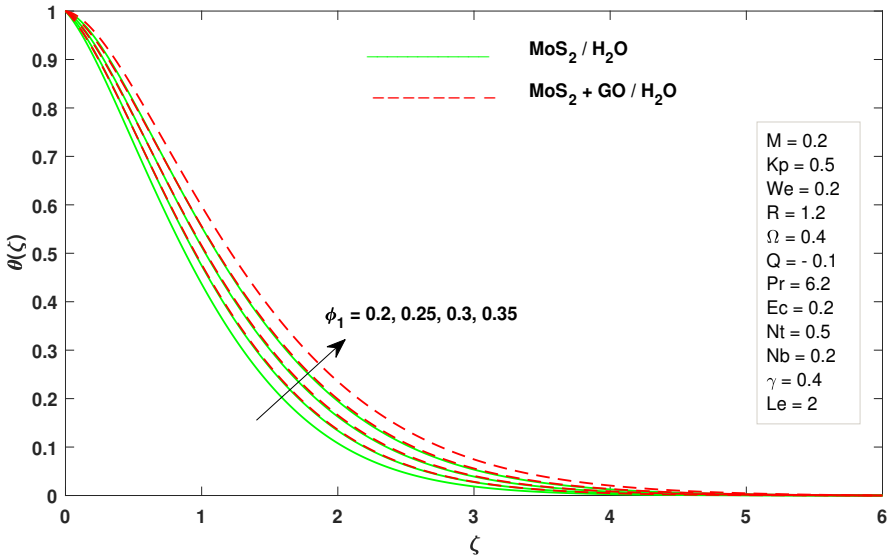

FIGURE 4.21: Effect of ϕ_1 on profile $\theta(\zeta)$

In conclusion, the investigation of the fluid temperature distribution reveals significant effects of various physical parameters on both the nanofluid and the hybrid nanofluid. Understanding these influences is vital for practical applications and provides valuable insights into fluid's behavior within different conditions and environments.

4.5.4 Analysis of the Concentration Profile

The concentration of nanoparticles within a fluid plays a significant role in determining various properties and applications of the fluid. For instance, the thermal and electrical conductivity of a nanofluid is directly related to the concentration of nanoparticles present in it. In this context, Figures 4.22 and 4.23 provide valuable insights into the effect of both the magnetic field parameter (M) and the porosity parameter (Kp) on the distribution of the nanoparticle concentration $\phi(\zeta)$.

Initially, as the magnetic field parameter (M) and the porosity parameter (Kp) increase, the fluid's movement is slowed down, which leads to an accumulation of nanoparticles and subsequently a higher nanoparticle concentration. The reduced fluid flow under the influence of the magnetic field causes nanoparticles to gather in specific regions, leading

to an initial rise in concentration.

However, as the concentration of nanoparticles increases, the interaction between the nanoparticles themselves and their surroundings becomes more significant. This interaction can result in particle aggregation, clustering and hindered movement, especially in regions with higher nanoparticles' concentration. As a consequence, there is a temporary decrease in the concentration profile due to these localized effects, counteracting an initial increase.

Subsequently, as the nanoparticle concentration reaches a certain critical point, the cumulative effect of nanoparticle-pore collisions in the porous medium become more pronounced. This contributes to a consistent rise in nanoparticle concentration beyond the initial fluctuations, resulting in a long-term increasing trend.

The fluctuating behavior is more pronounced in the hybrid nanofluid due to the presence of graphene oxide (GO) nanoparticles, which introduces additional complexities to the system. The GO nanoparticles can exhibit unique interactions with the other nanoparticles and the surrounding fluid, leading to more variations in concentration profiles.

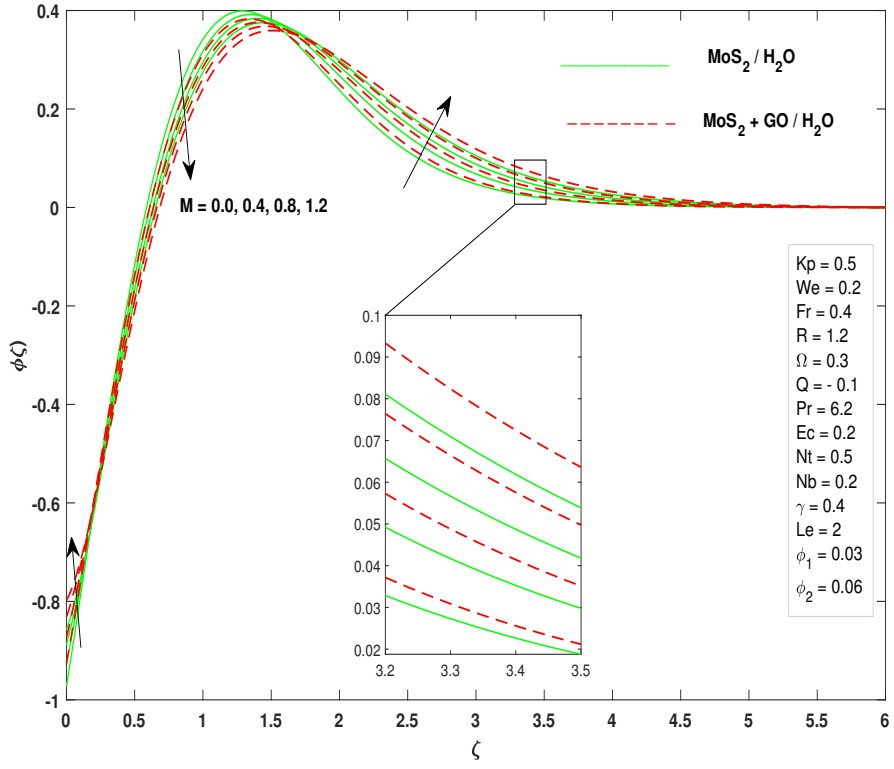

FIGURE 4.22: Effect of M on profile $\phi(\zeta)$

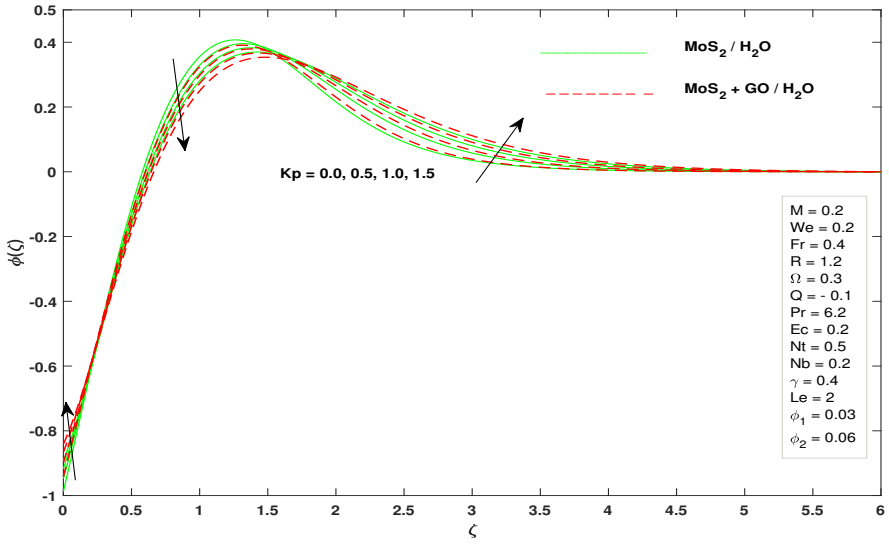

FIGURE 4.23: Effect of Kp on profile $\phi(\zeta)$

In Figures 4.24 and 4.25, we investigate the impact of two essential parameters, the non-Newtonian Williamson parameter (We) and the Forchheimer number (Fr), on the distribution of nanoparticle concentration $\phi(\zeta)$ within the fluid.

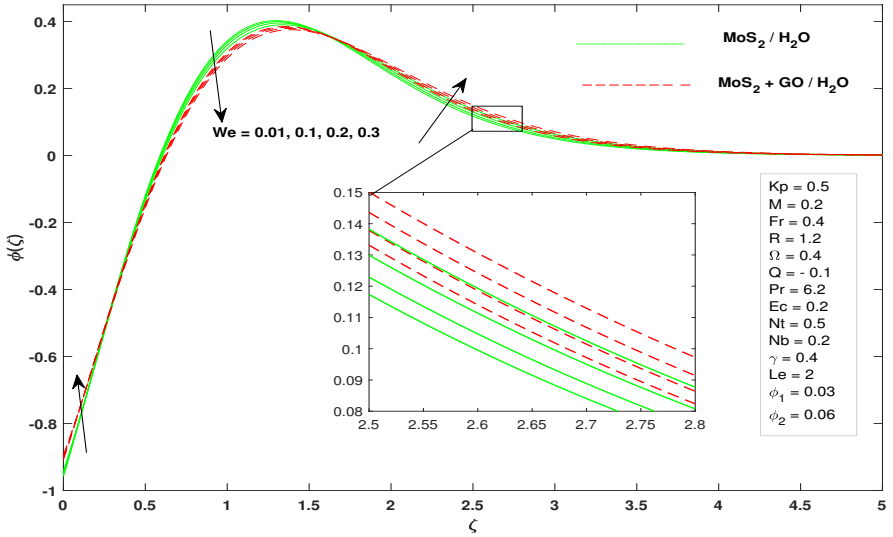

FIGURE 4.24: Effect of We on profile $\phi(\zeta)$

As the non-Newtonian Williamson parameter (We) and the Forchheimer number (Fr) increase, the nanoparticle concentration initially rises due to a reduction in the fluid movement caused by these parameters. The slowing fluid flow allows nanoparticles to accumulate in specific regions, leading to hike concentration. However, as the nanoparticle

concentration reaches a certain level, localized effects such as nanoparticle aggregation or hindered movement can lead to a temporary decrease in the concentration. Following this temporary dip, the nanoparticle concentration continues to rise steadily for both fluids. This continued increase is attributed to the cumulative impact of nanoparticle-pore collisions and the overall interactions among the nanoparticles within the fluid.

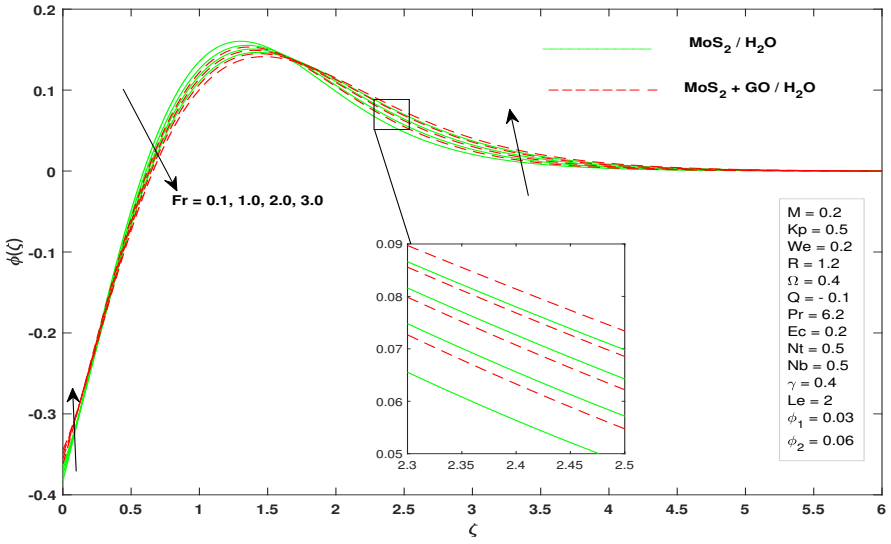

FIGURE 4.25: Effect of Fr on profile $\phi(\zeta)$

Figures 4.26 and 4.27 explore the impact of the nonlinear thermal radiation parameter (R) and the heat generation/absorption parameter (Q) on the distribution of nanoparticle concentration.

In Figure 4.26, as the nonlinear thermal radiation parameter increases, it results in stronger nanoparticle temperatures and thickening of the fluid's boundary layer, leading to an enhanced temperature distribution throughout both fluids. This increment initially stimulates nanoparticles' movement and accumulation, causing an initial rise in nanoparticles' concentration for both the nanofluid and the hybrid nanofluid. However, after reaching a certain critical point, localized effects, such as nanoparticle aggregation or hindered movement, cause a temporary decrease in the concentration profile for both fluids. Subsequently, beyond this critical point, the nanoparticle concentration resumes its upward trend in both fluids, driven by cumulative nanoparticle-pore collisions and fluid interactions.

In Figure 4.27, the effect of the heat generation/absorption parameter (Q) on nanoparticle concentration $\phi(\zeta)$ is evident for both fluids. Increasing the heat generation enhances

fluid's temperature and concentration, while heat absorption results in the opposite effect, as depicted in the figure. Similar to Figure 4.27, an initial rise in nanoparticles' concentration is observed for both fluids as the heat generation parameter increases. However, after reaching a bit away from the surface, the concentration profile temporarily decreases for both fluids due to localized effects. Beyond this critical point, the concentration of nanoparticles's consistently increase, influenced by the cumulative nanoparticle-pore collisions.

Indeed, the same situation can also be seen in the case of the effect of Eckert number (Ec) on nanoparticle concentration distribution, as shown in figure 4.28.

As the Eckert number (Ec) increases, convective heat transfer intensifies, initially raising nanoparticle concentration in both fluids. However, a temporary dip occurs beyond a specific height above the wall, likely due to localized effects. Subsequently, nanoparticle concentration continues to rise steadily for both the nanofluid and hybrid nanofluid, driven by cumulative nanoparticle-pore interactions.

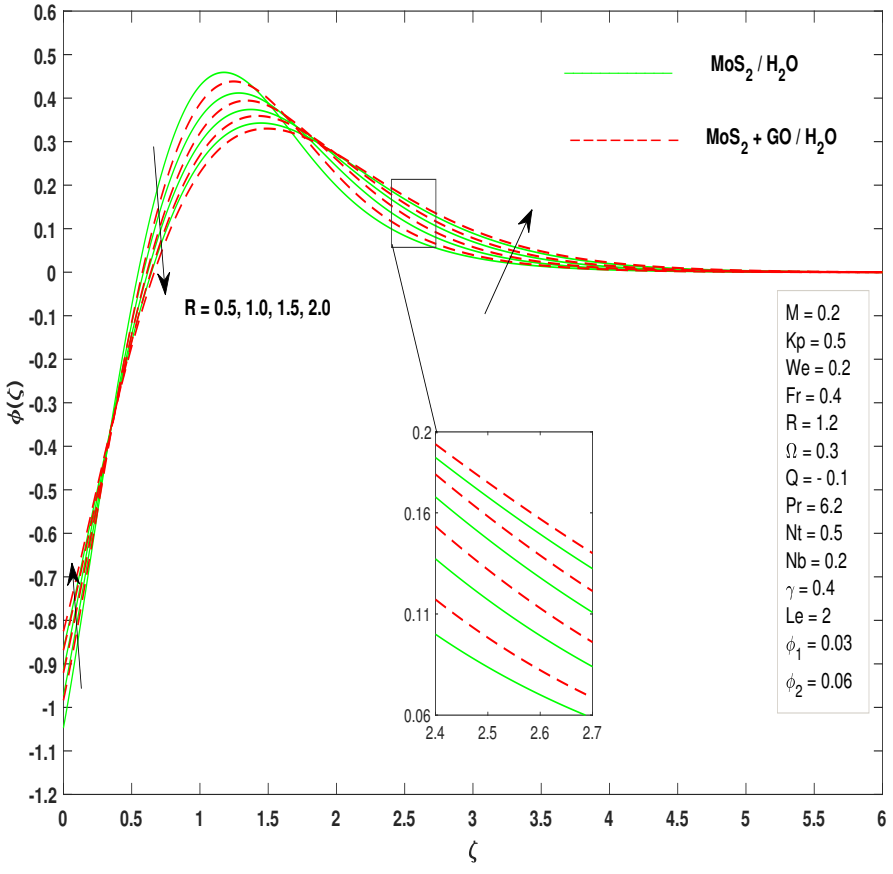

FIGURE 4.26: Effect of R on profile $\phi(\zeta)$

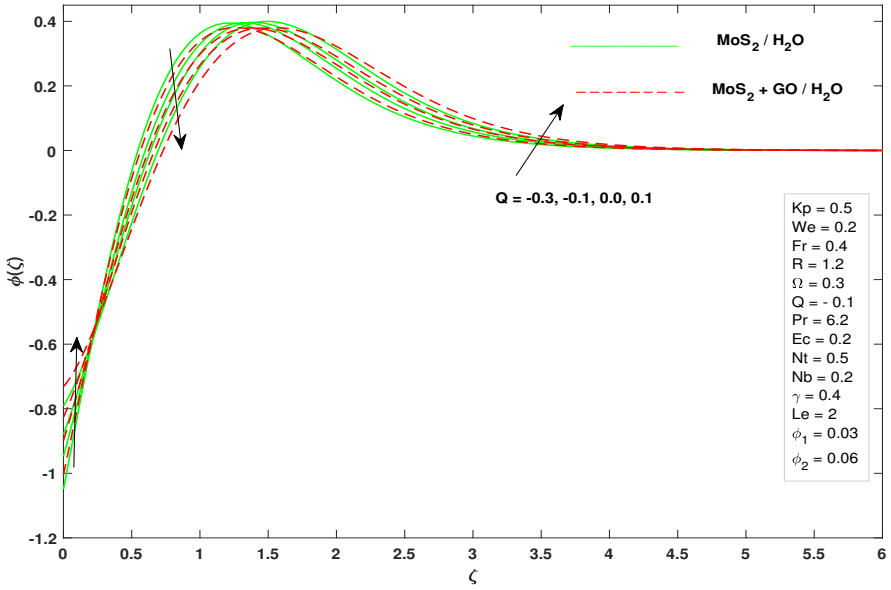

FIGURE 4.27: Effect of Q on profile $\phi(\zeta)$

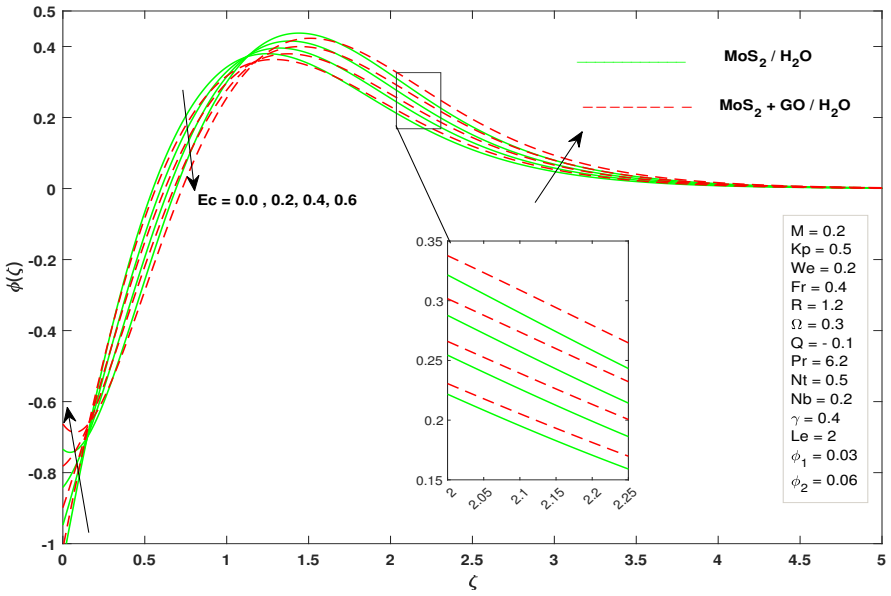

FIGURE 4.28: Effect of Ec on profile $\phi(\zeta)$

For both the fluids, Figures 4.29 and 4.30 demonstrate the negative impact of the Prandtl number (Pr) and the time relaxation parameter (Ω) on nanoparticle concentration. The observed scenario of initial decrease, followed by an increase and then a subsequent decrease in the concentration for both the Prandtl number and the time relaxation parameter (Ω) can be understood through the physical interactions within the fluids.

When the Prandtl number increases, the dominance of momentum diffusion over thermal diffusion results in reduction in the concentration. This happens because the fluid's momentum carries more energy and affects the nanoparticles movement, leading to a localized drop in the concentration. However, as the Prandtl number further increases, the thermal diffusion eventually catches up, leading to a temporary increase in nanoparticle concentration. At this point, the energy transfer from the fluid's momentum to the nanoparticles becomes more balanced, causing a transient rise in the concentration. Subsequently, after a particular height above the wall, the momentum diffusion begins to overpower the thermal diffusion significantly, resulting in a decline in the concentration again. The dominance of momentum diffusion leads to a decrease in the localized nanoparticle accumulation, causing the concentration to revert to its original decreasing pattern.

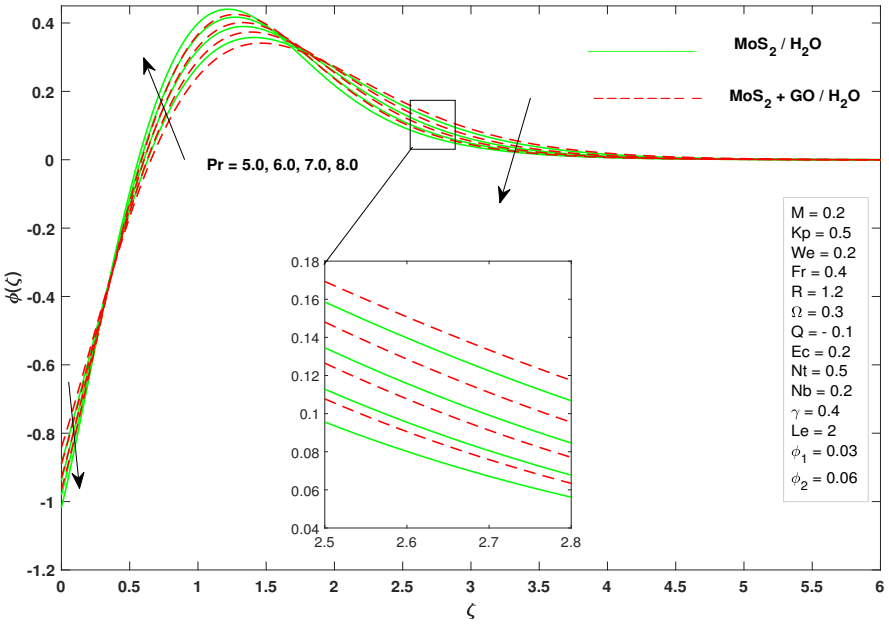

FIGURE 4.29: Effect of Pr on profile $\phi(\zeta)$

Similarly, for the time relaxation parameter (Ω), an initial decrease in the nanoparticle concentration is noticed owing to the effect of fluid movement on the nanoparticles. As Ω increases, the fluid's relaxation time becomes more significant, affecting the nanoparticles' behavior and leading to a temporary reduction in the concentration. However, as the relaxation effect stabilizes, a temporary increase in the nanoparticle concentration is observed. This occurs because the relaxation mechanism allows nanoparticles to accumulate in certain regions for a shorter period. Yet the overall influence of the fluid

momentum starts to dominate again, leading to a decrease in the concentration profile as before.

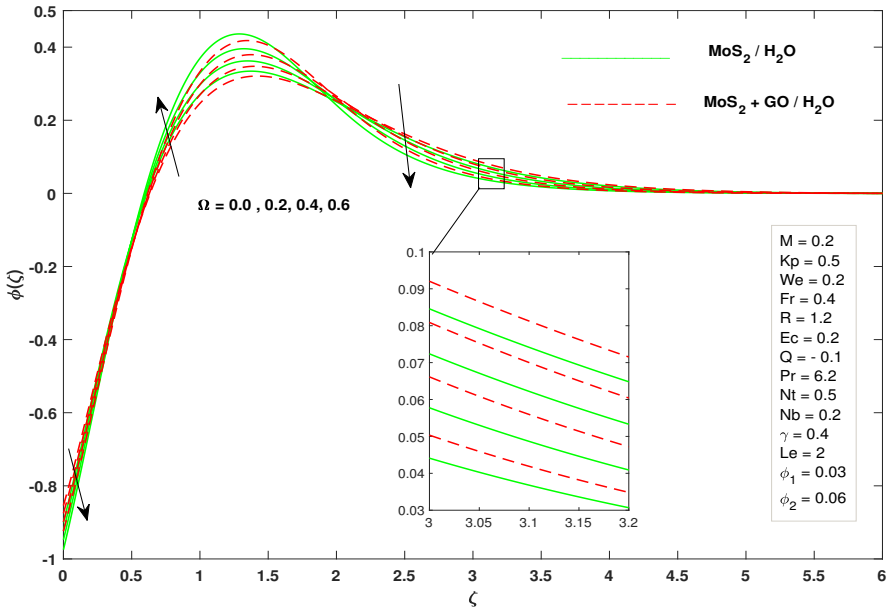

FIGURE 4.30: Effect of Ω on profile $\phi(\zeta)$

Figure 4.31 demonstrates the effect of the Brownian motion parameter (Nb) on the distribution of nanoparticle concentration within the fluid. Increasing this parameter leads to a reduction in the concentration of nanoparticles. Physically, Brownian motion refers to the random movement of nanoparticles within the fluid. When the Brownian motion parameter is enhanced, nanoparticles move more freely in all directions. This initially results in an increase in the nanoparticle-concentration as they spread uniformly throughout the fluid. However, as thermal diffusion effects become more significant due to factors like thermal radiation and thermophoresis, the enhanced Brownian motion becomes limited. This leads to a decrease in nanoparticle concentration after reached to the specific height above the wall.

Moreover, Figure 4.32 illustrates the impact of the thermophoresis parameter Nt on the distribution of concentration $\phi(\zeta)$. As this parameter increases, there is a subsequent increase in $\phi(\zeta)$. However, it is noteworthy that at the beginning, the concentration of $\phi(\zeta)$ initially exhibits a decreasing behavior. Physically, thermophoresis refers to the motion of nanoparticles due to temperature gradients in the fluid. When the thermophoresis parameter is enhanced, nanoparticles experience enhanced motion from hot to cold regions. This leads to an initial reduction in nanoparticle concentration in certain areas as

they migrate towards colder regions. However, as the thermophoresis effect intensifies further, nanoparticles accumulate more in regions with favorable temperature gradients, leading to a collective augmentation in the concentration of nanoparticles $\phi(\zeta)$ within the fluids.

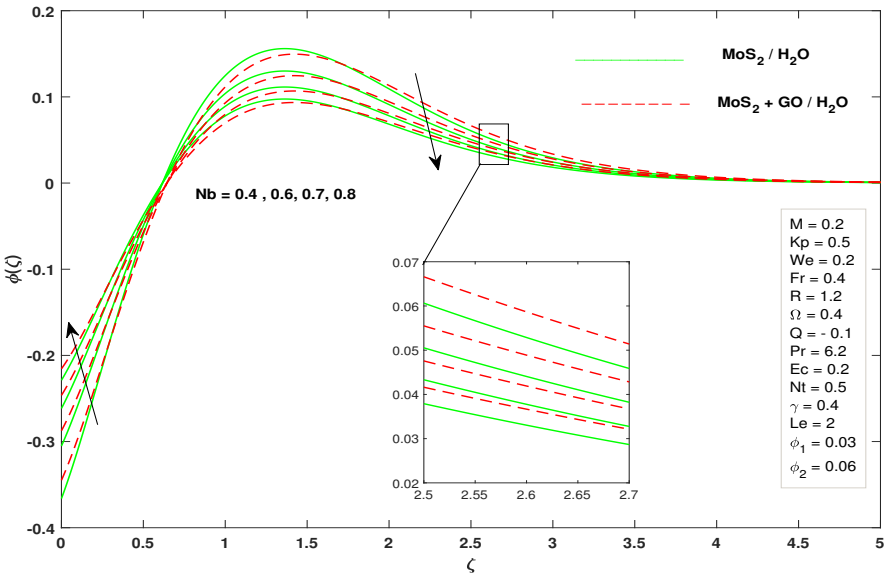

FIGURE 4.31: Effect of Nb on profile $\phi(\zeta)$

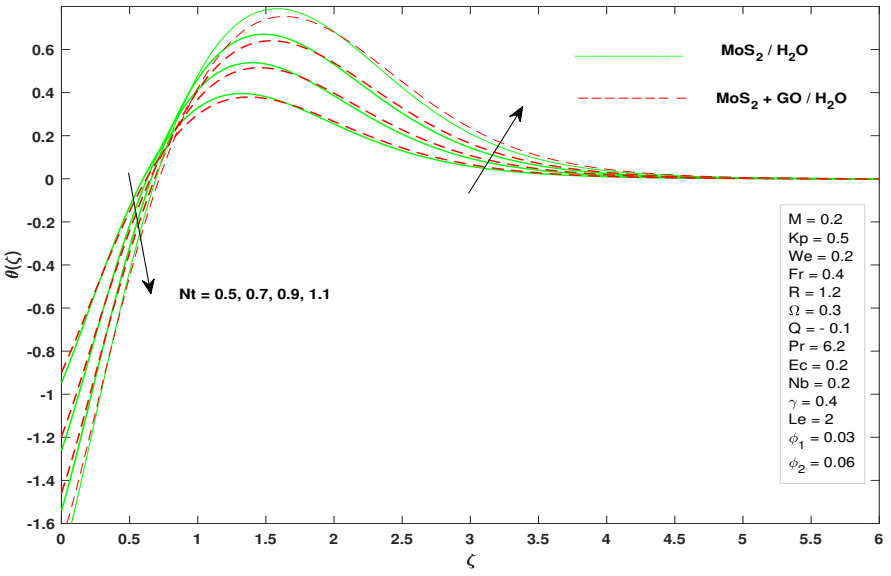

FIGURE 4.32: Effect of Nt on profile $\phi(\zeta)$

Figure 4.33 illustrates the influence of the Lewis number (Le) on the concentration ($\phi(\zeta)$). As the Lewis number increases, there is an inverse relationship, resulting in a

decrease in the nanoparticle-concentration. However, it is important to note that initially, there is an increasing behavior in the distribution of nanoparticle concentration.

Physically, the Lewis number indicates the ratio of thermal diffusivity to mass diffusivity within the fluid. When the Lewis number is increased, the dominant effect shifts towards mass diffusion, which tends to disperse the nanoparticles and decrease their concentration.

However, at the initial stage, other factors might temporarily influence the concentration, leading to the observed increase. These factors could include localized fluid flow patterns or initial variations in temperature gradients.

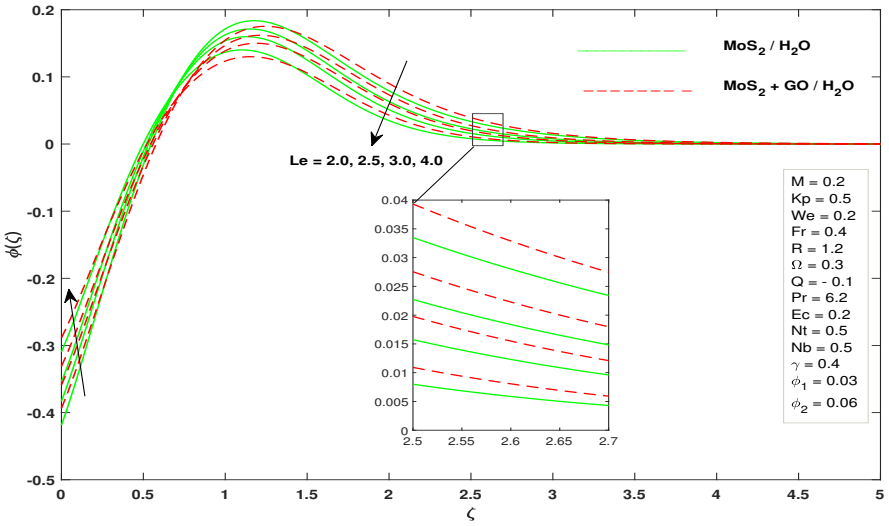

FIGURE 4.33: Effect of Le on profile $\phi(\zeta)$

Figure 4.34 illustrates the effect of the chemical reaction parameter (γ) on $\phi(\zeta)$. As the value of the chemical reaction parameter increases, there is an inverse relationship, resulting in a decrease in the nanoparticle-concentration. However, it is noteworthy that initially, the concentration of nanoparticles shows an uncertain behavior. Physically, the chemical reaction parameter represents the rate of chemical reactions within the fluid that may influence the behavior of nanoparticles. When the chemical reaction parameter is allowed to vary, a change in the concentration profile is naturally expected.

Figure 4.35 explores the impact of ϕ_1, which represents the volume fraction of MoS_2, on the concentration profile. As ϕ_1 increases, the concentration profile initially rises. However, at a specific height along the wall, the concentration profile starts to decrease before eventually returning to its normal increasing behavior beyond that height. This

behavior suggests a complex interaction between ϕ_1 and the distribution of concentration in the fluid, leading to this unique concentration profile pattern.

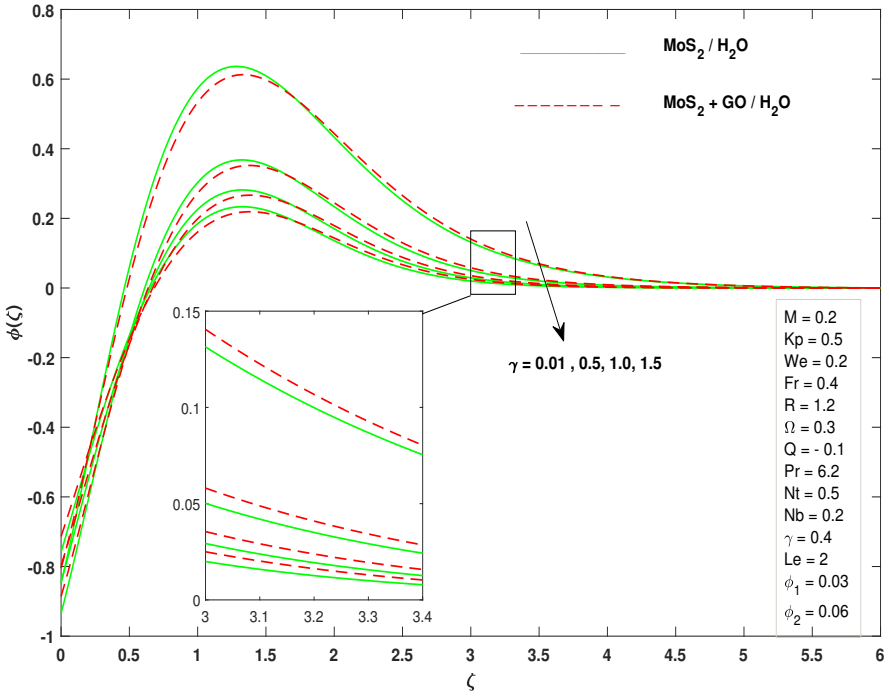

FIGURE 4.34: Effect of γ on profile $\phi(\zeta)$

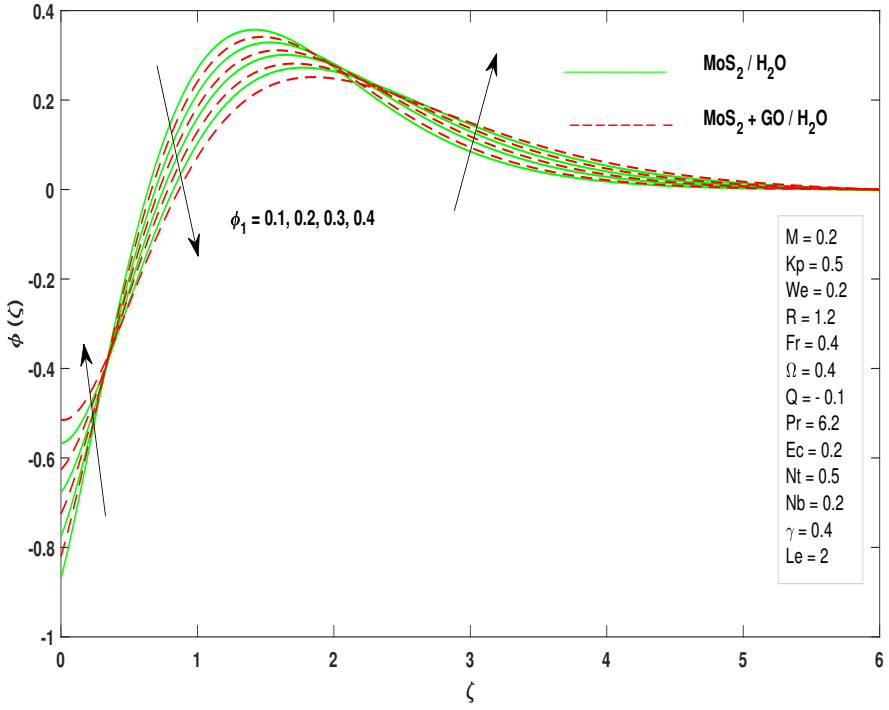

FIGURE 4.35: Effect of ϕ_1 on profile $\phi(\zeta)$

4.5.5 Graphically Behavior of Physical Quantities

Figure 4.36 illustrates the variation in the coefficient of skin friction concerning the non-Newtonian Williamson parameter (We) and the Forchheimer number (Fr). Evidently, the coefficient of skin friction increases with higher values of We.

In Figure 4.37, we examine $Re_x^{1/2}Cf_x$ for different values of M and Kp. It is evident that the coefficient of skin friction decreases with increasing values of these parameters. This suggests that elevated M and Kp lead to a more rapid fluid velocity gradient. Figure 4.38 explores the influence of the (R) and (Pr) on the $Re_x^{-1/2}Nu_x$. Here, an increase in the values of R and Pr leads to a decrease in the local Nusselt number. This implies a reduction in convective heat transfer relative to conductive heat transfer at a boundary within the fluid. Figure 4.39 demonstrates the fluctuation in $Re_x^{-1/2}Nu_x$ due to changes in Pr and Ω for both the fluids. Increasing values of Pr and Ω result in an enhancement of $Re_x^{-1/2}Nu_x$ for both fluids, with this enhancement being more pronounced for the hybrid nanofluid when compared with the nanofluid. Finally, Figure 4.40 reveals that the Sherwood number increases with higher values of the nonlinear thermal radiation parameter and decrease for higher values of Pr. Conversely, in Figure 4.41, the local Sherwood number decreases with increasing values of the Pr and $Omega$.

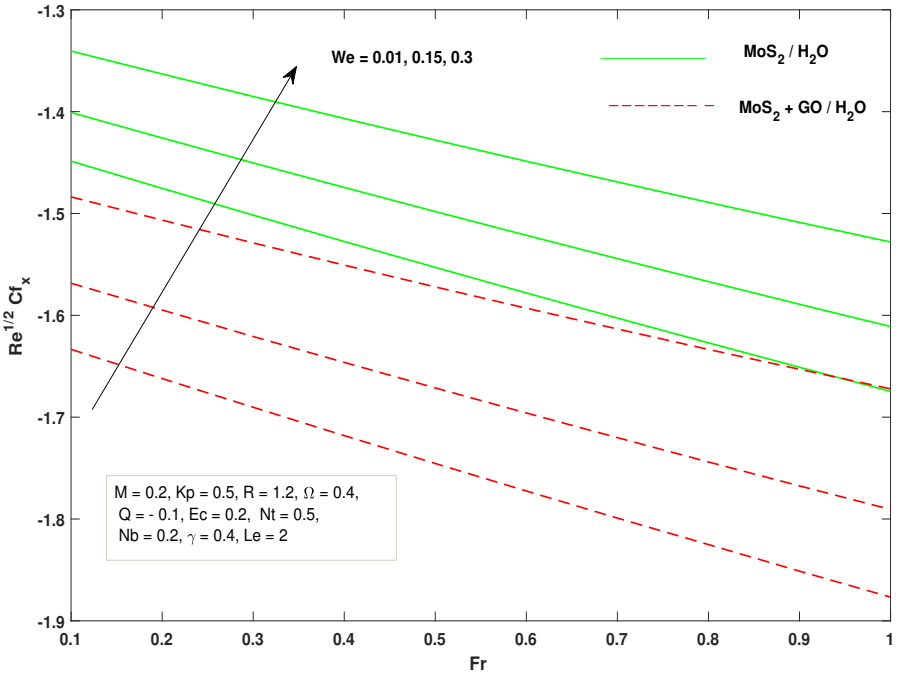

FIGURE 4.36: Skin fraction $Re_x^{1/2}Cf_x$ vs Fr for various values of We

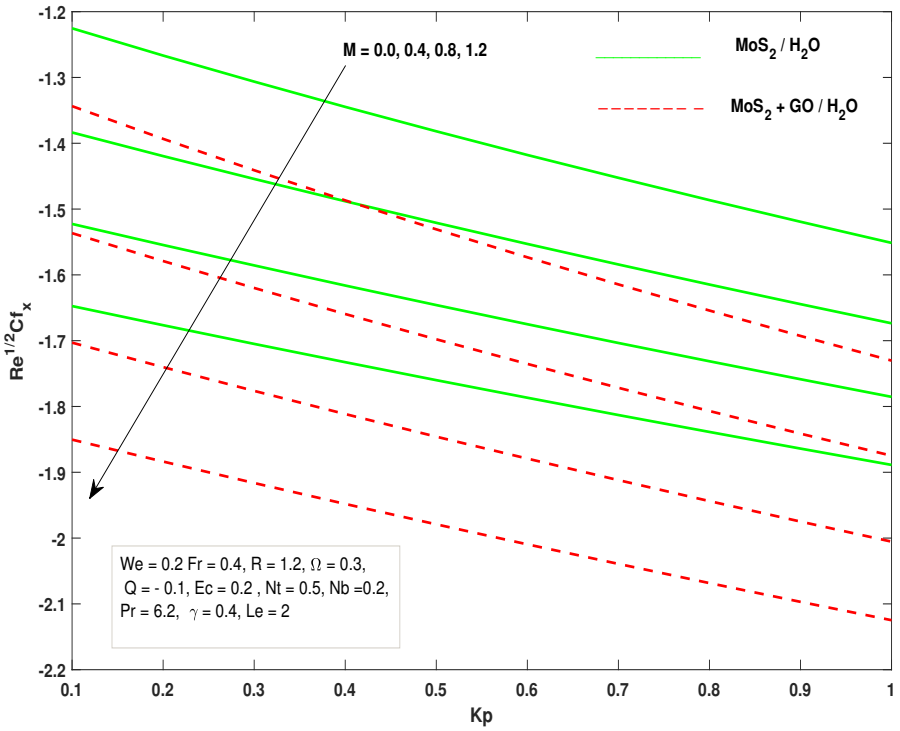

FIGURE 4.37: Skin fraction $Re_x^{1/2}Cf_x$ vs Kp for various values of M

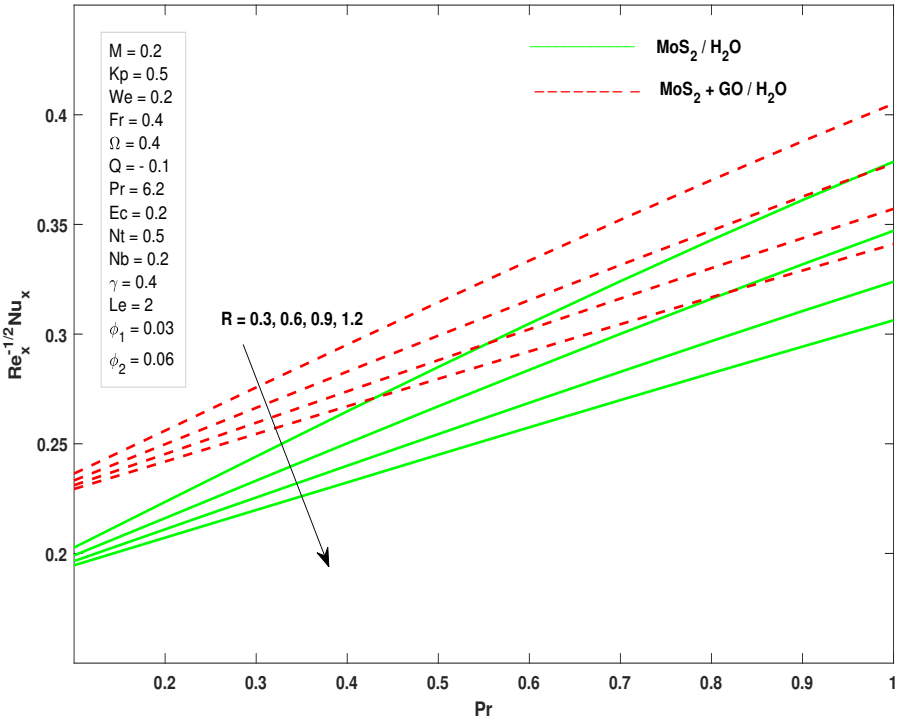

FIGURE 4.38: Local Nusselt number $Re_x^{-1/2}Nu_x$ vs Pr for various values of R

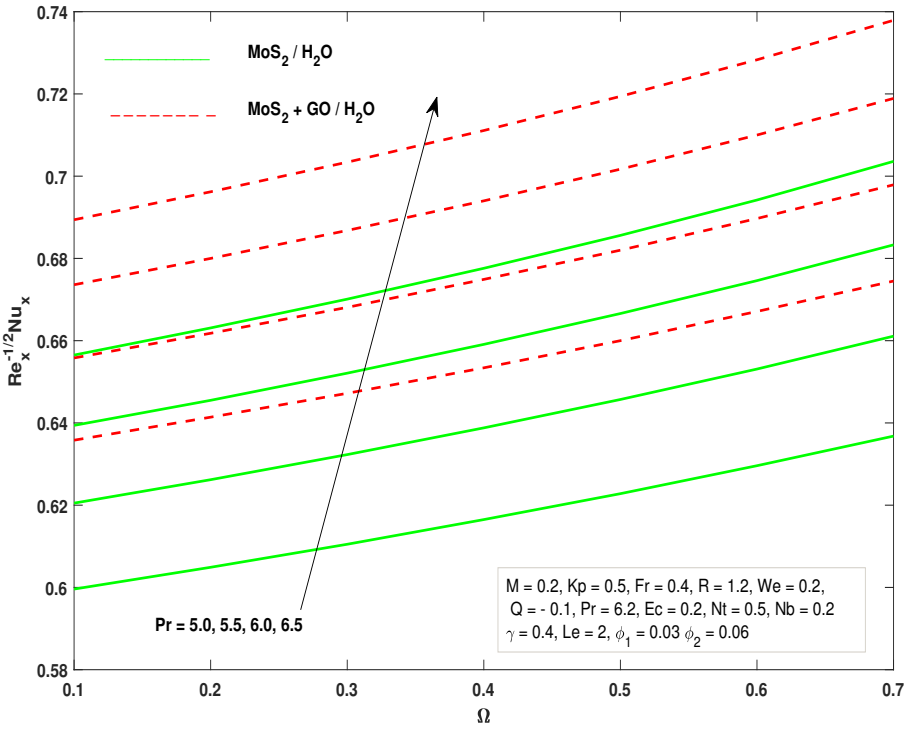

FIGURE 4.39: Local Nusselt number $Re_x^{-1/2}Nu_x$ vs Ω for various values of Pr

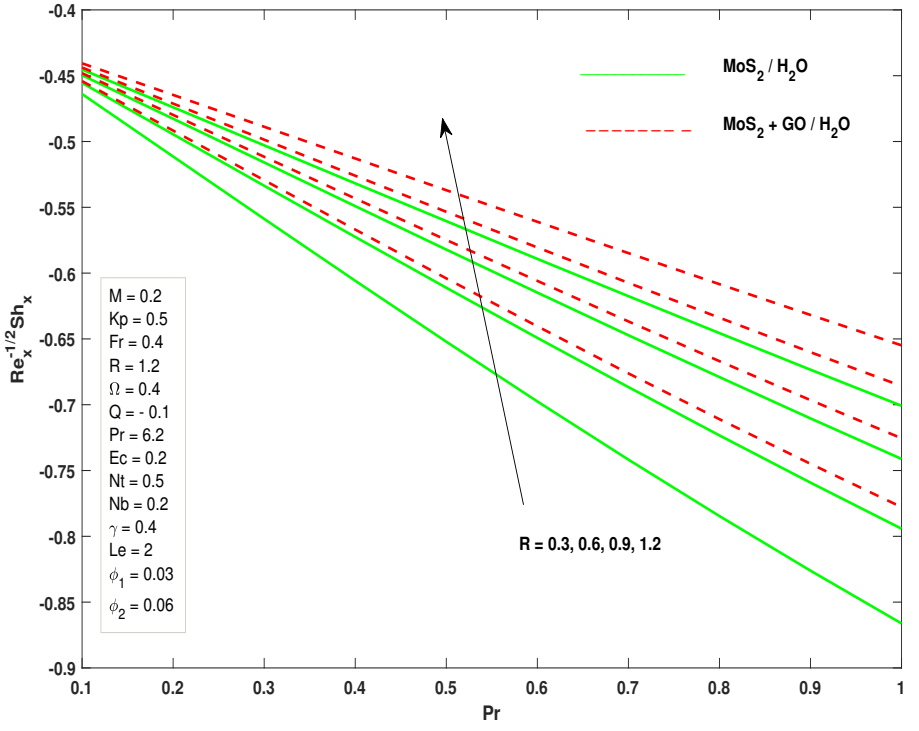

FIGURE 4.40: Local Sherwood number $Re_x^{-1/2}Sh_x$ vs Pr for various values of R

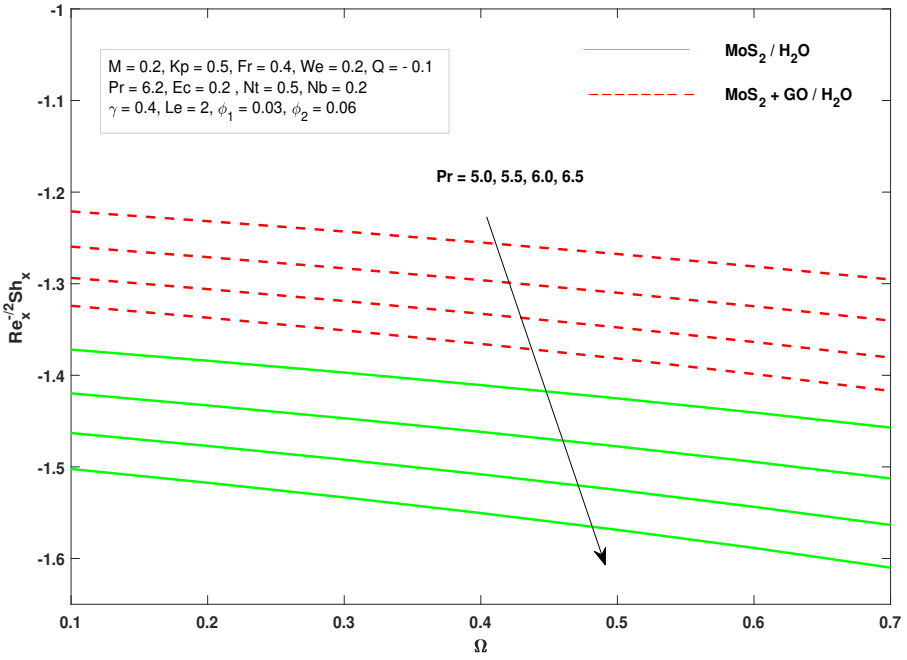

FIGURE 4.41: Local Sherwood number $Re_x^{-1/2}Sh_x$ vs Ω for various values of Pr

4.6 Verification of Code

The acquired results were verified by comparing them with the findings from existing literature sources [2, 17, 55]. A comprehensive comparison of the consistencies observed in various studies is summarized in Table 4.5, 4.6 and 4.7. It is worth noting that the present result reflected a convincing agreement with the some of the reported result in the literature. It should be noted that in table 4.5, '↑' stands for the increasing behavior whereas '↓' means the other way round.

TABLE 4.5: Comparing the current numerical outcomes with those were previously reported of skin fraction when $Fr = \Omega = \phi_1 = \phi_2 = 0, Nb = Nt = Kp = 0.5$, $Le = 2, Q = -0.1, Ec = 0.4$ and $Pr = 5$

	$We = 0.2$			$M = 0.5$	
M	**Bouslimi [2]**	**Present Result**	We	**Bouslimi [2]**	**Present Result**
0	-1.16631	-1.16633	0.1	-1.37752	-1.37752
0.5	-1.33621	-1.33621	0.2	-1.16631	-1.16633
1.0	-1.48296	-1.48296	0.3	-1.28774	-1.28774

TABLE 4.6: Comparison of the accuracy of the present result with the previous result

Increase	**Yahya et al. [17]**		**Bouslimi et al. [2]**			**Present result**		
parameter	$f'(\zeta)$	$\theta(\zeta)$	$f'(\zeta)$	$\theta(\zeta)$	$\phi(\zeta)$	$f'(\zeta)$	$\theta(\zeta)$	$\phi(\zeta)$
M	↓		↓	↑	↑	↓	↑	↑
Kp	↓		↓	↑	↑	↓	↑	↑
We	↓		↓			↓		
Ec		↑		↑	↑		↑	↑
Q		↑		↑	↑		↑	↑
Pr		↓		↓	↓		↓	↓
Le					↑			↑
γ					↓			↓
R				↑	↑		↑	↑
Nt				↑	↑		↑	↑
Nb					↓			↓

TABLE 4.7: Comparison of $-f''(0)$ with variation of magnetic parameter M when $We = Kp = Fr = \phi_1 = \phi_2 = 0$

M	**Ali et al. [56]**	**Asjad et al. [55]**	**Present outcomes**
0.0	1.00000	1.00000	1.00048
0.2	1.09545	1.09545	1.09559
0.5	1.22474	1.22474	1.22477
1.0	1.41421	1.41421	1.41423
1.2	1.48324	1.48324	1.48325
1.5	1.58114	1.58114	1.58114

Chapter 5

Conclusions

In this research thesis, we conducted a comprehensive investigation into the impact of various physical parameters on the velocity, temperature, and concentration profiles of nanoparticles within two different fluids, namely nanofluid (MoS_2/H_2O) and hybrid nanofluid ($MoS_2 + GO/H_2O$) based on the Williamson fluid model. The parameters examined included non-Newtonian Williamson parameter (We), Forchheimer number (Fr), porosity parameter (Kp), nonlinear thermal radiation parameter, time relaxation parameter (Ω), Prandtl number (Pr), thermophoresis parameter (Nt), Brownian motion parameter (Nb), chemical reaction parameter (γ), Lewis number (Le), Eckert number (Ec), and magnetic field coefficient (M).

- Non-Newtonian Williamson parameter (We) and Forchheimer number (Fr) inversely affected fluid velocity, leading to reduced flow rates. Magnetic field parameter (M) caused a decrease in fluid velocity due to Lorentz force.
- Cattaneo-Christov heat flux and heat generation/absorption parameter (Q) positively impacted fluid temperature, enhancing heat transfer and thermal diffusion.
- Prandtl number (Pr) negatively affected fluid temperature due to dominance of momentum diffusion over thermal diffusion.
- The concentration profile is influenced by the thermophoresis parameter (Nt) and Lewis number (Le), resulting in an augmentation in the concentration.

- Brownian motion parameter (Nb) and chemical reaction parameter (γ) led to a decrease in nanoparticle concentration. Time relaxation parameter (Ω) shaped transient behavior within the fluid.

- Regarding certain parameters, a variable behavior in nanoparticle concentration is noted within a specific interval above the wall. Understanding parameter effects crucial for optimizing nanofluid systems in various engineering applications.

- The investigation led to observe an enhancement in thermal and electrical properties, paving the way for nanofluid technology advancements.

Bibliography

[1] R. V. Williamson, "The flow of pseudoplastic materials," *Industrial & Engineering Chemistry*, vol. 21, no. 11, pp. 1108–1111, 1929.

[2] J. Bouslimi, M. Omri, R. Mohamed, K. Mahmoud, S. Abo-Dahab, and M. Soliman, "Williamson nanofluid flow over a stretching sheet through a porous medium under effects of Joule heating, nonlinear thermal radiation, heat generation/absorption, and chemical reaction," *Advances in Mathematical Physics*, vol. 2021, 2021.

[3] B. Jalili, A. D. Ganji, P. Jalili, S. S. Nourazar, and D. Ganji, "Thermal analysis of Williamson fluid flow with Lorentz force on the stretching plate," *Case Studies in Thermal Engineering*, vol. 39, p. 102374, 2022.

[4] K. Guedri, M. S. Hashmi, K. Al-Khaled, M. I. Khan, N. Khan, S. U. Khan, and A. M. Galal, "Numerical simulation for two-phase dusty thermally developed marangoni forced convective flow of Williamson material: a finite difference scheme," *ZAMM-Journal of Applied Mathematics and Mechanics/Zeitschrift für Angewandte Mathematik und Mechanik*, vol. 103, no. 3, p. e202100206, 2023.

[5] P. Kumar, R. S. Yadav, and O. Makinde, "Numerical study of Williamson fluid flow and heat transfer over a permeable stretching cylinder with the effects of Joule heating and heat generation/absorption," *Heat Transfer*, 2023.

[6] S. Shaheen, M. Arain, K. S. Nisar, A. Albakri, M. Shamshuddin, F. O. Mallawi, *et al.*, "A case study of heat transmission in a Williamson fluid flow through a ciliated porous channel: A semi-numerical approach," *Case Studies in Thermal Engineering*, vol. 41, p. 102523, 2023.

[7] S. JANGID, R. MEHTA, and M. K. SHARMA, "Williamson fluid flow and heat transfer analysis over a stretched sheet along with Newtonian heating in the existence of thermal radiative, Buoyancy, and Viscid dissipative impression," 2023.

[8] M. Taj and T. Salahuddin, "A three dimensional frictional flow study of Williamson fluid with chemical reaction," *Materials Science and Engineering: B*, vol. 291, p. 116305, 2023.

[9] S. U. Choi and J. A. Eastman, "Enhancing thermal conductivity of fluids with nanoparticles," tech. rep., Argonne National Lab.(ANL), Argonne, IL (United States), 1995.

[10] J. Buongiorno, "Convective transport in nanofluids," 2006.

[11] W. Khan and I. Pop, "Boundary-layer flow of a nanofluid past a stretching sheet," *International journal of heat and mass transfer*, vol. 53, no. 11-12, pp. 2477–2483, 2010.

[12] S. Nadeem, S. Hussain, and C. Lee, "Flow of a Williamson fluid over a stretching sheet," *Brazilian journal of chemical engineering*, vol. 30, pp. 619–625, 2013.

[13] M. M. Bhatti and M. M. Rashidi, "Effects of thermo-diffusion and thermal radiation on Williamson nanofluid over a porous shrinking/stretching sheet," *Journal of Molecular Liquids*, vol. 221, pp. 567–573, 2016.

[14] M. Krishnamurthy, B. Prasannakumara, B. Gireesha, and R. S. R. Gorla, "Effect of chemical reaction on MHD boundary layer flow and melting heat transfer of Williamson nanofluid in porous medium," *Engineering Science and Technology, an International Journal*, vol. 19, no. 1, pp. 53–61, 2016.

[15] T. Hayat, M. Kiyani, A. Alsaedi, M. I. Khan, and I. Ahmad, "Mixed convective three-dimensional flow of Williamson nanofluid subject to chemical reaction," *International Journal of Heat and Mass Transfer*, vol. 127, pp. 422–429, 2018.

[16] A. Zhu, H. Ali, M. Ishaq, M. S. Junaid, J. Raza, and M. Amjad, "Numerical study of heat and mass transfer for Williamson nanofluid over stretching/shrinking sheet along with Brownian and thermophoresis effects," *Energies*, vol. 15, no. 16, p. 5926, 2022.

[17] A. U. Yahya, N. Salamat, W.-H. Huang, I. Siddique, S. Abdal, and S. Hussain, "Thermal charactristics for the flow of Williamson hybrid nanofluid $MoS_2 + ZnO$ based with engine oil over a streched sheet," *Case Studies in Thermal Engineering*, vol. 26, p. 101196, 2021.

[18] W. Jamshed, S. U. Devi, and K. S. Nisar, "Single phase based study of $ag - cu/eo$ Williamson hybrid nanofluid flow over a stretching surface with shape factor," *Physica Scripta*, vol. 96, no. 6, p. 065202, 2021.

[19] M. Amjad, I. Ahmed, K. Ahmed, M. S. Alqarni, T. Akbar, and T. Muhammad, "Numerical solution of magnetized Williamson nanofluid flow over an exponentially stretching permeable surface with temperature dependent viscosity and thermal conductivity," *Nanomaterials*, vol. 12, no. 20, p. 3661, 2022.

[20] A. Alhowaity, H. Hamam, M. Bilal, and A. Ali, "Numerical study of Williamson hybrid nanofluid flow with thermal characteristics past over an extending surface," *Heat transfer*, vol. 51, no. 7, pp. 6641–6655, 2022.

[21] U. Mahabaleshwar, A. Vishalakshi, and H. I. Andersson, "Hybrid nanofluid flow past a stretching/shrinking sheet with thermal radiation and mass transpiration," *Chinese Journal of Physics*, vol. 75, pp. 152–168, 2022.

[22] A. M. Alqahtani, M. Bilal, M. Usman, T. R. Alsenani, A. Ali, and S. R. Mahmuod, "Heat and mass transfer through mhd Darcy Forchheimer Casson hybrid nanofluid flow across an exponential stretching sheet," *ZAMM-Journal of Applied Mathematics and Mechanics/Zeitschrift für Angewandte Mathematik und Mechanik*, p. e202200213, 2023.

[23] H. Waqas, U. Farooq, D. Liu, M. Abid, M. Imran, and T. Muhammad, "Heat transfer analysis of hybrid nanofluid flow with thermal radiation through a stretching sheet: A comparative study," *International Communications in Heat and Mass Transfer*, vol. 138, p. 106303, 2022.

[24] P. S. Reddy, P. Sreedevi, and A. J. Chamkha, "Hybrid nanofluid heat and mass transfer characteristics over a stretching/shrinking sheet with slip effects," *Journal of Nanofluids*, vol. 12, no. 1, pp. 251–260, 2023.

[25] R. I. Yahaya, N. M. Arifin, F. M. Ali, and S. S. P. M. Isa, "Hybrid nanofluid flow with multiple slips over a permeable stretching/shrinking sheet embedded in a porous medium," *Journal of Advanced Research in Fluid Mechanics and Thermal Sciences*, vol. 106, no. 2, pp. 143–152, 2023.

[26] J. B. J. Fourier, *Théorie analytique de la chaleur*. Gauthier-Villars et fils, 1888.

[27] C. Cattaneo, "Sulla conduzione del calore," *Atti Sem. Mat. Fis. Univ. Modena*, vol. 3, pp. 83–101, 1948.

[28] C. Christov, "On frame indifferent formulation of the Maxwell–Cattaneo model of finite-speed heat conduction," *Mechanics research communications*, vol. 36, no. 4, pp. 481–486, 2009.

[29] M. B. Ashraf, A. Tanveer, S. Ulhaq, *et al.*, "Effects of Cattaneo-Christov heat flux on MHD Jeffery nano fluid flow past a stretching cylinder," *Journal of Magnetism and Magnetic Materials*, vol. 565, p. 170154, 2023.

[30] E. A. Algehyne, A. F. Alharbi, A. Saeed, A. Dawar, M. Ramzan, and P. Kumam, "Analysis of the MHD partially ionized go-ag/water and $Go-Ag$/kerosene oil hybrid nanofluids flow over a stretching surface with Cattaneo–Christov double diffusion model: A comparative study," *International Communications in Heat and Mass Transfer*, vol. 136, p. 106205, 2022.

[31] A. Salmi, H. A. Madkhali, B. Ali, M. Nawaz, S. O. Alharbi, and A. Alqahtani, "Numerical study of heat and mass transfer enhancement in Prandtl fluid MHD flow using Cattaneo-Christov heat flux theory," *Case Studies in Thermal Engineering*, vol. 33, p. 101949, 2022.

[32] K. Muhammad, T. Hayat, S. Momani, and S. Asghar, "Fdm analysis for squeezed flow of hybrid nanofluid in presence of Cattaneo-Christov (CC) heat flux and convective boundary condition," *Alexandria Engineering Journal*, vol. 61, no. 6, pp. 4719–4727, 2022.

[33] K. Latha, M. G. Reddy, D. Tripathi, O. A. Bég, S. Kuharat, H. Ahmad, D. U. Ozsahin, and S. Askar, "Computation of stagnation coating flow of electro-conductive ternary Williamson hybrid nanofluid with a Cattaneo–Christov heat flux model and magnetic induction.," *Scientific Reports*, vol. 13, no. 1, 2023.

[34] K. Jabeen, M. Mushtaq, T. Mushtaq, and R. M. A. Muntazir, "A numerical study of boundary layer flow of Williamson nanofluid in the presence of viscous dissipation, bioconvection, and activation energy," *Numerical Heat Transfer, Part A: Applications*, pp. 1–22, 2023.

[35] U. Farooq, M. Imran, N. Fatima, S. Noreen, M. Tahir, A. Akgül, M. De la Sen, and A. M. Galal, "Cattaneo-Christov heat flux model in radiative flow of

($Fe_3o_4 - -TiO_2$/Transformer oil) and ($Cu - -Tio_2$/Transformer oil) magnetized hybrid nanofluids past through double rotating disks," *Case Studies in Thermal Engineering*, vol. 45, p. 102905, 2023.

[36] A. A. Hussaini, A. G. Madaki, S. A. Kabiru, A. Barde, and I. Abdullahi, "Numerical approach for convective magnetohydrodynamic (MHD) nanofluid flow with impermeable stretching surface," *SCIENCETECH*, vol. 3, no. 1, pp. 1–16, 2022.

[37] B. Jalili, S. Sadighi, P. Jalili, and D. D. Ganji, "Numerical analysis of MHD nanofluid flow and heat transfer in a circular porous medium containing a cassini oval under the influence of the Lorentz and buoyancy forces," *Heat Transfer*, vol. 51, no. 7, pp. 6122–6138, 2022.

[38] A. A. Hussaini and A. T. Abdulkadir, "Physical effects of heat generation/absorption on MHD nanofluid flow over a stretching surface," *Int. J. Adv. Eng. and Mang.(IJAEM)*, vol. 4, no. 6, pp. 1464–1478, 2022.

[39] S. Sarala, E. Geetha, M. Mageswari, and M. R. Madhavi, "Effects of heat and mass transmission with radiation on MHD nanofluid flow past over an oscillating plate using chemical reaction," in *AIP Conference Proceedings*, vol. 2707, AIP Publishing, 2023.

[40] S. Sadighi, M. Jabbari, H. Afshar, and H. A. D. Ashtiani, "MHD heat and mass transfer nanofluid flow on a porous cylinder with chemical reaction and viscous dissipation effects: Benchmark solutions," *Case Studies in Thermal Engineering*, vol. 40, p. 102443, 2022.

[41] A. Dawar, A. Wakif, T. Thumma, and N. A. Shah, "Towards a new MHD non-homogeneous convective nanofluid flow model for simulating a rotating inclined thin layer of sodium alginate-based Iron oxide exposed to incident solar energy," *International Communications in Heat and Mass Transfer*, vol. 130, p. 105800, 2022.

[42] S. Sivasankaran, T. Chandrapushpam, M. Bhuvaneswari, S. Karthikeyan, and A. Alzahrani, "Effect of chemical reaction on double diffusive MHD squeezing copper water nanofluid flow between parallel plates," *Journal of Molecular Liquids*, vol. 368, p. 120768, 2022.

[43] K. Raghunath, "Study of heat and mass transfer of an unsteady magnetohydrodynamic (MHD) nanofluid flow past a vertical porous plate in the presence of chemical reaction, radiation and Soret effects," *Journal of Nanofluids*, vol. 12, no. 3, pp. 767–776, 2023.

[44] M. R. Zangooee, K. Hosseinzadeh, and D. D. Ganj, "Investigation of three-dimensional hybrid nanofluid flow affected by nonuniform MHD over exponential stretching/shrinking plate," *Nonlinear Engineering*, vol. 11, no. 1, pp. 143–155, 2022.

[45] J. Jiang, H. Zhao, and Y. Zhang, "Two dimensional MHD nanofluid flow analysis of fractional dual-phase-lag heat conduction between inclined cylinders with variable thickness," *International Journal of Numerical Methods for Heat & Fluid Flow*, vol. 33, no. 5, pp. 1637–1660, 2023.

[46] W. Li, U. Farooq, H. Waqas, A. M. Alharthi, N. Fatima, A. M. Hassan, T. Muhammad, and A. Akgül, "Numerical simulations of Darcy-forchheimer flow of radiative hybrid nanofluid with Lobatto-Iiia scheme configured by a stretching surface," *Case Studies in Thermal Engineering*, p. 103364, 2023.

[47] S. Nandi and D. Barman, "Unsteady MHD hybrid nanofluid flow over a convectively heated linear stretching cylinder with velocity slip: A comparative study," *International Journal of Modern Physics B*, p. 2450284, 2023.

[48] E. J. Shaughnessy, *Introduction to Fluid Mechanics*. 2005.

[49] R. Bansal, *A Textbook of Fluid Mechanics and Hydraulic Machines*. Laxmi Publications, 2010.

[50] S. Som, *Introduction to Heat Transfer*. PHI Learning Pvt. Ltd., 2008.

[51] R. E. Collins, "Flow of fluids through porous materials," 1976.

[52] J. N. Reddy and D. K. Gartling, *The Finite Element Method in Heat Transfer and Fluid Dynamics*. CRC press, 2010.

[53] J. Kuneš, "Thermomechanics," *Dimensionless Physical Quantities in Science and Engineering. Elsevier, Oxford*, pp. 173–283, 2012.

[54] B. Ali, R. A. Naqvi, D. Hussain, O. M. Aldossary, and S. Hussain, "Magnetic rotating flow of a hybrid nano-materials hybrid base fluid over an extending surface involving activation energy: FE simulation," *Mathematics*, vol. 8, no. 10, p. 1730, 2020.

[55] M. I. Asjad, M. Zahid, B. Ali, F. Jarad, *et al.*, "Unsteady MHD Williamson fluid flow with the effect of bioconvection over permeable stretching sheet," *Mathematical Problems in Engineering*, vol. 2022, 2022.

[56] B. Ali, Y. Nie, S. A. Khan, M. T. Sadiq, and M. Tariq, "Finite element simulation of multiple slip effects on MHD unsteady maxwell nanofluid flow over a permeable stretching sheet with radiation and thermo-diffusion in the presence of chemical reaction," *Processes*, vol. 7, no. 9, p. 628, 2019.

Turnitin Originality Report

Investigation of a Williamson Hybrid Nanofluid Flow using the Cattaneo-Christov Heat Flux, Magnetic Field, Forchheimer Flow and Chemical Reaction by Hassan Shahzad

From CUST Library (MS Thesis)

- Processed on 13-Sep-2023 09:37 PKT
- ID: 2164775255
- Word Count: 21661

Similarity Index
18%
Similarity by Source

Internet Sources:
14%
Publications:
13%
Student Papers:
4%

Graduate Studies Office
18%
Within Limits

sources:

1 1% match (Internet from 03-Feb-2023)
https://thesis.cust.edu.pk/UploadedFiles/MMT183010-Muhammad%20Qayyum%20Khan.pdf

2 1% match (Internet from 02-Feb-2023)
https://thesis.cust.edu.pk/UploadedFiles/MMT183011-Muhammad%20Asif%20Khan.pdf

3 1% match (Internet from 04-Feb-2023)
https://thesis.cust.edu.pk/UploadedFiles/Nimra%20Shanakhat-MMT183003.pdf

4 1% match (Internet from 06-Jan-2023)
https://www.ingentaconnect.com/contentone/asp/jon/2016/00000005/00000003/art00007?crawler=true

5 1% match (J. Bouslimi, M. Omri, R. A. Mohamed, K. H. Mahmoud, S. M. Abo-Dahab, M. S. Soliman. "MHD Williamson Nanofluid Flow over a Stretching Sheet through a Porous Medium under Effects of Joule Heating, Nonlinear Thermal Radiation, Heat Generation/Absorption, and Chemical Reaction", Advances in Mathematical Physics, 2021)
J. Bouslimi, M. Omri, R. A. Mohamed, K. H. Mahmoud, S. M. Abo-Dahab, M. S. Soliman. "MHD Williamson Nanofluid Flow over a Stretching Sheet through a Porous Medium under Effects of Joule Heating, Nonlinear Thermal Radiation, Heat Generation/Absorption, and Chemical Reaction", Advances in Mathematical Physics, 2021

6 1% match (M. Asif Zahoor Raja, M. Shoaib, Ghania Zubair, M. Ijaz Khan, R.J. Punith Gowda, B.C. Prasannakumara, Kamel Guedri. "Intelligent neuro-computing for entropy generated Darcy–Forchheimer mixed convective fluid flow", Mathematics and Computers in Simulation, 2022)
M. Asif Zahoor Raja, M. Shoaib, Ghania Zubair, M. Ijaz Khan, R.J. Punith Gowda, B.C. Prasannakumara, Kamel Guedri. "Intelligent neuro-computing for entropy generated Darcy–Forchheimer mixed convective fluid flow", Mathematics and Computers in Simulation, 2022

7 1% match (Internet from 18-Mar-2023)
https://dr.ntu.edu.sg/bitstream/10356/160809/2/1-s2.0-S2214157X21003592-main.pdf

8 < 1% match (Internet from 16-Dec-2022)
https://thesis.cust.edu.pk/UploadedFiles/MMT173034.pdf

9 < 1% match (Internet from 09-Jan-2023)
https://thesis.cust.edu.pk/UploadedFiles/Ayesha%20Maqbool-MMT183019.pdf

10 < 1% match (Internet from 19-Jan-2023)
https://thesis.cust.edu.pk/UploadedFiles/Abida%20Begum-MMT135013.pdf

11 < 1% match (Internet from 17-Jan-2023)
https://thesis.cust.edu.pk/UploadedFiles/Adeel%20Tahir-MA131014.pdf